Solving the partial differential equation for pricing barrier options via trigonometric expansions

MSc Thesis

TU Delft

QUANT

SOLVING THE PARTIAL DIFFERENTIAL EQUATION FOR PRICING BARRIER OPTIONS VIA TRIGONOMETRIC EXPANSIONS

MSc THESIS

by

Sofia Maria MARQUES DA ROCHA FELICIANO PEREIRA

to obtain the degree of Master of Science
at the Delft University of Technology,
to be defended publicly on October 27, 2023 at 14:00.

Student number:	5553113	
Project duration:	Feb 1, 2023 - Oct 27, 2023	
Thesis commitee:	Dr. F. Fang	TU Delft, supervisor
	Prof.Dr.ir. C. Vuik	TU Delft
	Prof.Dr. A. Papapantoleon	TU Delft
	Dr. X. Shen	FFQuant, supervisor

ABSTRACT

Barrier options, although highly liquid financial derivatives, present notable pricing challenges. In this thesis, we present a novel pricing approach for valuing continuously-monitored knock-out barrier option within the framework of stochastic volatility models.

The underlying process is firstly modelled under geometric Brownian motion and, subsequently, under Heston's stochastic volatility model. A key insight is that the value of a barrier option can be expressed as a single-dimensional integral, whereby the integrand involves the so-called survival density function, which captures the barrier-breaching information. Therefore, the option can be valued using the one-dimensional COS method for European options, once the Fourier series coefficients of the survival density are obtained.

The coefficients of the sine series expansion of the survival density function are in fact a continuous function, which is closely related to the characteristic function of the density. This motivates us to directly recover that function, which we refer to as the target function herewith, by selecting an appropriate series expansion for it. Thereafter, we insert this series expansion into the partial differential equation (PDE) that the target function should satisfy, which can be derived from the pricing PDE. This results in a linear system, solving which we obtain the coefficients needed to reconstruct the target function. Notably, this approach is particularly advantageous when the reference values of option prices are limited or unavailable, as it relies solely on the PDE to calibrate the series coefficients.

Our choice of series expansion is driven by the need for precise global and local approximations. Our research shows that a proper expansion for the target function can be built up from integrating a two-dimensional Fourier series of its first derivative with respect to time, marking our second pivotal insight. That results in a trigonometric expansion that significantly enhances the accuracy compared to a direct Fourier series expansion on the target function. Finally, our third pivotal insight: applying a change of variables further improves error convergence.

Extensive testing results suggest that, for similar accuracy levels, our approach greatly outperforms Monte Carlo simulations in terms of computation time. It also demonstrates superior computational efficiency and accuracy compared to other advanced numerical methods in the existing literature. The benefits of this method become even more prominent when pricing a large number of options simultaneously.

Numerical tests reveal algebraic convergence for the series expansion reconstruction. For the option price, theoretical error analysis aligns with our findings, also predicting algebraic convergence.

Keywords. Barrier option, Geometric Brownian Motion model, Heston's model, Pricing PDE, COS method, Fourier series, Monte Carlo simulation.

PREFACE

As I come to the end of this thesis project, I can not help but think about the past two years that made my master in Applied Mathematics at TU Delft; all the friends I made along the way, all the things I learnt in and outside of classrooms, all the memories I made. This thesis marks the end of my studies in Applied Mathematics and while challenging, these past five years were also very rewarding. For that reason, I would like to acknowledge some people that were a part of this journey.

Firstly, I would like to express my gratitude to my supervisors, Dr. Fang and Dr. Shen, for the possibility to work on this project at FF Quant. Your guidance, patience, continuous feedback and insightful comments played an important role in enhancing my research skills and critical thinking, ultimately culminating in the successful completion of my thesis.

To Gijs, I know you think acknowledgments are "corny" but I could not not thank you for all the hours of discussion, motivational talks and always being available for me. To Zoé and Felix, my partners in this thesis journey, I definitely could not have done it without you. My gratitude goes beyond this past 9 months as Felix has been my friend and study buddy for the entire master and Zoé was my first friend in Delft, helping me around since day one. Also, my sincere thanks to those that I met in Delft and made this experience so enjoyable and memorable.

In addition, I would like to express my appreciation for my friends back in Portugal for always making it feel like distance is just a detail. In particular, I would like to thank Tomás, Luís, Inês, (my other) Tomás and Matilde for being by my side during my whole studies in Applied Mathematics. As much as life has changed, our friendship and my appreciation for you has been a constant variable. To my best friend Maria, you helped me more in the past few months than you can imagine and I am very grateful for that.

Finally, I would like to thank my family, whose unconditionally support and caring helped me through this master, and especially through this thesis project. Words are not enough to describe how important your support was (and is) to me. Last but not least, a special mention to Carla for always being there for me.

Sofia Pereira
Delft, October 2013

List of Figures

LIST OF TABLES

List of Abbreviations

BS Black-Scholes 2

ch.f. characteristic function 2

FTC Fundamental Theorem of Calculus 23

GBM Geometric Brownian Motion 1

IVBP initial boundary value problem 41

LHS left-hand side 33

MC Monte Carlo 2

PDE Partial Differential Equation 3

pdf probability density function 2

RHS right-hand side 33

SDE Stochastic Differential Equation 10

CONTENTS

1

INTRODUCTION

One of the most important issues in quantitative finance is that of pricing derivative instruments. The valuation of options, in particular, takes a pivotal role in effective risk management and portfolio optimization. However, under certain underlying asset models, closed-form solutions do not exist, and thus, multiple numerical methods have been proposed and studied in the literature, aiming to obtain accurate option prices efficiently.

There are different types of options, such as European options, American options and exotic options. Among the last category, one finds Asian options, Bermudan options, and Barrier options. Specifically, barrier options are path-dependent options whose payoff is contingent on whether the underlying price breaches a predetermined level - the barrier -, during the lifetime of the option contract.

Barrier options are one of the most liquid exotic derivatives - especially in the foreign exchange (FX) markets. Their popularity can be attributed to the fact that they are cheaper than European options, as the payoff opportunities are more limited. In fact, barrier options were created to offer hedging capabilities at a lower premium cost, typically appealing to purchasers with very precise speculations on the market's moving.

An important feature of barrier options is whether the barrier-crossing is monitored in continuous or discrete time. Barrier option contracts that assume continuous monitoring require a continuous verification on whether the barrier is breached at any time before the expiration date. One of the most liquid barrier options in FX markets are continuously-monitored calls and puts (see e.g. [1]–[4]). For that reason, in this thesis, we shall focus on continuously-monitored barrier options. Alternatively, one can consider just daily/weekly/monthly monitoring which makes the barrier option more expensive because chances of the barrier getting breached are smaller (cf. [4]). A detailed discussion of the valuation of discrete barriers can be found in [5].

Despite the high liquidity, a closed-form pricing formula for continuously-monitored barrier options is not available unless we assume a Geometric Brownian Motion (GBM) process for the underlying asset, as proposed by Black and Scholes [6]. Under the GBM

framework, analytical formulae have been developed by, for example, Merton [7], Heynen and Kat [8] and Kunitomo and Ikeda [9].

However, the Black-Scholes (BS) framework does not sufficiently capture the leptokurtic features observed in financial market data, and subsequently more advanced models have been developed to better reflect the volatility smiles and skews implied in market traded options. One type of such models are the so-called *stochastic volatility models*, which assume that the volatility evolves stochastically. The most prominent stochastic volatility models include the square-root process introduced by Heston [10], the stochastic volatility model developed by Hull and White [11], the model proposed by Stein and Stein [12], under which the volatility follows an arithmetic Ornstein–Uhlenbeck process, and the SABR model by Hagan et al. [13]. However, Heston's model is a popular model adopted in the industry, and as such, it is one of the model choices of this thesis.

As opposed to the BS framework, not so many analytical results have been obtained in the literature for barrier option pricing under stochastic volatility models. Section 1.1 is devoted to a literature review on the most recent research on this topic.

1.1. LITERATURE REVIEW

Existing numerical methods for option pricing include Monte Carlo (MC) simulation, finite difference schemes that directly solve the corresponding pricing PDE [14], tree-based methods such as [15] and [16], Fourier-based methods including the COS method in [17] and [18] and other FFT-based methods (on the basis of Fast Gauss or the Hilbert Transform) [19]–[21]. On top of this, there have been recent efforts in using machine learning to directly approximate the valuation formulas.

MC simulation methods are often used for the valuation of financial products which exhibit some form of path dependency in practice. Notice, however, that it is too slow for the trading environment due to the slow error convergence rate. That is, one usually needs a large number of sample paths. Moreover, in the context of continuously-monitored barrier options, a large number of time steps is also required, leading to notable computational inefficiencies.

A different and a very efficient approach to computing option values involves the use of Fourier techniques. One of the most popular methods of this type is the COS method, which was introduced by Fang and Oosterlee in [22] to price European options. The essence of the method lies in recovering the probability density function (pdf) through its Fourier pair, i.e. the characteristic function (ch.f.), semi-analytically. It has been applied to pricing barrier options under Heston's model in [17]. It consists of a one-dimensional method that relies on the pdf of the log-variance at current time, conditioned on the log-variance at a past time, for which a closed-form solution is available. However, our testing results indicate that for certain parameter sets this method exhibits significant pricing difficulties. An alternative, the two-dimensional COS method introduced by Ruijter and Oosterlee [18], employs a similar approach but uses the two-dimensional ch.f.. Nevertheless, its scope of application is even narrower, as it is designed for variance rather than log-variance, particularly challenging due to the skewed nature of the variance density function. Moreover, both methods are developed for discretely-monitored barrier options and the computational speed is not optimal for

weekly- and daily-monitored barrier options.

All the methods presented thus far directly address the computation of the expectation within the valuation formula for a barrier option. Simultaneously, the Feynman-Kac theorem provides a connection between the expectation of the option's payoff value and the solution of the corresponding pricing Partial Differential Equation (PDE). Therefore, another way to compute option values is to solve the corresponding pricing PDE numerically, using, for instance, the finite difference method. The main benefit of this approach is that the option's value can be generated for the entire discretization range of the underlying stock values simultaneously. However, it requires a large number of discretization steps for an accurate outcome for path-dependent derivatives. Plus, the difficulties mentioned for the COS methods are also present in the finite difference scheme.

Lastly, existing machine learning techniques for option pricing in the literature rely on given reference values for the training step, which can only be computed via the aforementioned numerical methods. Furthermore, for neural networks, there can be concerns related to interpretability, as they often operate as "black-box" algorithms, preventing a full understanding of the process.

In summary, the majority of the previous methods are more suitable for discretely-monitored barrier options. The reason is that, in continuous time, the derivation of the first hitting time (of the barrier level) for stochastic volatility models poses a mathematically challenging problem.

Under Heston's model, the availability of analytical results is very limited, but they exist in two cases. The first case involves zero drift and zero correlation between the variance and the underlying price. The barrier option price, conditioned on the integrated variance, is determined by a one-dimensional integration. This conditional expectation must then be further solved to yield the unconditional expectation, by integrating with the density of the integrated variance, as seen in previous works [2], [3].

When the correlation is non-zero, closed-form formulas are not available and perturbation methods are often employed. Perturbation methods consider a small parameter ϵ, allowing for an asymptotic solution constructed through a series expansion in ϵ. This approach has been explored in various studies, namely [3], [23]–[26].

A more recent paper from 2022 develops a methodology that is different from the ones mentioned above. For one-dimensional diffusion models, the classical reflection principle (cf. [27]) is used to derive the barrier option pricing formulas under the BS model [28]; He and Lin [29] have explored this idea in the context of Heston's model to obtain a pricing formula that needs to be solved via numerical integration.

Their procedure can be split in two steps. First, they reduce the dimensionality of the problem by assuming that all the future information of the volatility is known at the current time. Under this assumption, the Heston's model becomes a time-dependent BS model through a series of variable transformations. Using the reflection principle, an analytical approximation for the barrier option price $M(h_T, v_T) := V(t, x|\mathscr{F}_T)$ is derived, where $h_T = \int_t^T v_S ds$. In the second step, they regard the target barrier option price as the expectation of the obtained conditional price with respect to the volatility, $V(t, x, v) = \mathbb{E}[M(h_T, v_T)|v_t]$. They recur to the COS method to recover an approximation for the density function in $V(t, x, v) = \int_0^{+\infty} M(h_T, v_T) f(h_T|v_t, v_T) dh_T$. In the end, the

option pricing formula depends on an integral that needs to be numerically computed, thereby leading to an increased computational time.

1.2. THESIS OBJECTIVE AND OUTLINE

This thesis contributes to the existing literature with a novel approach to pricing continuously-monitored barrier options recurring to the pricing PDE. This method comprises three main components: determining the most suitable expansion form for getting the survival ch.f. of a knock-out option; finding the coefficients of this expansion via inserting it in the PDE to yield a linear system; and applying the one-dimensional COS method for pricing the respective option.

The central theoretical foundation of our method is that the barrier-hitting probability can be incorporated into the so-called survival density function. This enables us to employ the one-dimensional COS formula by Fang and Oosterlee [22], typically used for pricing European options, to value barrier options.

As a result, we focus on recovering the survival pdf and determining the coefficients of its sine series expansion. These coefficients are, in fact, a continuous function, which is closely related to the survival ch.f.. Building on this insight and inspired by prior research conducted at FF Quant [30], we are driven to directly reconstruct that function, which we refer to as the target function herewith, using another series expansion. In our case, a proper expansion for the target function is a trigonometric expansion, which we build up step by step and it is a result of integrating a two-dimensional Fourier series expansion of its first derivative with respect to time. This leads to another key insight: accuracy of a Fourier series approximation can be enhanced by expanding the derivative of the target function rather than the function itself. Additionally, error convergence speed of the trigonometric expansion can be further improved by applying a change of variables to the target function, so that the skewness is reduced.

Finally, the main idea behind this method is to obtain the coefficients of the trigonometric expansion directly from the PDE it satisfies, instead of by training on a set of reference values. This is achieved by evaluating the PDE at various training points. Once we obtain the coefficients of the trigonometric expansion, we have a series expansion-based approximation of the coefficients of the survival pdf's series. Lastly, using the COS method, we compute the price of a barrier option.

The outline of this thesis is as follows. Chapter 2 lays the essential mathematical framework for formulating and understanding our approach. Chapter 3 presents a preliminary analysis for the Heat equation, a simpler PDE for which there are known solutions. This forms the foundation of our later derivations regarding more complex pricing PDEs. Our methodology is developed step by step in Chapter 4, under the assumption that the underlying asset price follows a GBM. Subsequently, in Chapter 5 we extend our method to Heston's model, addressing challenges that arise from the additional dimension of the stochastic variance. Both Chapters 4 and 5 include numerical results, wherein we evaluate the accuracy of our approach by comparing it to the closed-form solution for GBM in Chapter 4 and to a MC simulation for Heston's model in Chapter 5. Chapter 6 is dedicated to further performance improvements of our approach. Moreover, Chapter 7 provides a final comparison between our method and other existing methods in the

literature for pricing barrier options. The error is analysed from a theoretical perspective in Chapter 8. Finally, Chapter 9 summarizes all the findings, draws a conclusion on merits and demerits of our approach, and suggests future research directions.

2

MATHEMATICAL FRAMEWORK

In this chapter, all the relevant mathematical tools are presented to formulate, model and solve the option pricing problem.

2.1. STOCHASTIC CALCULUS

The purpose of this section is to introduce relevant definitions and theorems from the field of stochastic calculus. The contents of this section are based on [31] and [32].

Definition 2.1.1 (Filtration)**.** *Let $(\Omega, \mathscr{F}, \mathbb{P})$ be a probability space. A filtration on $(\Omega, \mathscr{F}, \mathbb{P})$ is a family of sub σ-fields $\{\mathscr{F}_t,\ t \geq 0\}$ of $\mathscr{F}$ indexed by $t \in [0, \infty)$, such that $\mathscr{F}_s \subset \mathscr{F}_t$ for every $s \leq t \leq \infty$.*

Definition 2.1.2 (Adapted process)**.** *A process $X = \{X_t,\ t \geq 0\}$ is said to be adapted to a filtration $\{\mathscr{F}_t,\ t \geq 0\}$ if for all $t \geq 0$, X_t is $\mathscr{F}_t$ measurable.*

Definition 2.1.3 (Martingale)**.** *Let $M := \{M_t,\ t \geq 0\}$ be a process defined on the probability space $(\Omega, \mathscr{F}, \mathbb{P})$ equipped with a filtration $\{\mathscr{F}_t,\ t \geq 0\}$. Then M is said to be a martingale if*

- *M is an adapted process.*
- *For all $t \geq 0$, M_t is integrable.*
- *M satisfies the martingale property,*

$$\mathbb{E}[M_t | \mathscr{F}_s] = M_s, \quad \forall\ 0 \leq s < t.$$

Definition 2.1.4 (Brownian Motion)**.** *A real-valued process $\{W_t,\ t \geq 0\}$ is called a Brownian motion if*

- *$W_0 = 0$.*
- *Normally distributed increments: For all $0 \leq s < t$, $W_t - W_s \simeq N(0, t - s)$.*

- *Independent increments: For* $0 \le t_0 < t_1 < \cdots < t_n$, *the random variables* $Y_i := W_{t_i} - W_{t_{i-1}}$, $i = 1, \ldots, n$ *are independent.*
- *All sample paths are continuous: The map* $t \mapsto W_t$ *is continuous.*

Definition 2.1.5 (Stopping time)**.** *A stopping time* τ *is a function from* Ω *to* $\{0, 1, 2, \ldots, \} \cup \{\infty\}$ *such that* $\{\tau = t\} \in \mathscr{F}_t, \forall\, t < \infty$.

Definition 2.1.6 (Local Martingale)**.** *An right continuous with left limits adapted process* L *is said to be a local martingale if there exist stopping times* $\tau^n \uparrow \infty$ *such that for each* n, *the process* M^n *defined by* $M_t^n := L_{t \wedge \tau^n}$ *is a martingale.*

Definition 2.1.7 (Semimartingale)**.** *A stochastic process* $X = \{X_t,\ t \ge 0\}$ *is called a semimartingale if it can be decomposed as follows*

$$X = X_0 + M + A,$$

where the random variable X_0 *is finite and* $\mathscr{F}_0$*-measurable, the stochastic process* M *is a local martingale and the stochastic process* A *has finite variation.*

Definition 2.1.8 (Itô Integral)**.** *For any square-integrable adapted process* Y_t *with continuous sample paths, the Itô integral is given by*

$$I(T) = \int_0^T Y_t dW_t := \lim_{m \to \infty} I_m(T), \quad \text{in } L^2.$$

Here, $I_m(T) = \int_0^T Y_t^m dW_t$ *for some elementary process* $Y_t^m = \sum_{j=0}^{n-1} \eta_j \mathbb{1}_{[t_j, t_{j+1})}$, *satisfying*

$$\lim_{m \to \infty} \mathbb{E}\left[\int_0^T (Y_t^m - Y_t)^2 dt\right] = 0,$$

where η_j *is* $\mathscr{F}_{t_j}$ *measurable for all* $j = 0, 1, \ldots, n-1$ *and square-integrable.*

Theorem 2.1.1 (Itô Isometry)**.** *For any stochastic process* Y_t, *satisfying the usual regularity conditions, the following equality holds,*

$$\mathbb{E}\left[\left(\int_0^T Y_t dW_t\right)^2\right] = \int_0^T \mathbb{E}[(Y_t)^2] dt.$$

Theorem 2.1.2 (Itô's Formula)**.** *Let* $f \in C^2(\mathbb{R})$ *and consider a continuous semimartingale* X *with decomposition* $X = M + A$. *Then, the stochastic process* $(f(X_t))_{t \ge 0}$ *is also a semimartingale and holds*

$$f(X_t) = f(X_0) + \int_0^t \frac{\partial f}{\partial x}(X_u) dX_u + \frac{1}{2} \int_0^t \frac{\partial^2 f}{\partial x^2}(X_u) d[X]_u,$$

with $[X]$ *denotes the quadratic variation of the process* $(X_t)_{t \ge 0}$.

Itô's formula is often expressed in differential form,

$$df(X_t) = \frac{\partial f}{\partial x}(X_t) dX_t + \frac{1}{2} \frac{\partial^2 f}{\partial x^2}(X_t) d[X]_t.$$

2.2. OPTION BASICS

This section presents the basic concepts used in the context of option pricing, which will be used throughout this thesis. The definitions, prepositions and explanations presented are based on [31], [33] and [34].

An option is a financial contract which gives its holder the right (but not the obligation) to purchase from the writer a certain asset for a predetermined price at a future time.

Options trading represents a significant portion of overall trading activity in many financial markets as they are extremely attractive to investors, both for speculation and hedging. The European call and put options are the most basic option which can be traded, and their formal definitions are presented below.

Definition 2.2.1 (European Call Option)**.** *A European call option is a contract signed between two parties at some time t, from which the right arises, to buy an asset S (underlying), for a pre-defined price K (strike), at a certain time in the future $T > 0$ (maturity).*

Definition 2.2.2 (European Put Option)**.** *A European call option is a contract signed between two parties at some time t, from which the right arises, to sell an asset S (underlying), for a pre-defined price K (strike), at a certain time in the future $T > 0$ (maturity).*

At maturity time T, the holder of the option can either exercise or can choose to not trade in the asset. Therefore, the payoffs of a European call and put option at maturity, T, are given by

$$V_{call}(T,S) := (S_T - K)^+,$$
$$V_{put}(T,S) := (K - S_T)^+,$$

where S_T denotes the value of the underlying asset at maturity time and K the strike price.

There also exist more complicated types of options, as for instance, exotic options. These are called *exotic* due to the presence of exotic features in their payoff structure, such as path-dependent attributes, where the final payoff depends the trajectory of the underlying asset's price over the option's lifespan. Furthermore, exotic options may involve multiple underlying assets. These options are exclusively traded in the over-the-counter (OTC) market, since they are customized by financial institutions to meet the specific needs and preferences of their clients. These types of options cannot be replicated by a finite combination of standard products (like European call and put options, future contracts, etc.). One example of such options are barrier options.

Barrier options can be classified in *knock-in* options, which only become active in the event that the predetermined barrier price is reached, otherwise they expire worthless; or *knock-out* options, where the right to exercise the option ceases to exist in the event that the predetermined barrier price is breached. Using this classification, we can distinguish four main types of barrier options:

- Up-and-out: spot price starts below the barrier level and has to move up for the option to be knocked out.

- Down-and-out: spot price starts above the barrier level and has to move down for the option to become null and void.
- Up-and-in: spot price starts below the barrier level and has to move up for the option to become activated.
- Down-and-in: spot price starts above the barrier level and has to move down for the option to become activated.

In this thesis, we focus on up-and-out barrier options. Let $\tau := \inf\{\tilde{t} \geq t : S_{\tilde{t}} \leq B\}$ be the first time that the process S_t breaches the barrier, B. Then, the payoffs of an up-and-out barrier call and put option at maturity T are given by

$$V^B_{call}(T,S) := (S_T - K)^+ \mathbb{1}_{\{\tau<T\}},$$
$$V^B_{put}(T,S) := (K - S_T)^+ \mathbb{1}_{\{\tau<T\}}.$$

Notice that if the barrier is not crossed, then the payoff becomes that of a European option.

The generalization of the this definition to other barrier types is trivial. In particular, given a formula for a up-and-out option, the corresponding down-and-out option can be found from the relation: in + out = European.

2.2.1. UNDERLYING PROCESS DYNAMICS

The asset price is not a deterministic value, but rather a continuous stochastic process. Therefore, it is not known at future time points, and has to be modelled according to a suitable stochastic process. This thesis will consider two different models for representing asset price dynamics, namely GBM and Heston's stochastic volatility model. The former is most commonly used asset price process in finance, while the later is one of the most popular models within the class of stochastic volatility models. For that reason, this section is dedicated to introducing these models.

GEOMETRIC BROWNIAN MOTION

A process S_t is said to follow a GBM process, when it satisfies the following Stochastic Differential Equation (SDE),

$$dS_t = \mu S_t dt + \sigma S_t dW^{\mathbb{P}}_t,$$

where μ denotes the drift parameter, i.e. a constant deterministic growth rate of the stock, and σ is the (constant) volatility parameter. The amount by which an asset price differs from its expected value is determined by σ. The above SDE is defined under the real-world probability measure $\mathbb{P}$.

Definition 2.2.3 (Risk-neutral measure)**.** *A probability measure $\mathbb{Q}$ on $(\Omega, \mathcal{F})$ is called a martingale measure or risk-neutral measure if the discounted asset price process is a $\mathbb{Q}$-martingale, i.e. S_t is an adapted process and $\mathbb{E}^{\mathbb{Q}}[e^{-r\Delta t} S_{t+1} \mid \mathcal{F}_t] = S_t$, for all $t \geq 0$.*

Under the risk-neutral measure $\mathbb{Q}$, the underlying stock price is assumed to follow a GBM, given by

$$dS_t = rS_t dt + \sigma S_t dW_t^{\mathbb{Q}},$$

where $\mu = r$, the risk-free interest rate. Note that throughout this thesis we assume constant interest rate, r.

HESTON'S MODEL

In order to deal with the non-constant implied volatility observed in the market, Heston proposed a stochastic volatility model [10], wherein the instantaneous variance process follows a mean-reverting square root process. We consider two SDEs, one for the underlying asset price S_t, and the other for the variance process v_t, as follows

$$\begin{cases} dS_t &= rS_t dt + \sqrt{v_t} S_t dW_1^{\mathbb{Q}}, \\ dv_t &= \kappa(\bar{v} - v_t)dt + \gamma\sqrt{v_t} dW_2^{\mathbb{Q}}, \end{cases}$$

with correlation ρ between the Brownian motions, i.e. $dW_1^{\mathbb{Q}} dW_2^{\mathbb{Q}} = \rho dt$. Parameters $\kappa \geq 0$, $\bar{v} \geq 0$ and $\gamma > 0$ are called the speed of mean reversion, the long-term mean of the variance process and the volatility of the volatility, respectively. The SDEs are described under the risk-neutral measure $\mathbb{Q}$.

The dynamics can also be expressed in terms of two independent Brownian motions, $\widetilde{W}_1^{\mathbb{Q}}$ and $\widetilde{W}_2^{\mathbb{Q}}$, as follows

$$\begin{cases} dS_t = & rS_t dt + \sqrt{v_t} S_t d\widetilde{W}_1^{\mathbb{Q}}, \\ dv_t = & \kappa(\bar{v} - v_t)dt + \gamma\sqrt{v_t}\left(\rho d\widetilde{W}_1^{\mathbb{Q}} + \sqrt{1-\rho^2} d\widetilde{W}_2^{\mathbb{Q}}\right). \end{cases} \tag{2.1}$$

Notice that, to avoid negative volatilities, the asset's variance is modeled by a so-called CIR process [35]. This process can be recognized as a mean reverting square-root process, which prevents negative values for v_t. If v_t reaches zero it subsequently becomes positive. It is the Feller condition, $2\kappa\bar{v} \geq \gamma^2$, which guarantees that v_t stays positive; otherwise, if the Feller condition is not satisfied, v_t may reach zero [36].

2.2.2. OPTION VALUATION

In the field quantitative finance, a lot of research is devoted to finding the *fair* value of an option before expiry time $t < T$. The price should be "fair" in the sense that it is acceptable by both the buyer and the seller of the derivative. One of the key principles on which option valuation theory rests is the no-arbitrage principle, which states that in an efficient market there should be no gain without risk. The concept of arbitrage is formally presented in the following definition.

Definition 2.2.4 (Arbitrage)**.** *An investment strategy is called an arbitrage if the value process V of the strategy satisfies the following:*

- $V_0 \leq 0$ *(zero initial cost)* ,
- $\mathbb{P}(V_T > (1+r)V_0) > 0$,

- $\mathbb{P}(V_T \geq (1+r)V_0) = 1$,

where r denotes the risk-free interest rate in a money-savings account and T the maturity.

In other words, the no-arbitrage principle assures that there is never an opportunity to make a risk-free profit that gives a greater return than that provided by the interest from a bank deposit.

One of the most important results in option value theory is the derivation of the PDE by Black and Scholes for the valuation of European options [6]. Based on the assumption of a GBM process for the asset price S_t, the value of an European option can be represented as the solution of the following PDE, with appropriate terminal conditions,

$$\frac{\partial V}{\partial t} + rS\frac{\partial V}{\partial S} + \frac{1}{2}\sigma^2 S^2 \frac{\partial^2 V}{\partial S^2} - rV = 0. \tag{2.2}$$

The derivation of the BS PDE can be done via a replication portfolio or martingale approach. The concept of the replicating portfolio is to create a portfolio of the underlying asset and a risk-free asset that replicates the payoff of the option. In other words, by adjusting the amount of the underlying asset and the risk-free asset in the portfolio, one can create a combination of these two assets that has the same value as the option at any point in time. By the no-arbitrage principle, two portfolios with identical cash flows in the future must have the same value as of the valuation date. Therefore, the value of the option must be equal to the value of the replicating portfolio at any point in time. Using the replication strategy, Black and Scholes were able to derive the pricing PDE for European options.

An alternative approach to derive the pricing PDE is to apply the theory of martingales. By the First Fundamental Theorem of Asset Pricing (cf. [34]), there exists an equivalent martingale measure in case the no-arbitrage principle holds. Thus, this second approach involves the construction of a risk neutral probability measure $\mathbb{Q}$, according to which we have

$$\begin{aligned} V(t,S) &= \mathbb{E}^{\mathbb{Q}}\left[e^{-r(T-t)}V(T,S)\middle|\mathscr{F}_t\right] \\ &= \mathbb{E}^{\mathbb{Q}}\left[e^{-r(T-t)}f(T,S)\middle|S_t = s\right], \end{aligned} \tag{2.3}$$

where $f(T,S)$ denotes the payoff function of the option.

In particular, for an up-and-out barrier option, let $\tau_B := \inf\{\tilde{t} \geq t : S_{\tilde{t}} \geq B\}$ be the first time that the process S_t hits the upper barrier B. Then, the value of such option at time $t < T$ can be written as

$$V(t,s) = e^{-r(T-t)}\mathbb{E}\left[f(T,S)\mathbb{1}_{\{\tau_B > T\}}|S_t = s\right]. \tag{2.4}$$

The value of the option can be derived either by solving the pricing PDE (2.2), or by evaluating the discounted expected payoff obtained from (2.3). By the no-arbitrage principle, these approaches should then lead to the same value. The equivalence of both approaches is proved in the famous Feynman-Kac theorem, which takes the discounted expectation as the closed-form solution to the BS PDE. We are particularly interested in the solution via the Feynman-Kac formula, and for that reason, we present the formulation for the BS model below.

Proposition 2.2.1 (Feynman-Kac formula for BS model)**.** *Let $V(t,S)$ be a sufficiently differentiable function of time t and stock price S_t. Suppose that $V(t,S)$ satisfies the following PDE, with constant interest rate r, and volatility σ,*

$$\frac{\partial V}{\partial t} + rS\frac{\partial V}{\partial S} + \frac{1}{2}\sigma^2 S^2 \frac{\partial^2 V}{\partial S^2} - rV = 0,$$

with a final condition given by $V(T,S) = f(T,S)$. The solution $V(t,S)$ at any time $t < T$ is then provided by

$$V(t,S) = \mathrm{e}^{-r(T-t)}\mathbb{E}^{\mathbb{Q}}[f(T,S) \mid \mathscr{F}_t],$$

where the expectation is taken under the measure $\mathbb{Q}$, with respect to a process S_t, which is defined by

$$dS_t = rS_t dt + \sigma S_t dW_t^{\mathbb{Q}}.$$

Under the GBM model for the underlying, an analytical formula for the option value can be obtained by solving the BS PDE with appropriate final time and boundary conditions. From [33], the formula for the value of an up-and-out call with initial value S_0 at time $t = 0$, barrier level B, strike K, maturity T, interest rate r and volatility σ is given by

$$\begin{aligned} V(t,S) = S\left(\Phi(d_1) - \Phi(e_1) - \left(\frac{B}{S}\right)^{1+2r/\sigma^2}(\Phi(f_2) - \Phi(g_2))\right) \\ - Ke^{-r(T-t)}\left(\Phi(d_2) - \Phi(e_2) - \left(\frac{B}{S}\right)^{-1+2r/\sigma^2}(\Phi(f_1) - \Phi(g_1))\right), \end{aligned} \tag{2.5}$$

where $\Phi(\cdot)$ stands for the cumulative distribution function of a standard normal distribution and

$$\begin{aligned} d_1 &= \frac{\ln(S/K) + (r + \frac{1}{2}\sigma^2)(T-t)}{\sigma\sqrt{T-t}}, \\ d_2 &= \frac{\ln(S/K) + (r - \frac{1}{2}\sigma^2)(T-t)}{\sigma\sqrt{T-t}}, \\ e_1 &= \frac{\ln(S/B) + (r + \frac{1}{2}\sigma^2)(T-t)}{\sigma\sqrt{T-t}}, \\ e_2 &= \frac{\ln(S/B) + (r - \frac{1}{2}\sigma^2)(T-t)}{\sigma\sqrt{T-t}}, \\ f_1 &= \frac{\ln(S/B) - (r - \frac{1}{2}\sigma^2)(T-t)}{\sigma\sqrt{T-t}}, \\ f_2 &= \frac{\ln(S/B) - (r + \frac{1}{2}\sigma^2)(T-t)}{\sigma\sqrt{T-t}}, \\ g_1 &= \frac{\ln(SK/B^2) - (r - \frac{1}{2}\sigma^2)(T-t)}{\sigma\sqrt{T-t}}, \\ g_2 &= \frac{\ln(SK/B^2) - (r + \frac{1}{2}\sigma^2)(T-t)}{\sigma\sqrt{T-t}}. \end{aligned}$$

Identically, Heston derived a pricing PDE for when the asset price process is modelled according to his stochastic volatility model [10]. The value of an European option can be represented as the solution of the following PDE, with appropriate terminal conditions,

$$\frac{\partial V}{\partial t} + rS\frac{\partial V}{\partial S} + \kappa(\bar{v} - v)\frac{\partial V}{\partial v} + \rho\gamma v S\frac{\partial^2 V}{\partial S \partial v} + \frac{1}{2}vS^2\frac{\partial^2 V}{\partial S^2} + \frac{1}{2}\gamma^2 v\frac{\partial^2 V}{\partial v^2} - rV = 0. \tag{2.6}$$

For the Heston's model, there is unfortunately no closed-form solution to the respective pricing PDE.

GREEKS

The Greeks of an option measure the sensitivity of the value of a derivative product or a financial portfolio to changes in a certain parameter value while holding the other parameters fixed.

The most common Greek is the Delta of an option, widely used for hedging purposes. The Delta for an option measures the sensitivity of the option value V to small changes in the asset price S, denoted by $\Delta := \frac{\partial V}{\partial S}$. The Gamma corresponds to the second derivative with respect to S and it is denoted $\Gamma := \frac{\partial^2 V}{\partial S^2}$, where V is the value of the option. For instance, according to the BS model, for an European call option,

$$\Delta_{\text{call}} = \Phi(d_1),$$
$$\Delta_{\text{put}} = \Phi(d_1) - 1,$$

where

$$d_1 = \frac{\ln(S/K) + (r + \frac{\sigma^2}{2})T}{\sigma\sqrt{T}} \text{ and } d_2 = d_1 - \sigma\sqrt{T}.$$

2.3. FOURIER SERIES EXPANSIONS

The contents of this section are modified from the paper [37].

Given a piecewise smooth function, it is possible to construct a global expansion using orthogonal basis functions, such as cosine and sine functions in the Fourier series expansion. Nevertheless, it is not generally true that, for an arbitrary function f, the Fourier series will converge at each particular point x to the value $f(x)$. To ensure that convergence does hold it is necessary to impose extra constraints on f, namely Dirichlet conditions: *A piecewise function f must be periodic with at most a finite number of discontinuities, and/or a finite number of minima or maxima within one period. In addition,* $\int_0^T |f(x)|dx < \infty$. [38]. Consequently, regarding continuity and differentiability, the weakest condition for a function to be represented by a Fourier series is that it is piecewise continuous.

Suppose that f is smooth on $[0,\pi]$, then there are three ways in which f may be represented by a Fourier series. These are the half-range Fourier-cosine series, the half-range Fourier-sine series and the full-range Fourier series, represented respectively as follows:

$$f(\theta) = \sum_{k=0}^{\infty}{}' A_k \cos(k\theta), \tag{2.7}$$

$$f(\theta) = \sum_{k=1}^{\infty} B_k \sin(k\theta), \tag{2.8}$$

$$\begin{aligned} f(\theta) &= \frac{A_0}{2} + \sum_{k=1}^{\infty} A_k \cos(2k\theta) + B_k \sin(2k\theta) \\ &= \sum_{k=-\infty}^{+\infty} c_k e^{i2k\theta} \text{ (in exponential format)}, \end{aligned} \tag{2.9}$$

where $c_0 = A_0, c_k = (A_k - iB_k)/2$ for $k > 0$ and $(A_{-k} + iB_{-k})/2$ for $k < 0$. $\sum'$ indicates that the first term is multiplied by half.

The use of the term "half-range" refers to the fact that the function f, although defined in $[0,\pi]$, has been extended into the interval $[-\pi,\pi]$ as an even-valued function in the case of the half-range cosine series (so that sine contributions vanish) and as an odd-valued function in the case of the half-range sine series (so that the constant and cosine contributions vanish). Therefore, the approximation of the function is obtained by periodically repeating f with period 2π. We shall refer to the half-range series as Fourier-cosine and -sine series from here onward.

The best trigonometric approximation in the L^2-norm is the Fourier truncated series, as described in Theorem 2.3.1. This result also applies to the Fourier-sine and -cosine series.

Theorem 2.3.1. *The truncated Fourier series at level N, $S_N f$, is the best approximation of f in $\mathscr{L}_N$[1] in the L^2-norm on $[0,\pi]$, i.e.*

$$\|f - S_N f\|_2 = \min_{g \in \mathscr{L}_N} \|f - g\|_2.$$

Proof. Consider $S_N f = \sum_{k=-N}^{N} c_k e^{i2k\theta}$ to be the truncated Fourier series and $P_N f = \sum_{k=-N}^{N} \hat{c}_k e^{i2k\theta}$ to be a general trigonometric approximation for f. The norm of the approximation error is given by

$$\begin{aligned} \|f - P_N f\|_2^2 &= \left\| \sum_{k=-N}^{N} (c_k - \hat{c}_k) e^{i2k\theta} + \sum_{|k|=N+1}^{\infty} c_k e^{i2k\theta} \right\|_2^2 \\ &= \pi \left(\sum_{k=-N}^{N} |c_k - \hat{c}_k|^2 + \sum_{|k|=N+1}^{\infty} |c_k|^2 \right), \end{aligned}$$

which is minimized by setting $\hat{c}_k = c_k$ for $|k| \le N$. □

For functions supported on any other finite interval $[a,b] \in \mathbb{R}$, the series expansion can easily be obtained via a change of variables,

$$\theta := \frac{x-a}{b-a}\pi, \quad x = \frac{b-a}{\pi}\theta + a.$$

[1] $\mathscr{L}_N$ is the linear space of trigonometric polynomials with degree $\le N$.

Then, one period will correspond to the interval $[2a-b, b]$ and the series expansions for f in $[a, b]$ read

$$f(x) = \sum_{k=0}^{\infty}{}' A_k \cos\left(k\pi \frac{x-a}{b-a}\right), \tag{2.10}$$

$$f(x) = \sum_{k=1}^{\infty} B_k \sin\left(k\pi \frac{x-a}{b-a}\right), \tag{2.11}$$

$$f(x) = \frac{A_0}{2} + \sum_{k=1}^{\infty} A_k \cos\left(2k\pi \frac{x-a}{b-a}\right) + B_k \sin\left(2k\pi \frac{x-a}{b-a}\right). \tag{2.12}$$

These expansions exist for any real function with finite support and the coefficients A_k and B_k, in (2.10), (2.11) and (2.12), are provided by

$$\text{for cosine series: } A_k = \frac{2}{b-a}\int_a^b f(x)\cos\left(k\pi \frac{x-a}{b-a}\right)dx, k \geq 0, \tag{2.13}$$

$$\text{for sine series: } B_k = \frac{2}{b-a}\int_a^b f(x)\sin\left(k\pi \frac{x-a}{b-a}\right)dx, k \geq 1, \tag{2.14}$$

$$\text{for Fourier series: } \begin{cases} A_k &= \frac{1}{b-a}\int_a^b f(y)\cos\left(2k\pi \frac{y-a}{b-a}\right)dy, k \geq 0, \\ B_k &= \frac{1}{b-a}\int_a^b f(y)\sin\left(2k\pi \frac{y-a}{b-a}\right)dy, k \geq 1. \end{cases} \tag{2.15}$$

2.3.1. CONVERGENCE OF FOURIER SERIES

This section contains some general theory on the convergence of Fourier-series, mostly taken from [39]. Theorems on pointwise convergence, differentiation and integration of Fourier series are presented. Plus, the different types of convergence rates are discussed, together with the corresponding series truncation error. The main result is then found in proposition 2.3.7, which shows the convergence rate of the Fourier-cosine series for different classes of functions.

Theorem 2.3.2 (Pointwise convergence of Fourier series)**.** *Take $S_N f(x)$ to be the Fourier sum approximation of function f truncated at level N. Suppose that $f(x)$ is continuous with a continuous derivative except at perhaps a finite number of points (in a period). Let c be a discontinuity point, then $S_N f(c) \to \frac{1}{2}(\lim_{x\to c^-} f(x) + \lim_{x\to c^+} f(x))$ as $N \to \infty$.*

Theorem 2.3.3 (Differentiation of Fourier series)**.** *If f is a piecewise smooth function on $[0, \pi]$ and it is also continuous, then the Fourier series of f can be differentiated term by term provided that $f(0) = f(\pi)$ [40].*

Theorem 2.3.4 (Integration of Fourier series)**.** *A Fourier series of a piecewise smooth function f can always be integrated term by term and the result is a convergent infinite series that always converges to the integral of f for $x \in [0, \pi]$ [40].*

The two theorems above are also valid for Fourier-cosine and -sine series, only that the relevant interval is $[-\pi, \pi]$, where the function f is evenly or oddly extended, respectively.

Definition 2.3.1 (Algebraic Index of Convergence). *The algebraic index of convergence* $n(\geq 0)$ *is the largest number for which*

$$\lim_{k\to\infty} |A_k| k^n < \infty, \qquad k >> 1,$$

where the A_k *are the coefficients of the series. An alternative definition is that if the coefficients of a series,* A_k*, decay asymptotically as*

$$A_k \sim \mathcal{O}\left(\frac{1}{k^n}\right), \qquad k >> 1,$$

then n *is the algebraic index of convergence.*

Definition 2.3.2 (Exponential Index of Convergence). *If the algebraic index of convergence* $n(\geq 0)$ *is unbounded – in other words, if the coefficients,* A_k*, decrease faster than* $1/k^n$ *for any finite* n *– the series is said to have exponential convergence. Alternatively, if*

$$A_k \sim \mathcal{O}\left(e^{-\gamma k^r}\right), \qquad k >> 1,$$

with γ*, constant, the 'asymptotic rate of convergence', for some* $r > 0$*, then the series shows exponential convergence. The exponent* r *is the index of convergence.*
For $r < 1$*, the convergence is called subgeometric.*
For $r = 1$*, the convergence is either called supergeometric with*

$$A_k \sim \mathcal{O}\left(k^{-n} e^{-(k/j)\ln(k)}\right),$$

(for some $j > 0$*), or geometric with*

$$A_k \sim \mathcal{O}\left(k^{-n} e^{-\gamma k}\right). \tag{2.16}$$

Proposition 2.3.5 (Series truncation error of algebraically converging series). *It can be shown that the series truncation error of an algebraically converging series behaves like*

$$\sum_{k=K}^{\infty} \frac{1}{k^n} \sim \frac{1}{(n-1)(K-1)^{n-1}}.$$

The proof can be found in [41].

Proposition 2.3.6 (Series truncation error of geometrically converging series). *If a series has geometrical convergence, then the error after truncation of the expansion after* K *terms,* $E_T(K-1)$*, reads*

$$E_T(K-1) \sim P^* e^{-(K-1)\nu}.$$

Here, constant $\nu > 0$ *is called the asymptotic rate of convergence of the series, which satisfies*

$$\nu = \lim_{n\to\infty} (-\log|E_T(n)|/n),$$

and $P^* > 0$ *denotes a factor which varies less than exponentially with* $K-1$ *.*

Proposition 2.3.7 (Convergence of Fourier-cosine series)**.** *If $g(x) \in C^\infty([a,b] \subset \mathbb{R})$, then its Fourier-cosine series expansion on $[a,b]$ has geometric convergence. The constant γ in 2.16 is determined by the location in the complex plane of the singularities nearest to the expansion interval. Exponent n is determined by the type and strength of the singularity. If a function $g(x)$, or any of its derivatives, is discontinuous, its Fourier-cosine series coefficients show algebraic convergence. Integration-by-parts shows that the algebraic index of convergence, n, is at least as large as n', with the n'-th derivative of $g(x)$ integrable.*

References to the proof of this proposition are available in [39].

2.3.2. FILTERS

When discussing Fourier series, it is natural to address the case in which the existence of discontinuities destroys the convergence of the global approximation, even in regions for which the underlying function is analytic. In this context, filters can be applied. This section is modified from [42]–[44] and it presents relevant definitions and concepts related to filters.

As a result of discontinuities, the Fourier partial sums oscillate in value near the jumps at the discontinuity points and feature non-uniform convergence. This characteristic behavior is called the Gibbs phenomenon. But the Gibbs phenomenon has a global effect on top of the already described local effect. Even though the error between the approximation and the actual function decays as we move away from the jumps, the decay rate is limited to first-order [43]. Thus, the existence of one or more discontinuities slows down the convergence rate throughout the domain. In short, spectral accuracy is lost.

Nevertheless, there are two interchangeable processes available for recovering the rapid convergence in the piecewise smooth case. These are mollification, carried out in the physical space, and filtering, carried out in the Fourier space.

Filtering accelerates convergence when pre-multiplying the Fourier coefficients by a rapidly decreasing function $\varphi(k/N)$ as $k \uparrow N$. This function, called the *filter* is continuous and only modifies high frequency modes, not the low modes.

Filtering may remove the Gibbs phenomenon from a discontinuity, but the error depends on the distance to the discontinuity. If the filter is well-chosen, the convergence rate away from the discontinuity will improve. Since the approximation will be smoothed, convergence very close to the jump will not improve.

The order of a filter determines the rate at which the error produced by the filtering decays. Thus, its accuracy is described by its order.

Definition 2.3.3. *A filter is of order m if for any fixed $k > 0$*

$$\varphi\left(\frac{k}{N}\right) \sim \mathcal{O}\left(\frac{1}{N^m}\right), \text{ for } N \to \infty.$$

Equivalently a filter is m-order accurate if it satisfies

$$\varphi^{(k)}(0) = \delta_{k0} \text{ for } k = 0, 1, \ldots, m.$$

One example of a order 1 filter is the Lanczos filter, defined as

$$\varphi(\eta) = \frac{\sin(\pi\eta)}{\pi\eta}.$$

Another example is the exponential filter of order m, $\varphi(\eta) = e^{-\alpha\eta^m}$ Note that $\varphi(1) = e^{-\alpha}$, and thus, formally the exponential filter does not satisfy the definition of the filter. However, in practice a large α is often sufficient to restore that property.

On the one hand, for an already analytic function (such that its spectral series is converging exponentially), it is desirable to use a filter of high order to keep the advantages of having a high order spectral method when computing smooth solutions. Hence, one needs a filter of order m to make sure the filtered spectral series converges at order m, i.e. that the errors produced by the filtering are $\mathcal{O}(1/N^m)$.

On the other hand, for a function that is not smooth (such that its unfiltered spectral series converges only at algebraic rate), one can recover the true solution with $\mathcal{O}(1/N^m)$ accuracy at any fixed point away from the discontinuities by using a filter of order m [44].

2.3.3. OPTION PRICING VIA FOURIER-COSINE (SINE) SERIES

This section replicates the works of [22] and derives the COS (and sine counterpart) formula for European-style options by replacing the density function by its Fourier-cosine (sine) series.

Suppose that f is a transitional pdf with known ch.f., ϕ. Since the density function forms a Fourier pair with its ch.f., the latter is defined formally by the equation

$$\phi(\omega) = \int_{\mathbb{R}} f(y) e^{i\omega y} dy. \tag{2.17}$$

Following the steps of [22], we recover f through the respective ch.f.. Consider the cosine series expansion of f,

$$f(y|x) = \sum_{k=0}^{\infty}{}' A_k(x) \cos\left(k\pi \frac{y-a}{b-a}\right),$$

where A_k is computed as in (2.13). For the sine series expansion of f, we have

$$f(y|x) = \sum_{k=1}^{\infty} B_k(x) \sin\left(k\pi \frac{y-a}{b-a}\right),$$

where B_k is computed as in (2.14).

Due to the conditions for the existence of a Fourier transform, the integrands in (2.17) have to decay to zero at $\pm\infty$ and we can truncate the integration range in a proper way without losing accuracy.

Suppose $[a,b] \subset \mathbb{R}$ is chosen such that the truncated integral approximates the infinite counterpart very well, i.e.

$$\phi_1(\omega; x) = \int_a^b f(y|x) e^{i\omega y} dy \approx \int_{\mathbb{R}} f(y|x) e^{i\omega y} dy = \phi(\omega; x). \tag{2.18}$$

Then, the coefficients are given, respectively, by

$$A_k(x) = \frac{2}{b-a} \mathrm{Re}\left\{\phi_1\left(\frac{k\pi}{b-a}; x\right) \exp\left(-ik\pi \frac{a}{b-a}\right)\right\}, \tag{2.19}$$

$$B_k(x) = \frac{2}{b-a} \mathrm{Im}\left\{\phi_1\left(\frac{k\pi}{b-a}; x\right) \exp\left(-ik\pi \frac{a}{b-a}\right)\right\}. \tag{2.20}$$

It then follows from (2.18) that $A_k \approx F_k$ and $B_k \approx G_k$ with

$$F_k(x) = \frac{2}{b-a}\text{Re}\left\{\phi\left(\frac{k\pi}{b-a};x\right)\exp\left(-ik\pi\frac{a}{b-a}\right)\right\}, \tag{2.21}$$

$$G_k(x) = \frac{2}{b-a}\text{Im}\left\{\phi\left(\frac{k\pi}{b-a};x\right)\exp\left(-ik\pi\frac{a}{b-a}\right)\right\}. \tag{2.22}$$

We now replace A_k by F_k in the series expansion of f on $[a,b]$ (and proceed in the same way for B_k), i.e.

$$f_1(y|x) = \sum_{k=0}^{\infty}{}'F_k(x)\cos\left(k\pi\frac{y-a}{b-a}\right), \tag{2.23}$$

$$f_1(y|x) = \sum_{k=1}^{\infty}G_k(x)\sin\left(k\pi\frac{y-a}{b-a}\right), \tag{2.24}$$

and truncate the series summation such that

$$f_2(y|x) = \sum_{k=0}^{N-1}{}'F_k(x)\cos\left(k\pi\frac{y-a}{b-a}\right), \tag{2.25}$$

$$f_2(y|x) = \sum_{k=1}^{N}G_k(x)\sin\left(k\pi\frac{y-a}{b-a}\right). \tag{2.26}$$

In this way, we are able to recover the transitional pdf from the respective ch.f.. Now, recall that the value of an option is given by

$$V(x,t) = e^{-r(T-t)}\mathbb{E}[V(y,T)|\mathscr{F}_t] = e^{-r(T-t)}\mathbb{E}[V(y,T)|x] = e^{-r(T-t)}\int_{\mathbb{R}}V(y,T)f(y|x)dy. \tag{2.27}$$

Since the density rapidly decays to zero as $y \to \pm\infty$, we truncate the infinite integration range without losing significant accuracy to $[a,b] \subset \mathbb{R}$, and we obtain approximation V_1,

$$V_1(x,t) = e^{-r(T-t)}\int_a^b V(y,T)f(y|x)dy. \tag{2.28}$$

By plugging in the cosine series approximation for the transitional density function, we obtain

$$\begin{aligned}V_2(x,t) &= e^{-r(T-t)}\int_a^b V(y,T)\sum_{k=0}^{N-1}{}'F_k(x)\cos\left(k\pi\frac{y-a}{b-a}\right)dy \\ &= e^{-r(T-t)}\int_a^b V(y,T)\sum_{k=0}^{N-1}{}'\frac{2}{b-a}\text{Re}\left\{\phi\left(\frac{k\pi}{b-a};x\right)e^{-ik\pi\frac{a}{b-a}}\right\}\cos\left(k\pi\frac{y-a}{b-a}\right)dy.\end{aligned} \tag{2.29}$$

Define $V_k := \frac{2}{b-a}\int_a^b V(y,T)\cos\left(k\pi\frac{y-a}{b-a}\right)dy$, then the value of the option can be written as

$$V_2(x,t) = e^{-r(T-t)}\sum_{k=0}^{N-1}{}'\text{Re}\left\{\phi\left(\frac{k\pi}{b-a};x\right)e^{-ik\pi\frac{a}{b-a}}\right\}V_k. \tag{2.30}$$

Alternatively, for the sine series, we have

$$V_2(x,t) = e^{-r(T-t)} \int_a^b V(y,T) \sum_{k=1}^{N} G_k(x) \sin\left(k\pi \frac{y-a}{b-a}\right) dy$$
$$= e^{-r(T-t)} \int_a^b V(y,T) \sum_{k=1}^{N} \frac{2}{b-a} \mathrm{Im}\left\{\phi\left(\frac{k\pi}{b-a}; x\right) e^{-ik\pi \frac{a}{b-a}}\right\} \sin\left(k\pi \frac{y-a}{b-a}\right) dy. \tag{2.31}$$

Plus, we define $V_k := \frac{2}{b-a} \int_a^b V(y,T) \sin\left(k\pi \frac{y-a}{b-a}\right) dy$ accordingly, and thus the value of the option can be written as

$$V_2(x,t) = e^{-r(T-t)} \sum_{k=1}^{N} \mathrm{Im}\left\{\phi\left(\frac{k\pi}{b-a}; x\right) e^{-ik\pi \frac{a}{b-a}}\right\} V_k. \tag{2.32}$$

The formulas above can be understood as the combination of two parts: firstly, the inner product of two sets of Fourier-cosine (sine) coefficients, one for density and the other for payoff; and secondly, the Fourier-cosine (sine) coefficients for density can be approximated by the respective ch.f.. Moreover, the coefficients for the payoff, V_k, can be obtained analytically for both European call or put options (cf. [22]).

2.4. COLLOCATION METHODS

The explanations in this section are adapted from [45] and [46].

A collocation method is a numerical method for solving integral and differential equations. Collocation is a further continuation of interpolation. While collocation sets the constraint that the function must satisfy a differential equation at certain points in the domain called *collocation points*, normal interpolation sets constraints on the value of the function itself.

Given a differential equation, assume it can be written in the form $\mathscr{L}(u) = 0$, where $\mathscr{L}$ is the differential equation operator and u is the solution function. For example, the BS pricing PDE operator is such that

$$\mathscr{L}_{BS}(u) = \frac{\partial u}{\partial t} + rS\frac{\partial u}{\partial S} + \frac{1}{2}\sigma^2 S^2 \frac{\partial^2 u}{\partial S^2} - ru.$$

Similarly to interpolation, we approximate the solution to the PDE by a function u^h of the form

$$u^h(x) = \sum_{n=1}^{N} c_n u_n^h(x), \tag{2.33}$$

where $u_n^h(\cdot)$ denote the basis functions. Hence, the PDE now reads $\mathscr{L}(u^h) \approx 0$.

The goal is to find a solution to the PDE by determining the N coefficients, c_n. For that reason, we choose a finite number of collocation points, x_i, with $i = 1, \ldots, M$. The solution is determined from the condition that equation (2.33) is satisfied at the collocation points.

Expanding u^h for each constraint results in a system of equations with M equations. To ensure existence and uniqueness of the solution, we prescribe that the number of

degrees of freedom N equals the number of constraints M. We are left with an uniquely determined linear system that needs to be solved for the coefficients c_n. Note that, if the PDE contains initial or boundary conditions, these should be accounted for in the constraints.

For many cases in the literature, polynomials, such as Legendre, Laguerre, and Chebyshev polynomials, are a natural choice for the basis functions. Other choices for basis functions include non-polynomial basis functions, such as the Fourier series. Also, an usual approach involves selecting collocation points in a manner that aligns with the roots of orthogonal polynomials, similar to the process employed in Gauss quadrature.

2.5. TENSORS

This section introduces basic concepts in tensor calculus that will play a crucial role in the explanation of our approach in Chapter 5. The material presented here draws from the work of [47].

A tensor is a multi-dimensional array. The number of dimensions of a tensor is denominated *order*. For example, a first-order tensor is a vector, a second-order tensor is a matrix, and tensors of order three or higher are called higher-order tensors. An Nth-order tensor $\mathscr{A}$ has N sets of indices $\{i_n\}_{n=1,\cdots,N}$ and $i_n = 1, \cdots, I_n$ to indicate one specific element. Hence, $\mathscr{A} \in \mathbb{R}^{I_1 \times \cdots \times I_N}$. For example, for a third-order tensor $\mathscr{A} \in \mathbb{R}^{I_1 \times I_2 \times I_3}$, the elements are denoted $\mathscr{A}[i_1, i_2, i_3] = A_{i_1,i_2,i_3}$.

Another relevant concept for higher-order tensors is that of tensor *fibers*. Fibers are the higher-order analogue of matrix rows and columns. A fiber is defined by fixing every index but one. When extracted from the tensor, fibers are always assumed to be oriented as column vectors. For example, a matrix column is a one-dimensional fiber and a matrix row is a two-dimensional fiber. Third-order tensors have column, row, and tube fibers, as is illustrated in Figure 2.1.

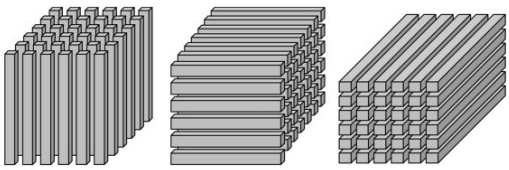

Figure 2.1: Fibers and slices of a third-order tensor [48].

In this thesis, we will only go as far as third-order tensors. For the operations that will be performed, it is of relevance to transform tensors into a vector, on which well-studied matrix-vector operations can be applied. Reordering the elements of a Nth-order tensor array into a vector is called *vectorization*. There exists different ways of vectorizing a tensor, but the ordering of the elements is not important as long as it is consistent across related calculations. As an example, consider a tensor $\mathscr{A} \in \mathbb{R}^{4\times3\times2}$ which can be arranged as a 24-element vector by stacking up all the tube fibers vertically in order as follows

$$\text{vec}(\mathscr{A}) = \begin{pmatrix} a_{111} \\ a_{112} \\ a_{121} \\ a_{122} \\ a_{131} \\ a_{132} \\ a_{211} \\ \vdots \\ a_{411} \\ a_{412} \\ a_{421} \\ a_{422} \\ a_{431} \\ a_{432} \end{pmatrix}$$

On top of this, a few matrix products will be of importance in the sections that follow, and their definitions are introduced below.

Definition 2.5.1 (Kronecker Product)**.** *The Kronecker product of matrices $A \in \mathbb{R}^{I\times J}$ and $B \in \mathbb{R}^{K\times L}$ is denoted with $A \otimes B \in \mathbb{R}^{IK\times JL}$, and is defined by*

$$A \otimes B = \begin{pmatrix} a_{11}B & a_{12}B & \cdots & a_{1J}B \\ a_{21}B & a_{22}B & \cdots & a_{2J}B \\ \vdots & \vdots & \ddots & \vdots \\ a_{I1}B & a_{I2}B & \cdots & a_{IJ}B \end{pmatrix}$$

Let $\mathbf{a}, \mathbf{b} \in \mathbb{R}$ be column vectors, then an important result that shall be used later is that $\text{vec}(\mathbf{a}\mathbf{b}^\top) = \mathbf{b} \otimes \mathbf{a}$, where $\text{vec}(\cdot)$ is the vectorization operator. This operator is linear.

2.6. OTHER RELEVANT THEOREMS

Theorem 2.6.1 (First Fundamental Theorem of Calculus (FTC))**.** *Let f be a continuous real-valued function defined on a closed interval $[a, b]$. Let F be the function defined, for all $x \in [a, b]$, by*

$$F(x) = \int_a^x f(t)\,dt.$$

Then F is uniformly continuous on $[a, b]$ and differentiable on the open interval (a, b), and

$$F'(x) = f(x),$$

for all $x \in (a, b)$ so F is an antiderivative of f.

Corollary 2.6.1.1. *If f is a real-valued continuous function on $[a, b]$ and F is an antiderivative of $f \in [a, b]$ then*

$$\int_a^b f(t)\,dt = F(b) - F(a).$$

3

PRELIMINARY ANALYSIS: HEAT EQUATION

In this chapter, we focus on the Heat equation. The relevance of such PDE lies in the existence of a well-established solution represented as a series expansion [49]. This allows us to gain more understanding and insights into Fourier methods within the context of PDEs, which will subsequently be applied to build up our own approach to solve more complex PDEs.

3.1. SOLVING THE HEAT EQUATION

Let us consider the 1D Heat equation, for which there is only one spatial variable. We consider a metal bar with a length 2π (and negligible thickness), and we take x as the variable that indicates the distance of a point on the bar. Let $u(t,x)$ be a function that indicates the temperature at distance x and at time t. The heat transfer in the rod satisfies the following PDE with boundary conditions,

$$\begin{cases} \dfrac{\partial u}{\partial t} = \dfrac{1}{2}\dfrac{\partial^2 u}{\partial x^2} \text{ for } 0 < x < 2\pi, 0 < t, \\ u(t,0) = 0, \\ u(t,2\pi) = 0, \\ u(0,x) = f(x). \end{cases} \tag{3.1}$$

The two conditions following the equation are called the Dirichlet conditions. It means that the bar boundaries are kept at zero temperature. The last condition states that the initial distribution of temperatures (that is, when $t = 0$) is given by function f.

Without the constraints of the initial and boundary conditions, there are infinitely many solutions to the Heat equation. The above PDE can be solved by applying the method of separation of variables, meaning that we assume solutions of the form $u(x,t) =$

$X(x)T(t)$. Notice this is not the only possible type of solution. From this assumption, it follows that

$$X(x)T'(t) = \frac{1}{2}X''(x)T(t) \implies \frac{T'(t)}{\frac{1}{2}T(t)} = \frac{X''(x)}{X(x)}.$$

Note that we are looking for non-trivial solutions, hence, it should hold that $X(x) \neq 0$ and $T(t) \neq 0$. The boundary condition $u(t,0) = 0$ leads to $X(0) = 0$, and $u(t,2\pi) = 0$ implies that $X(2\pi) = 0$. The initial condition $u(0,x) = f(x)$ leads to $X(x) = f(x)$ and $T(0) = 1$.

3

Notice that each side depends only on one variable, which means that we can write that each side is equal to a constant $-\lambda \in \mathbb{R}$, i.e.

$$\frac{T'(t)}{\frac{1}{2}T(t)} = \frac{X''(x)}{X(x)} = -\lambda,$$

which yields

$$\begin{cases} X''(x) + \lambda X(x) = 0, \\ T'(t) + \frac{1}{2}\lambda T(t) = 0. \end{cases} \tag{3.2}$$

The second equation in (3.2) has solution $T(t) = ce^{-\frac{1}{2}\lambda t}$. Accounting for the initial condition $T(0) = 1$, we conclude that $T(t) = e^{-\frac{1}{2}\lambda t}$.

For the first equation in (3.2), for $\lambda \leq 0$, we obtain only the trivial solution $X(x) = 0$; for $\lambda > 0$, the general solution is of the form $X(x) = c_1\cos(\sqrt{\lambda}x) + c_2\sin(\sqrt{\lambda}x)$. Using the boundary conditions, we have that

$$\begin{cases} X(0) = c_1\cos(\sqrt{\lambda}0) + c_2\sin(\sqrt{\lambda}0) = 0 \\ X(2\pi) = c_1\cos(\sqrt{\lambda}2\pi) + c_2\sin(\sqrt{\lambda}2\pi) = 0 \end{cases} \implies \begin{cases} c_1 = 0, \\ c_2\sin(\sqrt{\lambda}2\pi) = 0. \end{cases}$$

To yield a non-trivial solution, we need that $c_2 \neq 0$ and $\sin(\sqrt{\lambda}2\pi) = 0$, which implies that $\sqrt{\lambda}2\pi = k\pi$, or equivalently, $\lambda = \left(\frac{k}{2}\right)^2$, with $k \in \mathbb{Z}$.

Because the Heat equation is linear, any linear combination of solutions is also a solution. Thus, by the superposition principle, the desired solution is of the following form

$$u(t,x) = \sum_{k=1}^{\infty} B_k e^{-\frac{1}{2}\left(\frac{k}{2}\right)^2 t}\sin\left(k\pi\frac{x}{2\pi}\right) = \sum_{k=1}^{\infty} B_k e^{-k^2t/8}\sin(kx/2). \tag{3.3}$$

It can be seen that when $t = 0$, $u(0,x)$ reduces to a Fourier-sine series. It then follows that B_k are the sine series coefficients of $u(0,x) = f(x)$, i.e.

$$B_k = \frac{2}{2\pi}\int_0^{2\pi} f(y)\sin(ky/2)dy, \tag{3.4}$$

which, inserting to (3.3) and interchanging the summation and the integration, leads to

$$u(t,x) = \frac{1}{\pi}\int_0^{2\pi} f(y)\sum_{k=1}^{\infty} e^{-k^2t/8}\sin(kx/2)\sin(ky/2)dy. \tag{3.5}$$

3.2. APPROXIMATION USING 2D FOURIER SERIES

Equation (3.3) shows that the solution $u(t,x)$ can be written in the form of a series of sine functions of x with coefficients decaying exponentially in time. To be able to recover the solution function of more complicated PDEs, we now consider approximating $u(t,x)$ using a 2D Fourier series for the variables x and t. We start by constructing the expansion for the t-dimension, i.e. analysing how to properly expand $e^{-k^2 t/8}$ via a Fourier-cosine or -sine series.

3.2.1. t-DIMENSION

First consider a cosine series expansion to approximate the function $e^{-k^2 t/8}$ on a finite interval, such as $[0,1]$. Note that a Fourier-cosine series expansion is obtained by applying Fourier series expansion to an even extension of the original function, in our case on the interval $[-1,1]$, i.e.

$$g(t) = \begin{cases} e^{k^2 t/8} & \text{if } -1 \le t < 0, \\ e^{-k^2 t/8} & \text{if } 0 \le t \le 1. \end{cases}$$

For a given k, the respective cosine expansion in $[0,1]$ reads

$$e^{-k^2 t/8} \approx {\sum_{n=0}^{N-1}}' \beta_{k,n} \cos(n\pi t),$$

where $\beta_{k,n}$ are the Fourier-cosine series coefficients.

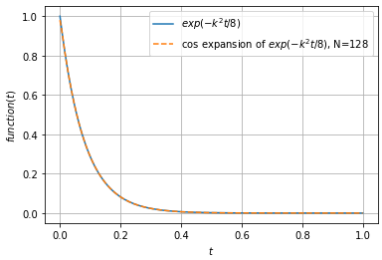

Figure 3.1: Cosine series expansion of $e^{-k^2 t/8}$ in the interval $[0,1]$, for $k = 10$.

Since we will eventually insert the expansion into the Heat equation - which requires the first order derivative with respect to time -, we need to check the convergence behavior of the time-dimension derivative of the series expansion. From Theorem 2.3.3, we can take the derivative of the cosine series expansion of $e^{-k^2 t/8}$. For a given k, the derivative in $[0,1]$ reads

$$-k^2/8 e^{-k^2 t/8} \approx -{\sum_{n=0}^{N-1}}' \beta_{k,n} n\pi \sin(n\pi t),$$

which is a sine expansion. Recall that a Fourier-sine series expansion is obtained by applying Fourier series expansion to an odd extension of the original function. In our

case, the function is $-k^2/8e^{-k^2t/8}$ and the odd extension is performed on the interval $[-1,1]$ as follows

$$g'(t) = \begin{cases} k^2/8e^{k^2t/8} & \text{if } -1 \le t < 0, \\ -k^2/8e^{-k^2t/8} & \text{if } 0 \le t \le 1. \end{cases}$$

3

Notice that there is a discontinuity at $t = 0$ and it can be seen in Figure 3.2a that there is Gibbs phenomenon at the discontinuity.

Theorem 2.3.2 indicates that if $f(t)$ is continuous at a then the left and right hand limits are equal and we have $S_N(a) \to f(a)$, but if $f(t)$ has a jump at a then $S_N(a)$ converges to the average of the left and right hand limits. This latter case is confirmed by Figure 3.2b, wherein the sine series at the discontinuity converges to $\frac{1}{2}(g'(0^-) + g'(0^+)) = \frac{1}{2}(k^2/8 - k^2/8) = 0$.

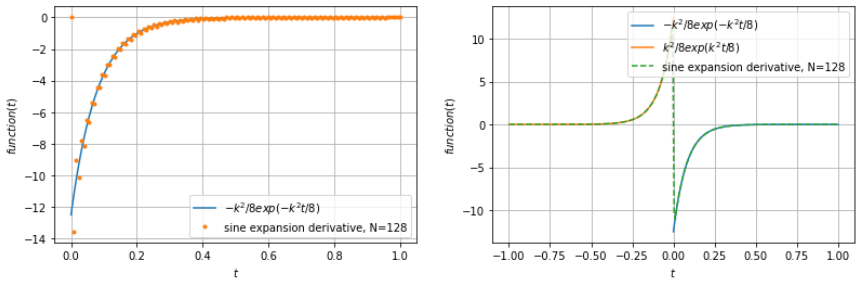

(a) Interval $[0,1]$. (b) Interval $[-1,1]$.

Figure 3.2: Derivative of the cosine expansion of $e^{-k^2t/8}$ against actual function $g'(t)$, for $k = 10$.

One way to circumvent the issue of Gibbs phenomenon at $t = 0$ is to construct a cosine series on a wider interval $[0-\varepsilon, 1+\varepsilon]$, for $\varepsilon > 0$ big enough, while the domain of interest for time is still $[0,1]$. That is, for a given k, we have

$$e^{-k^2t/8} \approx {\sum_{n=0}^{N-1}}' \beta_{k,n} \cos\left(n\pi \frac{t-\varepsilon}{1+2\varepsilon}\right), 0 \le t \le 1, \tag{3.6}$$

where $\beta_{k,n}$ are the Fourier-cosine series coefficients.

However, recall that the Gibbs phenomenon entails not only failure in convergence at a discontinuity but also a slowed convergence rate in regions distant from the discontinuity. In fact, even away from the new discontinuity ($t = -\varepsilon$), oscillations persist. This is illustrated in Figure 3.3.

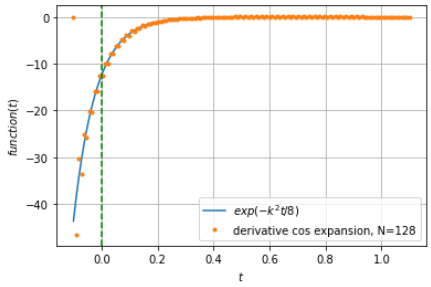

Figure 3.3: Sine expansion of the derivative of $e^{-k^2 t/8}$ in the interval $[-\varepsilon, 1+\varepsilon]$, for $k = 10$, $\varepsilon = 0.1$.

In addition to this, there is another, larger issue. So far, the example we analysed was for fixed k. Let us pay close attention to the form of the coefficients $\beta_{k,n}$ of the approximation for the exponential function,

$$\beta_{k,n} = 16k^2(1+2\varepsilon)\frac{e^{k^2\varepsilon/8} - e^{-k^2(1+\varepsilon)/8}\cos(k\pi)}{(1+2\varepsilon)^2 k^4 + 64n^2\pi^2}.$$

Notice that they also depend on the expansion terms for the x-dimension, given by the index k. For a big value of k, the coefficients eventually explode due to the fact that the lower endpoint of the expansion is negative, since $-\varepsilon < 0$. Because of this issue, the cosine expansion is not a good choice to approximate $e^{-k^2 t/8}$.

If we were to alternatively consider a Fourier-sine series expansion of $e^{-k^2 t/8}$ in $[0,1]$, there would be the limitation that for the endpoints of the interval, the function has value 0. Given the setting of our problem, it is not realistic to have $e^{-k^2 t/8} \approx 0$ at points $t = 0$ and $t = 1$.

Hence, we take a different approach. Since the aforementioned issues arise in the time-derivative of the approximation of the function, one idea is to directly approximate the derivative with respect to time by a Fourier series. Subsequently, by integrating, we can obtain an approximation for the original function. The derivative of $e^{-k^2 t/8}$ is a continuous function and, thus, Theorem 2.3.4 can be applied.

For a given k, the cosine expansion of the respective derivative in $[0,1]$ reads

$$-k^2/8 e^{-k^2 t/8} \approx {\sum_{n=0}^{N-1}}' \alpha_{k,n}\cos(n\pi t) = {\sum_{n=0}^{N-1}}' 2k^4 \frac{e^{-k^2/8}\cos(n\pi) - 1}{k^4 + 64n^2\pi^2}\cos(n\pi t),$$

whereby the coefficients $\alpha_{k,n}$ are solved analytically from the definition.

By taking the integral of the cosine expansion and applying the FTC, we obtain

$$
\begin{aligned}
& e^{-k^2 t/8} - 1 = \int_0^t -k^2/8 e^{-k^2 s/8} ds \\
\Longleftrightarrow & e^{-k^2 t/8} - 1 \approx \sum_{n=1}^{N-1} \alpha_{k,n} \int_0^t \cos(n\pi s)\, ds + \frac{1}{2}\alpha_{k,0} \int_0^t 1 ds \\
\Longrightarrow & e^{-k^2 t/8} \approx \sum_{n=1}^{N-1} \alpha_{k,n} \frac{1}{n\pi} \sin(n\pi t) + \frac{1}{2} t \alpha_{k,0} + 1.
\end{aligned} \tag{3.7}
$$

Notice that equation (3.7) is no longer a Fourier series for $e^{-k^2 t/8}$ due to the t-dependent term. We shall refer to this construction as a trigonometric expansion from here onward.

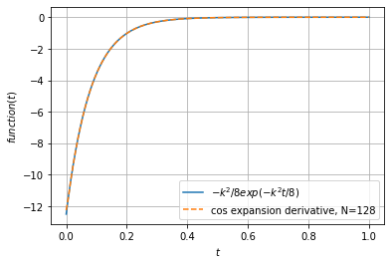

(a) Cosine expansion of the derivative of $e^{-k^2 t/8}$ in the interval $[0,1]$, for $k = 10$.

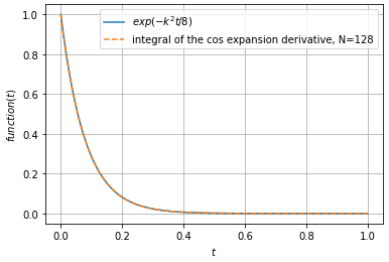

(b) $e^{-k^2 t/8}$ in the interval $[0,1]$ as the integral of the cosine expansion of the derivative, for $k = 10$.

By taking this approach, we are obtaining an approximation which is now continuous and differentiable at the point $t = 0$. This is because the actual expanded function, $-k^2/8 e^{-k^2 t/8}$, is at least continuous, and so taking its integral leads to a function which is differentiable and continuous.

Moreover, this is a global approximation for $e^{-k^2 t/8}$ (suitable for any t), and in particular, it is exact at point $t = 0$. The latter comes from the fact that we know the value of the function at initial time, and that information is used upon integration by using FTC.

Numerical tests show that our construction with the integral approximates the original exponential function well. In Figure 3.5, we present the convergence of the L^∞-norm error between the exact function $e^{-k^2 t/8}$ and the approximation (3.7) in the interval $[0,1]$, for different value of k.

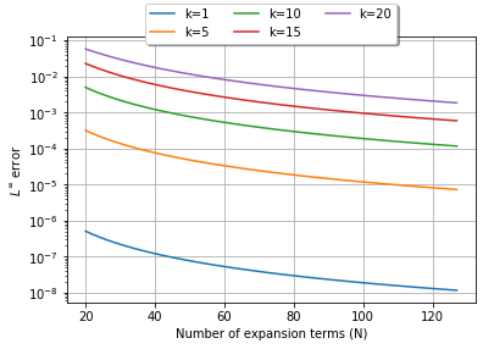

Figure 3.5: L^∞-norm error between integral approximation and the exact function $e^{-k^2 t/8}$, for different values of k.

The results indicate an algebraic convergence rate of the constructed trigonometric expansion. Furthermore, as the value of parameter k increases, the function $e^{-k^2 t/8}$ exhibits steeper behavior, leading to less precise approximations: even with $N = 128$ expansion terms, the approximation can only attain an accuracy of $\mathcal{O}(10^{-2})$ for $k = 20$. We conclude that achieving a reasonable approximation of an exponential function demands a substantial number of expansion terms.

Recall that how fast the series expansion converges is solely determined by how smooth the periodic extension of the function is. The weakest condition that guarantees convergence of a Fourier series is that the function is of class C^0 (continuous but not differentiable). When we first expand the derivative and then integrate that expansion, the smoothness of the expanded function has been improved by order 1. This is confirmed by numerical tests: if we would have taken a cosine series to directly approximate the exponential function,

$$e^{-k^2 t/8} \approx {\sum_{n=0}^{N-1}}' 16k^2 \frac{1 - e^{-k^2/8}\cos(n\pi)}{k^4 + 64n^2\pi^2} \cos(n\pi t),$$

the convergence would have been worse, as depicted in Figure 3.6.

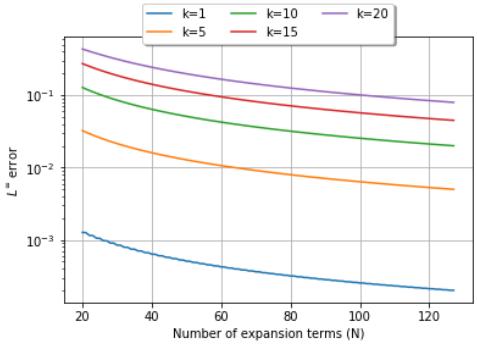

Figure 3.6: L^∞-norm error between cosine series approximation and the exact function $e^{-k^2 t/8}$, for different values of k.

3.2.2. TRIGONOMETRIC EXPANSION

Let us now consider the following particular problem for the Heat equation,

$$\begin{cases} \frac{\partial u_p}{\partial t} = \frac{1}{2}\frac{\partial^2 u_p}{\partial x^2}, \text{ for } 0 < x < 2\pi \text{ and } 0 < t \leq 1, \\ u_p(t,0) = 0, \\ u_p(t,2\pi) = 0, \\ u_p(0,x) = \sin(px/2). \end{cases} \tag{3.8}$$

Knowing, by Section 3.1, that a possible solution for this problem is of the form

$$u_p(t,x) = \sum_{k=1}^{\infty} B_k e^{-k^2 t/8} \sin(kx/2) = e^{-p^2 t/8} \sin(px/2),$$

where $B_k = 0$ for $k \neq p$ and $B_p = 1$, we approximate u_p using a 2D series expansion. As discussed in Section 3.2.1, we shall consider

$$\frac{\partial u_p}{\partial t} = \sum_{k=1}^{\infty} {\sum_{n=0}^{\infty}}' \alpha_{k,n} \cos(n\pi t) \sin(kx/2), \tag{3.9}$$

which yields

$$\begin{aligned} u_p &= \sum_{k=1}^{\infty} \left(\sum_{n=1}^{\infty} \alpha_{k,n} \frac{1}{n\pi} \sin(n\pi t) + \frac{1}{2} t \alpha_{k,0} \right) \sin(kx/2) + \sin(px/2) \\ \implies u_p &= \left(\sum_{n=1}^{\infty} \alpha_{p,n} \frac{1}{n\pi} \sin(n\pi t) + \frac{1}{2} t \alpha_{p,0} + 1 \right) \sin(px/2), \text{ since } \alpha_{k,n} = 0 \text{ for } k \neq p, \end{aligned} \tag{3.10}$$

where $\alpha_{k,n}$ denote the coefficients, analytically determined by

$$\alpha_{k,n} = -2 \int_0^1 k^2/8 e^{-k^2 t/8} \cos(n\pi t) dt = 2k^4 \frac{e^{-k^2/8} \cos(n\pi) - 1}{k^4 + 64 n^2 \pi^2}. \tag{3.11}$$

One particularity of this construction is that the boundary conditions $u_p(t,a) = u_p(t,b) = 0$ are automatically fulfilled for any coefficients $\alpha_{k,n}$, and the same holds for the initial condition. Plus, it allows us to recover a global approximation for u_p, suitable for any t and x in the PDE domain.

DETERMINING THE COEFFICIENTS

Let us now assume that the coefficients are in fact unknown, which is the case for later chapters wherein we solve more complicated PDEs. Truncating the series (3.10) by N, it yields

$$u_p \approx \sum_{k=1}^{N} \left(\sum_{n=1}^{N-1} A_{k,n} \frac{1}{n\pi} \sin(n\pi t) + \frac{1}{2} t A_{k,0} \right) \sin(kx/2) + \sin(px/2), \tag{3.12}$$

where $A_{k,n}$ denote the unknown coefficients. We shall refer to this construction as 2D trigonometric expansion for the function u_p, since the coefficients are unknown and the basis functions involved are trigonometric functions.

The coefficients $A_{k,n}$ can be stored as a second-order tensor (or matrix) as follows

$$A = \begin{pmatrix} A_{1,0} & A_{1,1} & \dots & A_{1,N-1} \\ A_{2,0} & A_{2,1} & \dots & A_{2,N-1} \\ \vdots & & & \vdots \\ A_{N,0} & \dots & \dots & A_{N,N-1} \end{pmatrix}.$$

Pluggling construction (3.12) into the PDE (3.8) leads to

$$\begin{aligned} &\frac{\partial u_p}{\partial t} = \frac{1}{2} \frac{\partial^2 u_p}{\partial x^2} \\ \iff &\sum_{k=1}^{N} \sum_{n=0}^{N-1}{}' A_{k,n} \cos(n\pi t) \sin(kx/2) \\ &+ \frac{1}{2} \sum_{k=1}^{N} \left(\sum_{n=1}^{N-1} A_{k,n} \frac{1}{n\pi} \sin(n\pi t) + \frac{1}{2} t A_{k,0} \right) \left(\frac{k}{2} \right)^2 \sin(kx/2) = -\frac{1}{2} \left(\frac{p}{2} \right)^2 \sin\left(px/2\right). \end{aligned} \tag{3.13}$$

By evaluating equation (3.13) at a specific data point $x \in [0, 2\pi]$ and $t \in [0, 1]$, we are left with an equation that needs to be solved for N^2 unknowns, the coefficients $A_{k,n}$.

With this in mind, we define a grid of training points with possible value combinations of x and t, through which we can build a linear system to solve the coefficients. The number of training data points per dimension is denoted with M. For the remainder of the analysis that follows, we will assume M different training values for both x and t, i.e. data points x_m, with $m = 1, \dots, M$ and t_ℓ, with $\ell = 0, \dots, M-1$.

CHOICE OF N AND M

Regarding N and M, there are three different choices when solving the linear system: $N < M$, $N > M$ and $N = M$. Observe that N^2 can be viewed as the degree of "flexibility" the model has in minimizing the misfit with the training data. At the same time, M^2 represents the level of "constraint" within the model, as the model tries to match these training data points when solving the system of equations.

Figure 3.7, which distinguishes between the accuracy for training and non-training data, shows the L^∞-norm between the left-hand side (LHS) and the right-hand side (RHS) of (3.13), for $p = 1$. The error in the coefficients is determined by $||A_{k,n} - \alpha_{k,n}||_\infty$.

The accuracy of the output for the non-training data is fully determined by the computed coefficients and hence these two error plots exhibit the same behaviour.

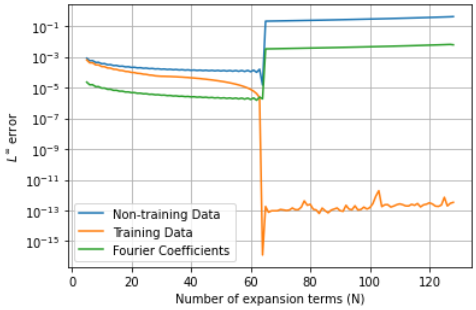

Figure 3.7: L^∞-norm error for for (non-)training data and the coefficients. $M = 64$ training points were used, for both dimensions, to determine the coefficients $A_{k,n}$.

- $N < M$. In this case, there are more training points than unknown coefficients. This is an overdetermined linear system and, therefore, there is no solution to this problem. The model can only minimize the distance between the RHS and the LHS of equation (3.13). However, the trigonometric expansion is a global approximation, thus the optimizer still returns coefficients that lead to an accurate approximation for non-training data. In this scenario, all three errors converge only algebraically with increasing N. The accuracy of the fitted function is limited by the series truncation error at level N.

- $N > M$. We are in the presence of an underdetermined linear system, for which there are infinite solutions. On the one hand, there is enough flexibility to accurately fit all of the training data. On the other hand, this gives room for *overfitting*, i.e. the training points are overly-fitted to, leading to a large deviation between the true coefficients of the global decomposition and the fitted ones. As a result, the error in the coefficients and in the non-training data increases significantly (as depicted in Figure 3.7), while the fitted function achieves machine precision for the training data.

- $N = M$. In this case, we have a uniquely determined linear system, for which there is a unique solution. This is because the degree of flexibility in the model corresponds to the degree of constraint, resulting in a fit that aligns with all training data points while providing an overall accurate approximation.

According to these results, we conclude that the optimal parameter choice is to take $N = M$ and directly solve a linear system to find the coefficients without recurring to minimization or optimization procedures.

Subsequently, we need to decide the number of training data points M for a satisfactory level of accuracy. For that, we tested the L^∞-norm error between the LHS and the RHS of (3.13), for $p = 1$. The results are shown in Figure 3.8, which unsurprisingly indicate that the higher the value of $N = M$, the better the accuracy.

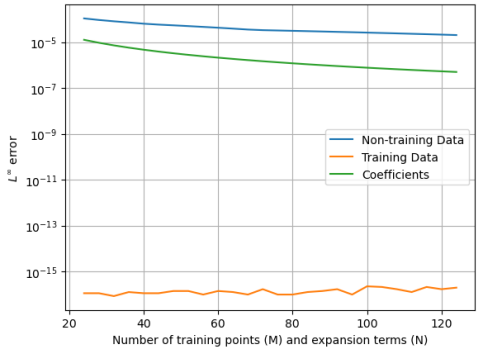

Figure 3.8: L^∞-norm error for (non-)training data and the coefficients. $M = N$ expansion terms and training points were used for both dimensions, to determine the coefficients $A_{k,n}$.

The LHS computed with the approximated coefficients $A_{k,n}$ can exactly match the RHS for all of the training data points, which results in a horizontal line close to machine precision for these points. The error in the non-training data and in the coefficients is determined by the series truncation error at level N. As N increases, the series truncation error decreases and there is an error decrease in the coefficients and in the non-training data. However, we see a very slow convergence rate as N and M increase. In fact, if we analyse the error in the coefficients for different values of p, we see an algebraic error convergence (cf. Figure 3.9).

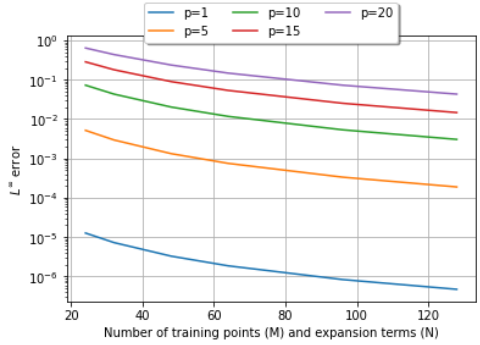

Figure 3.9: L^∞-norm error of the coefficients for different p, using $M = N$ expansion terms and training points. This is computed for different values of p.

Finally, we compute the L^∞-norm error between the exact function u_p and the approximation (3.12) whose coefficients are obtained via the PDE. Both are evaluated at the training points and the results are illustrated in Figure 3.10. Once again, we see a very slow convergence rate as N and M increase, and the minimum error attainable is of order $\mathcal{O}(10^{-6})$ for $p = 1$, and only $\mathcal{O}(10^{-1})$ for $p = 20$, by setting $N = M = 128$.

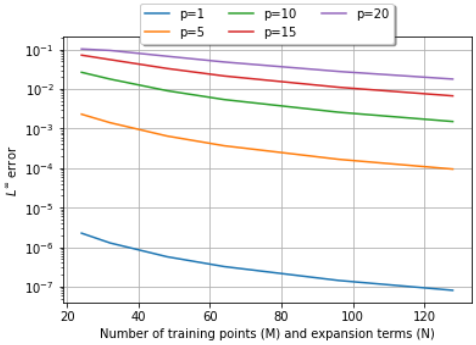

Figure 3.10: L^∞-norm error of approximation (3.12) against exact solution u_p, using $M = N$ for different values of p.

Finally, notice that the exact formulation for u_p (3.10) satisfies the Heat equation. However, we are assuming that u_p can be approximated by a trigonometric expansion of the form (3.12), which means that, once that approximation is plugged into the PDE, the value we obtain for the coefficients $A_{k,n}$ will make up for the fact that the approximation is truncated at level N. Even if that does not correspond to the analytical value, $\alpha_{k,n}$. As a result, the L^∞-norm error is smaller for the approximation of u_p than for the coefficients. This will be further discussed in Chapter 8.

4

Our approach: Pricing barrier options via trigonometric expansion under GBM model

In this chapter, we consider the case whereby the underlying process dynamics can be described by the GBM model. We start this research with the GBM model due to the availability of an analytical solution for the price of a barrier option. This choice allows us to readily benchmark and evaluate the effectiveness of our method while also acquiring valuable insights in order to extend it to more complex models.

The primary objective of this chapter is to introduce our novel approach for pricing up-and-out barrier options. To achieve this, we will begin with deriving a formula for the valuation of a barrier option in terms of a one-dimensional integral. Its integrand involves a density function that captures the barrier condition, which we refer to as the survival density function. This constitutes one of the key insights of this thesis and enables the direct application of the COS pricing method by Fang and Oosterlee [22].

Following this, we proceed to estimate the sine series coefficients of the survival pdf, which are closely related to the survival ch.f., via another series expansion. The choice of basis functions for this second approximation series is of utmost importance, and will be analysed in detail, taking into account the specific constraints of the problem at hand. The respective series coefficients are obtained from solving the corresponding PDE, which, in turn, is derived from the pricing PDE under the GBM model. Note that approximating the coefficients of the survival pdf's series and not the price directly allows us to obtain a fast pricing method through the application of the COS pricing formula.

Additionally, we derive an alternative formulation for the survival ch.f., capitalizing on the fact that the GBM pricing PDE can be reduced to the Heat equation, for which a solution exists in the form of a series.

Finally, numerical results are presented in the last section, where we benchmark the sine series coefficients of the survival pdf obtained via our approach against the alter-

native series formulation. We also compare the resulting option prices with their established closed-form solutions and compute the options' Greeks.

4.1. THE PRICING PDE

Let S_t be a stochastic process describing the asset price at time t, which will be the underlying for the financial derivative contract. $V(t,S)$ is the value of the contract at time t. Under the BS model, the underlying stock price is assumed to follow a GBM and its dynamics are given by

$$dS_t = rS_t dt + \sigma S_t dW_t^{\mathbb{Q}},$$

under the risk-neutral measure $\mathbb{Q}$, where r is the risk-free interest rate and σ the volatility.

Recall that the price of an option is given by the discounted expected payoff at time $t < T$ (maturity),

$$V(t,S) = e^{-r(T-t)}\mathbb{E}^{\mathbb{Q}}\left(V(T,S)|\mathscr{F}_t\right).$$

Then, using the Feynman-Kac theorem, the value of the option is the solution of the following pricing PDE,

$$\begin{cases} \frac{\partial V}{\partial t} + rS\frac{\partial V}{\partial S} + \frac{1}{2}\sigma^2 S^2 \frac{\partial^2 V}{\partial S^2} - rV = 0, \\ V(T,S) = f(S_T), \end{cases} \tag{4.1}$$

where $0 \le t \le T$ and $f(\cdot)$ stands for the payoff function of the option (either call, put or even other option types). The BS PDE is a parabolic PDE and its derivation was previously explained in Chapter 2. It is a well-posed PDE when accompanied by a final condition.

Performing a change of variable $S_t \mapsto X_t := \ln S_t$, such that now we have the log-asset price, the resulting pricing PDE reads

$$\begin{cases} \frac{\partial V}{\partial t} + \left(r - \frac{1}{2}\sigma^2\right)\frac{\partial V}{\partial X} + \frac{1}{2}\sigma^2 \frac{\partial^2 V}{\partial X^2} - rV = 0, \\ V(T,X) = f(X_T), \end{cases} \tag{4.2}$$

where $0 \le t \le T$.

4.1.1. VALUATION OF BARRIER OPTIONS

Up-and-out barrier options payoff only when the process S_t of the underlying asset price does not breach an agreed knock-out value, B, before the expiration of the option. This applies when the initial asset price, S_0, is less than B. In that case, the option's payoff mirrors that of a European option.

Let $\tau_B := \inf\{\tilde{t} \ge t : S_{\tilde{t}} \ge B \Leftrightarrow X_{\tilde{t}} \ge b\}$, with $b = \ln B$, be the first time that the process S_t hits the barrier level B. The payoff of an up-and-out barrier option is then given by $f(X_T)\mathbb{1}_{\{\tau_B > T\}}$, where $f(\cdot)$ is the payoff function of an European option.

Pricing an European option starts from the risk-neutral valuation formula, which is in essence an integration of the product of the probability density and the payoff function. Following the same reasoning as [50], the value of an up-and-out barrier option can be written in a similar format[1],

[1] Making use of the tower property of conditional expectations, i.e. $\mathbb{E}(XY) = \mathbb{E}[\mathbb{E}(XY|Y)]$.

$$
\begin{aligned}
V(t,x) &= e^{-r(T-t)}\mathbb{E}^{\mathbb{Q}}\left(f(X_T)\mathbb{1}_{\{\tau_B>T\}}|\mathscr{F}_t\right)\\
&= e^{-r(T-t)}\mathbb{E}^{\mathbb{Q}}\left(f(X_T)\mathbb{1}_{\{\tau_B>T\}}|X_t=x\right)\\
&= e^{-r(T-t)}\mathbb{E}^{\mathbb{Q}}\left[\mathbb{E}^{\mathbb{Q}}\left(f(X_T)\mathbb{1}_{\{\tau_B>T\}}|X_t=x,\mathbb{1}_{\{\tau_B>T\}}\right)\right]\\
&= 0\cdot\mathbb{P}(\tau_B\le T|X_t=x)+e^{-r(T-t)}\mathbb{E}^{\mathbb{Q}}[f(X_T)|X_t=x,\tau_B>T]\cdot\mathbb{P}(\tau_B>T|X_t=x)\\
&= e^{-r(T-t)}\left(\int_{\mathbb{R}} f(y)p(y|x,\tau_B>T)dy\right)\cdot\mathbb{P}(\tau_B>T|x)\\
&= e^{-r(T-t)}\int_{\mathbb{R}} f(y)\left(\int_T^{\infty} p(y|x,\tau_B)\cdot\mathbb{P}(\tau_B|x)d\tau_B\right)dy\\
&= e^{-r(T-t)}\int_{\mathbb{R}} f(y)\left(\int_T^{\infty} p(y,\tau_B|x)d\tau_B\right)dy\\
&= e^{-r(T-t)}\int_{\mathbb{R}} f(y)p(y,\tau_B>T|x)dy,
\end{aligned}
\tag{4.3}
$$

where $p(y,\tau_B>T|x)$ is the joint transition density function such that the realized path does not cross the barrier B (from below) before maturity T. We shall call this the *survival density function*. The corresponding ch.f. shall be denoted *survival ch.f.*.

As a result of the derivations outlined in (4.3), the barrier condition can be absorbed into the transitional pdf, and thereby into the respective ch.f. as well. This is a key insight from our approach.

One of the primary advantages of this derivation is that the COS pricing formula from [22] can be directly applied to barrier options, once the survival ch.f. is available. Furthermore, since the payoff function is identical to that of a European option, the payoff coefficients for the COS pricing formula remain the same, and a closed-form formula exists.

THE PRICING PDE FOR BARRIER OPTIONS

Notice that the expectation in (4.3) is evaluated only on the event that the barrier is not breached. A "localized" version of the Feynman-Kac theorem can be applied to such expectation [51]. Let $b=\ln B$ and choose a as low as possible, such that X can be considered close enough to $-\infty$ (i.e. $S\approx 0$). The option value $V(t,x)$, defined by the discounted expectation, satisfies a PDE of the same type as (4.2), but only in the domain whereby the payoff has a non-zero value, i.e. in a compact interval $[a,b]$ in which X can take values. In addition, boundary conditions for V can be established at the knock-out points. Then, under the GBM model, the theorem reads as follows.

Theorem 4.1.1 (Localized Feynman-Kac for GBM)**.** *Consider a process X_t whose dynamics are ruled by a GBM and take $\tau_{a\vee b}:=\inf\{\tilde{t}\ge t: X_{\tilde{t}}\le a\vee X_{\tilde{t}}\ge b\}$ to be the first time that the process X_t exits the interval (a,b). Let $f:[a,b]\to\mathbb{R}$ be a continuous payoff function with a compact support. Then,*

$$
\begin{aligned}
V(t,x) =& e^{-r(T-t)}\mathbb{E}^{\mathbb{Q}}[f(X_T)\mathbb{1}_{\{\tau_{a\vee b}>T\}}|\mathscr{F}_t]\\
=& e^{-r(T-t)}\mathbb{E}^{\mathbb{Q}}[f(X_T)\mathbb{1}_{\{\tau_{a\vee b}>T\}}|X_t=x]
\end{aligned}
$$

4

is the unique, bounded solution of the BS pricing PDE

$$\frac{\partial V}{\partial t}+\left(r-\frac{1}{2}\sigma^2\right)\frac{\partial V}{\partial X}+\frac{1}{2}\sigma^2\frac{\partial^2 V}{\partial X^2}-rV=0,\ \textit{for}\ a<X<b, 0\le t\le T,$$

with boundary and terminal conditions

$$\begin{aligned}V(t,a)&=0,\ \textit{for}\ 0\le t\le T,\\ V(t,b)&=0,\ \textit{for}\ 0\le t\le T,\\ V(T,X)&=f(X_T),\ \textit{for}\ a<X_T<b.\end{aligned}$$

4

Proof. We follow [52] and prove first the solution's uniqueness. Hence, assume that $u(t,x)$ is the solution of the above PDE and consider for $0\le t<T$ the process $M:=\{M_t, t\ge 0\}$ such that

$$M_t:=e^{-rt}u(t,X)$$

Using Itô's formula, we see that M is a $(\mathbb{Q},\mathbb{F})$-martingale, where $\mathbb{F}:=\{\mathscr{F}_t, t\ge 0\}$,

$$\begin{aligned}dM_t=&\left(e^{-rt}\frac{\partial u}{\partial t}-re^{-rt}u(t,x)+\left(r-\frac{1}{2}\sigma^2\right)e^{-rt}\frac{\partial u}{\partial X}+\frac{1}{2}\sigma^2e^{-rt}\frac{\partial^2 u}{\partial X^2}\right)dt+\sigma e^{-rt}\frac{\partial u}{\partial X}dW_t\\ =&\sigma e^{-rt}\frac{\partial u}{\partial X}dW_t\end{aligned}$$

since it does not contain any dt-terms.

M is bounded and, therefore, integrable. Hence,

$$\begin{aligned}M_t=\mathbb{E}^{\mathbb{Q}}[M_T|\mathscr{F}_t]&=\mathbb{E}^{\mathbb{Q}}[e^{-rT}f(X_T)\mathbb{1}_{\{\tau_{a\vee b}>T\}}|\mathscr{F}_t]\\ &=e^{-rt}\mathbb{E}^{\mathbb{Q}}[e^{-r(T-t)}f(X_T)\mathbb{1}_{\{\tau_{a\vee b}>T\}}|\mathscr{F}_t],\end{aligned}$$

which gives (uniquely) $u(t,X)=V(t,X)$.

Now we show that V is indeed a solution of the PDE. Clearly it satisfies the boundary and terminal conditions. Further, for $t<T$, $e^{-rt}V(t,X_t)$ is a $(\mathbb{Q},\mathbb{F})$-martingale since

$$\mathbb{E}^{\mathbb{Q}}[e^{-rT}V(T,X)|\mathscr{F}_t]=e^{-rt}\mathbb{E}^{\mathbb{Q}}[e^{-r(T-t)}f(X_T)\mathbb{1}_{\{\tau_{a\vee b}>T\}}|\mathscr{F}_t]=e^{-rt}V(t,X).$$

It can be proved that $V(t,X)$ is smooth and, consequently, using Itô's formula we deduce that $V(t,X)$ satisfies the PDE.

□

This theorem is the result of an argument followed by [53] and [54] as well.

Lastly, notice that the above theorem can also be applied to double-barrier and down-and-out barrier options. That only depends on the appropriate choice of the interval $[a,b]$.

4.2. BENCHMARK SOLUTION: SOLVING THE PDE THROUGH THE HEAT EQUATION

In this section, the pricing PDE is reduced to the a simpler PDE for which an analytical solution can be established. Our ultimate goal is to derive a formula for the survival ch.f., which will serve as a benchmark for our approach.

Following similar steps as [55], we start by transforming the differential equation into the Heat equation, for which there are known solutions [49]. Consider the following initial boundary value problem (IVBP),

$$\begin{cases} \frac{\partial V}{\partial t} + \left(r - \frac{1}{2}\sigma^2\right)\frac{\partial V}{\partial X} + \frac{1}{2}\sigma^2\frac{\partial^2 V}{\partial X^2} - rV = 0, \\ V(t,a) = 0, \text{ for } 0 \le t \le T, \\ V(t,b) = 0, \text{ for } 0 \le t \le T, \\ V(T,X) = f(X_T), \text{ for } a < X_T < b. \end{cases}$$

Step 1: Let us start by performing a change of variables, such that $t \mapsto \tau := \frac{1}{2}\sigma^2(T-t)$ and $x \mapsto z := x - a$. Then, the PDE becomes

$$\frac{\partial V}{\partial \tau} = \left(\frac{2r}{\sigma^2} - 1\right)\frac{\partial V}{\partial z} + \frac{\partial^2 V}{\partial z^2} - \frac{2r}{\sigma^2}V. \tag{4.4}$$

Setting $\kappa = \frac{2r}{\sigma^2}$, leads to

$$\begin{cases} \frac{\partial V}{\partial \tau} = (\kappa - 1)\frac{\partial V}{\partial z} + \frac{\partial^2 V}{\partial z^2} - \kappa V \text{ for } 0 < z < b - a, \\ V(\tau, 0) = 0, \\ V(\tau, b-a) = 0, \\ V(0,z) = f(z+a). \end{cases} \tag{4.5}$$

One more change of variables is needed in order to eliminate the last two terms on the RHS of the last equation. To this end, we set $V(\tau,z) = e^{\alpha(z+a)+\beta\tau}U(\tau,z)$. Computing the partial derivatives of V in terms of z and τ, it holds that

$$\begin{aligned} \frac{\partial V}{\partial \tau} &= \beta e^{\alpha(z+a)+\beta\tau}U + e^{\alpha(z+a)+\beta\tau}\frac{\partial U}{\partial \tau}, \\ \frac{\partial V}{\partial z} &= \alpha e^{\alpha(z+a)+\beta\tau}U + e^{\alpha(z+a)+\beta\tau}\frac{\partial U}{\partial z}, \\ \frac{\partial^2 V}{\partial z^2} &= \alpha^2 e^{\alpha(z+a)+\beta\tau}U + 2\alpha e^{\alpha(z+a)+\beta\tau}\frac{\partial U}{\partial z} + e^{\alpha(z+a)+\beta\tau}\frac{\partial^2 U}{\partial z^2}. \end{aligned} \tag{4.6}$$

Plugging these expressions into the PDE, and setting $\alpha = -\frac{1}{2}(\kappa - 1) = \frac{1}{2} - \frac{r}{\sigma^2}$ and $\beta = -\alpha^2 - \kappa = -\left(\frac{\sigma^2+2r}{2\sigma^2}\right)^2$, we have

$$\begin{cases} \frac{\partial U}{\partial \tau} = \frac{\partial^2 U}{\partial z^2}, 0 < z < b - a, \\ U(\tau, 0) = 0, \\ U(\tau, b-a) = 0, \\ U(0,z) = e^{-\alpha(z+a)}f(z+a). \end{cases} \tag{4.7}$$

Notice that this corresponds to the Heat equation for variables $0 \le z \le b-a$ and $0 \le \tau \le \frac{1}{2}\sigma^2 T$.

Step 2: To solve the Heat equation (4.7), we will use the method of separation of variables. That is, we assume solutions of the form $U(z,\tau) = Z(z)T(\tau)$. Following the same steps as in Chapter 3, we arrive at $Z_k(z) = B_k \sin\left(k\pi \frac{z}{b-a}\right)$, and $T_k(\tau) = e^{-\left(\frac{k\pi}{b-a}\right)^2 \tau}$, for $k \in \mathbb{Z}$.

Step 3: Because the Heat equation is linear, any linear combination of eligible solutions is also a solution. Then, the solution for the IVBP can be written as a linear combination of the separate solutions $U_k(\tau,z) = X_k(z)T_k(\tau)$, leading to a series expansion formulation. Hence, by the superposition principle, the desired solution is of the form

$$\begin{aligned} U(\tau,z) &= \sum_{k=1}^{\infty} B_k e^{-\left(\frac{k\pi}{b-a}\right)^2 \tau} \sin\left(k\pi \frac{z}{b-a}\right), 0 < z < b-a,\ 0 \le \tau \le \frac{1}{2}\sigma^2 T \\ \implies U(\tau,x) &= \sum_{k=1}^{\infty} B_k e^{-\left(\frac{k\pi}{b-a}\right)^2 \tau} \sin\left(k\pi \frac{x-a}{b-a}\right), a < x < b. \end{aligned} \tag{4.8}$$

When $\tau = 0$, $U(0,x)$ is also a Fourier-sine series expansion. It then follows that B_k are the sine series coefficients of $e^{-\alpha x} f(x)$, defined as follows

$$B_k = \frac{2}{b-a} \int_a^b e^{-\alpha y} f(y) \sin\left(k\pi \frac{y-a}{b-a}\right) dy. \tag{4.9}$$

This implies that

$$\begin{aligned} & U(\tau,x) = \sum_{k=1}^{\infty} B_k e^{-\left(\frac{k\pi}{b-a}\right)^2 \tau} \sin\left(k\pi \frac{x-a}{b-a}\right) \\ \implies & V(\tau,x) = e^{\alpha x + \beta \tau} \sum_{k=1}^{\infty} B_k e^{-\left(\frac{k\pi}{b-a}\right)^2 \tau} \sin\left(k\pi \frac{x-a}{b-a}\right) \\ \implies & V(t,x) = e^{-r(T-t)} \sum_{k=1}^{\infty} B_k e^{-\frac{1}{2}\sigma^2 (T-t)\left(\left(\frac{k\pi}{b-a}\right)^2 + \alpha^2\right)} e^{\alpha x} \sin\left(k\pi \frac{x-a}{b-a}\right) \\ \iff & V(t,x) = e^{-r(T-t)} \int_a^b \underbrace{e^{-\alpha y} f(y)}_{\text{payoff}} \\ & \underbrace{\frac{2}{b-a} \sum_{k=1}^{\infty} e^{-\frac{1}{2}\sigma^2 (T-t)\left(\left(\frac{k\pi}{b-a}\right)^2 + \alpha^2\right)} e^{\alpha x} \sin\left(k\pi \frac{x-a}{b-a}\right) e^{-\alpha y} \sin\left(k\pi \frac{y-a}{b-a}\right)}_{p(y,\tau_{a\vee b} > t|x)} dy. \end{aligned} \tag{4.10}$$

The formula for the survival density function $p(y,\tau_{a\vee b} > t|x)$ is confirmed by [56], which derives it via the Kolmogorov backward equation for the pdf.

Step 4: Since the survival pdf forms a Fourier pair with the survival ch.f., we get

$$\begin{aligned}\phi(\omega;t,x) &= \sum_{k=1}^{\infty} e^{-\frac{1}{2}\sigma^2(T-t)\left(\left(\frac{k\pi}{b-a}\right)^2+\alpha^2\right)} e^{\alpha x}\sin\left(k\pi\frac{x-a}{b-a}\right)\left(\frac{2}{b-a}\int_{-\infty}^{+\infty} e^{i\omega y}e^{-\alpha y}\sin\left(k\pi\frac{y-a}{b-a}\right)dy\right)\\ &\approx \sum_{k=1}^{\infty} e^{-\frac{1}{2}\sigma^2(T-t)\left(\left(\frac{k\pi}{b-a}\right)^2+\alpha^2\right)} e^{\alpha x}\sin\left(k\pi\frac{x-a}{b-a}\right)\left(\frac{2}{b-a}\int_{a}^{b} e^{i\omega y}e^{-\alpha y}\sin\left(k\pi\frac{y-a}{b-a}\right)dy\right).\end{aligned} \tag{4.11}$$

This result will be used for comparison of the results obtained with our approach, later in Section 4.5.

4.3. THE PDE FOR THE SURVIVAL CH.F.

From (4.3) and the sine formulation for the option price (2.32), we conclude that the price of a barrier option can be approximated by

$$V(t,x) \approx e^{-r(T-t)}\sum_{p=1}^{N}\text{Im}\left\{\phi\left(\frac{p\pi}{b-a},t;x\right)e^{-ip\pi\frac{a}{b-a}}\right\}V_p, \tag{4.12}$$

where ϕ is the survival ch.f. corresponding to $p(y,\tau_B > T|x)$. The coefficients V_p for European (and barrier) options are provided by

$$V_p := \frac{2}{b-a}\int_a^b V(T,y)\sin\left(p\pi\frac{y-a}{b-a}\right)dy, \tag{4.13}$$

where $V(T,y)$ is the option value at maturity T, i.e. the payoff function. For a call option, we have $V(y,T) = (e^y - K)^+$, for instance.

Let us denote by $\hat{\phi}_p(t,x) := \text{Im}\left\{\phi\left(\frac{p\pi}{b-a},t;x\right)e^{-ip\pi\frac{a}{b-a}}\right\}$ the coefficients for the survival pdf. Plugging formula (4.12) into the pricing PDE, we obtain

$$\begin{aligned}&\frac{\partial V}{\partial t}+\left(r-\frac{1}{2}\sigma^2\right)\frac{\partial V}{\partial X}+\frac{1}{2}\sigma^2\frac{\partial^2 V}{\partial X^2}-rV=0\\ \Longleftrightarrow\; &rV+e^{-r(T-t)}\sum_{p=1}^{N}\frac{\partial\hat{\phi}_p}{\partial t}V_p+\left(r-\frac{1}{2}\sigma^2\right)e^{-r(T-t)}\sum_{p=1}^{N}\frac{\partial\hat{\phi}_p}{\partial X}V_p+\frac{1}{2}\sigma^2e^{-r(T-t)}\sum_{p=1}^{N}\frac{\partial^2\hat{\phi}_p}{\partial X^2}V_p-rV=0\\ \Longleftrightarrow\; &\sum_{p=1}^{N}\left(\frac{\partial\hat{\phi}_p}{\partial t}+\left(r-\frac{1}{2}\sigma^2\right)\frac{\partial\hat{\phi}_p}{\partial X}+\frac{1}{2}\sigma^2\frac{\partial^2\hat{\phi}_p}{\partial X^2}\right)V_p=0,\ \text{for every } p\in\mathbb{N}.\end{aligned} \tag{4.14}$$

Notice that this is an inner product between a vector $\mathbf{v}$ with components V_p and a vector $\mathbf{u}$ with components $\frac{\partial\hat{\phi}_p}{\partial t}+\left(r-\frac{1}{2}\sigma^2\right)\frac{\partial\hat{\phi}_p}{\partial X}+\frac{1}{2}\sigma^2\frac{\partial^2\hat{\phi}_p}{\partial X^2}$, for $p=1,\ldots,N$, which is equal to zero. This means that the two vectors are orthogonal to each other, or one of them contains zero values. Since the formula for the coefficients V_p applies to any payoff function $V(T,y)$, for any possible vector $\mathbf{v}$, it can only be the case that $\mathbf{u}=\mathbf{0}$. That is, for every $p\in\mathbb{N}$, we conclude that

$$\frac{\partial\hat{\phi}_p}{\partial t}+\left(r-\frac{1}{2}\sigma^2\right)\frac{\partial\hat{\phi}_p}{\partial X}+\frac{1}{2}\sigma^2\frac{\partial^2\hat{\phi}_p}{\partial X^2}=0. \tag{4.15}$$

From the Feynman-Kac theorem 4.1.1, we have that $V(t,a) = V(t,b) = 0$, which implies that $\hat{\phi}_p(t,a) = \hat{\phi}_p(t,b) = 0$. For the terminal condition, $\sum_{p=1}^{N} \hat{\phi}_p(T,x)V_p$ corresponds to the sine series expansion of $V(T,x)$, i.e. $V(T,x) = \sum_{p=1}^{N} \sin\left(p\pi\frac{x-a}{b-a}\right) V_p$. Thus, it implies that $\hat{\phi}_p$ should correspond to the basis functions of the expansion, i.e. $\hat{\phi}_p(T,x) = \sin\left(p\pi\frac{x-a}{b-a}\right)$.

Following a common practice, we set $\tau := T - t$. Then, the terminal condition for $\hat{\phi}_p$ becomes an initial condition, $\hat{\phi}_p(0,x) = \sin\left(p\pi\frac{x-a}{b-a}\right)$ and $\frac{\partial\hat{\phi}_p}{\partial t} = -\frac{\partial\hat{\phi}_p}{\partial\tau}$.

To sum up, now we have to solve the following IVBP

$$\begin{cases} -\dfrac{\partial\hat{\phi}_p}{\partial\tau} + \left(r - \frac{1}{2}\sigma^2\right)\dfrac{\partial\hat{\phi}_p}{\partial X} + \dfrac{1}{2}\sigma^2\dfrac{\partial^2\hat{\phi}_p}{\partial X^2} = 0, a < X < b, \\ \hat{\phi}_p(\tau,a) = 0, \\ \hat{\phi}_p(\tau,b) = 0, \\ \hat{\phi}_p(0,x) = \sin\left(p\pi\frac{x-a}{b-a}\right), \end{cases} \tag{4.16}$$

with $\hat{\phi}_p$ a function of τ and x, i.e. $\hat{\phi}_p(\tau,x) := \text{Im}\left\{\phi\left(\frac{p\pi}{b-a},\tau;x\right)e^{-ip\pi\frac{a}{b-a}}\right\}$.

Having derived the PDE for $\hat{\phi}_p$ which will be solved in the following sections, we can now motivate the choice of computing the sine formula for the option price instead of the usual cosine formula. At the terminal time T (i.e. $\tau = 0$), the ch.f. ϕ equals $e^{i\omega X_T}$, which implies that

$$\phi\left(\frac{p\pi}{b-a},T;x\right)e^{-ip\pi\frac{a}{b-a}} = e^{ip\pi\frac{x-a}{b-a}}.$$

Hence, using the sine pricing formula (2.32), it follows that

$$V(T,x) = \sum_{p=1}^{N} \sin\left(p\pi\frac{x-a}{b-a}\right) V_p \implies V(T,a) = V(T,b) = 0,$$

as desired. On the other hand, at the terminal time, the cosine pricing formula (2.30) does not capture $V(T,a) = V(T,b) = 0$, because neither the coefficients V_p will be 0 at $x = a$ and $x = b$ nor the cosine basis functions. Moreover, there is nothing that guarantees orthogonality between the basis functions evaluated at $x = a$ and $x = b$ and the coefficients V_p. Thus, the value of the option would not be 0 at the boundaries $x = a$ and $x = b$ for the final time $t = T$, unless the following conditions were imposed when solving the PDE,

$$\sum_{p=0}^{N}{}'1 \cdot V_p = 0\,, \sum_{p=0}^{N}{}'(-1)^p \cdot V_p = 0.$$

Imposing such conditions would add one dimension to the problem, as we are now working with $\hat{\phi}_p$ directly and not with the option price V.

Furthermore, the choice to solve the PDE for $\hat{\phi}_p$ instead of the pricing PDE directly is motivated by the fact that solving the PDE for $\hat{\phi}_p$ enables the subsequent fast computation of option prices for multiple strike prices simultaneously, by taking advantage of the sine pricing formula (4.12).

4.4. APPROXIMATION FOR THE SURVIVAL CH.F.

A closed-form solution for $\hat{\phi}_p$ does not exist. Therefore, our goal is to find a formula for $\hat{\phi}_p$ by solving the respective PDE.

Previous work done in FF Quant [30] has indicated that the survival ch.f. can be recovered accurately from its Fourier series expansion. Building upon this insight, we came up with the idea of approximating $\hat{\phi}_p$ as a series expansion and insert it into the PDE (4.16) to yield a linear system where the unknowns are the coefficients of that expansion. This idea coincides with that of a collocation method, which is briefly explained in Section 2.4. However, there are a few distinct differences, which we will highlight as we develop the method step by step.

It is worth noting that in the context of PDE solving, the success of the method of separation of variables depends not only on the fact that a PDE is linear and homogeneous, but also on the boundary conditions being linear and homogeneous [57]. In (4.16), we encounter an IVBP with these characteristics. Hence, it is natural to consider an approximation for $\hat{\phi}_p$ featuring independent basis functions for each variable, mirroring the principle of separation of variables.

Furthermore, the initial condition in (4.16) suggests the use of a trigonometric basis function. Since the chosen approximation formula for $\hat{\phi}_p$ will be plugged in the PDE, it is important to guarantee the differentiability of the basis functions with respect to x and τ. This choice is in accordance with the need for differentiability, as sine and cosine functions are infinitely differentiable and form an orthogonal basis.

Additionally, Fourier series are global decompositions, providing optimal approximations on a finite support [39]. Recall that Fourier series is an example of a trigonometric series, but not all trigonometric series are Fourier series. Particularly, the truncated Fourier series provides the best approximation in the L^2-norm among all truncated trigonometric series (see Theorem 2.3.1).

For these reasons, we explore the idea of employing a 2D Fourier series expansion as an approximation for $\hat{\phi}_p$. We will consider the $x-$ and $\tau-$dimension separately in order to determine the most suitable approximation for each.

4.4.1. x-DIMENSION

Regarding the x-dimension, notice that we impose Dirichlet boundary conditions for x in (4.16). Therefore, it is intuitive to consider a sine expansion to approximate the x-dimension. This choice guarantees that the function takes on a value of 0 at the extremes $x = a$ and $x = b$.

This is corroborated by literature on the reflection method used to solve boundary value problems on a finite interval $(0, L)$ (see e.g. [57]). In the reflection method, one takes an odd extension of the data in the case of Dirichlet boundary conditions. Then, the resulting extended data is odd on the symmetric interval $(-L, L)$, and is extended to be periodic with period $2L$ to the rest of the real line. This is similar to the approximation produced by a sine series, as described in Section 2.3. Conversely, in the case of an even extension, whereby the solution is expressed as a cosine series, the solution to the PDE naturally satisfies Neumann boundary conditions.

To better visualize the idea of approximating the x-dimension with a sine series, let us isolate this dimension by writing it as function f_1 of x. Let $S_N f_1(x)$ denote the sine

expansion of f_1 truncated at level N on the domain $[a_1, b_1]$, then

$$f_1(x) \approx S_N f_1(x) = \sum_{k_1=1}^{N} A_{k_1} \sin\left(k_1\pi \frac{x-a_1}{b_1-a_1}\right), \tag{4.17}$$

where a_1 and b_1 are appropriate bounds for the sine expansion, i.e. $a_1 = a$ and $b_1 = b$.

4.4.2. τ-DIMENSION

Intuitively, one could now consider a sine or cosine expansion for $\hat{\phi}_p$. However, these particular formulations are not suitable for τ. As described in Section 4.2, we expect the τ-dimension to be described by an exponential function, with a dependency on the index of the series expansion for the x-dimension. Plus, from the analysis in Section 3.1, using sine or cosine series is not appropriate in such context. Thus, for the τ-dimension, we consider that the derivative with respect to τ is a cosine expansion and, thus, the original function is the integral of that cosine series. This has been tested in Chapter 3 to have a better convergence rate than applying a direct expansion of the function itself.

To illustrate the idea, we isolate what happens on this dimension by writing it as function f_2 of τ. Let $S_N f_2'(\tau)$ denote the cosine expansion of f_2' truncated at level $N-1$ on the domain $[a_2, b_2]$. Then, we have that

$$\begin{aligned} f_2'(\tau) \approx S_N f_2'(\tau) &= {\sum_{k_2=0}^{N-1}}' A_{k_2} \cos\left(k_2\pi \frac{\tau-a_2}{b_2-a_2}\right) \\ \implies T_N f_2(\tau) &= \sum_{k_2=1}^{N-1} A_{k_2} \frac{b_2-a_2}{k_2\pi} \sin\left(k_2\pi \frac{\tau-a_2}{b_2-a_2}\right) + \frac{1}{2} A_{k,0}(\tau-a_2) + f_2(a_2), \end{aligned} \tag{4.18}$$

where the FTC was used, and a_2 and b_2 are appropriate bounds for the cosine expansion. Notice that this is not a sine series due to the presence of the term $\frac{1}{2}A_{k,0}(\tau-a_2)$. For that reason, we shall refer to the approximation of f_2 as trigonometric expansion, denoted $T_N f_2(x)$.

4.4.3. TRIGONOMETRIC EXPANSION

Taking into account the aforementioned reasoning, we choose to expand the partial derivative of $\hat{\phi}_p$ with respect to τ as follows

$$\frac{\partial \hat{\phi}_p}{\partial \tau}(\tau, x) \approx {\sum_{k=1}^{N}}' {\sum_{k_2=0}^{N-1}}' A_{k_1,k_2} \cos\left(k_2\pi \frac{\tau-a_2}{b_2-a_2}\right) \sin\left(k_1\pi \frac{x-a_1}{b_1-a_1}\right), \tag{4.19}$$

where $a_1 = a$, $b_1 = b$ and $a_2 \geq 0$ since that is the minimum value that the time to maturity τ can assume. Then,

$$\begin{aligned} \hat{\phi}_p(\tau, x) \approx T_N \hat{\phi}_p(\tau, x) &= \int_{a_2}^{\tau} \frac{\partial \hat{\phi}_p}{\partial s}(s, x)\, ds + \hat{\phi}_p(a_2, x) \text{ by the FTC} \\ &= \sum_{k_1=1}^{N} \sum_{k_2=1}^{N-1} A_{k_1,k_2} \frac{b_2-a_2}{k_2\pi} \sin\left(k_2\pi \frac{\tau-a_2}{b_2-a_2}\right) \sin\left(k_1\pi \frac{x-a_1}{b_1-a_1}\right) \\ &\quad + \sum_{k_1=1}^{N} \frac{1}{2} A_{k_1,0}(\tau-a_2) \sin\left(k_1\pi \frac{x-a_1}{b_1-a_1}\right) + \hat{\phi}_p(a_2, x). \end{aligned} \tag{4.20}$$

Since $\hat{\phi}_p(a_2, x)$ is only known at initial time ($\tau = 0$), we must have $a_2 = 0$, and thus,

$$T_N\hat{\phi}_p = \sum_{k_1=1}^{N}\sum_{k_2=1}^{N-1} A_{k_1,k_2}\frac{b_2-a_2}{k_2\pi}\sin\left(k_2\pi\frac{\tau-a_2}{b_2-a_2}\right)\sin\left(k_1\pi\frac{x-a_1}{b_1-a_1}\right) + \sum_{k_1=1}^{N} A_{k_1,0}\frac{1}{2}\tau\sin\left(k_1\pi\frac{x-a_1}{b_1-a_1}\right) + \sin\left(p\pi\frac{x-a_1}{b_1-a_1}\right), \text{ with } a_2 = 0. \tag{4.21}$$

While we start with a 2D Fourier series representation of $\frac{\partial\hat{\phi}_p}{\partial\tau}$, we do not have a Fourier series expansion for $\hat{\phi}_p$. We will refer to this construction $T_N\hat{\phi}_p$ in (4.21) as a 2D trigonometric expansion for the function $\hat{\phi}_p$, since the basis functions involved are trigonometric functions. It is worth noting that, this is not a simple application of Fourier basis in the context of collocation methods. Instead, we expand the derivative of the original function using a Fourier series and obtain the original function upon integration while taking into account the boundary conditions.

Notice that the boundary conditions $\hat{\phi}_p(\tau, a_1) = \hat{\phi}_p(\tau, b_1) = 0$ are automatically fulfilled for any coefficients A_{k_1,k_2} and the same for the initial condition. In fact, considering this specific structure for approximating $\hat{\phi}_p$ allows us to recover a global approximation suitable for any τ and x, and in particular, it is possible to obtain accurate local approximations for the boundaries and initial time.

Furthermore, the coefficients are now defined by the two-dimensional integrals. They can be stored as a second-order tensor (or matrix)

$$A = \begin{pmatrix} A_{1,0} & A_{1,1} & \dots & A_{1,N-1} \\ A_{2,0} & A_{2,1} & \dots & A_{2,N-1} \\ \vdots & & & \vdots \\ A_{N,0} & \dots & \dots & A_{N,N-1} \end{pmatrix}$$

To ultimately find $\hat{\phi}_p$, we can plug in formula (4.21) in the PDE and obtain the following expression in terms of matrix-vector product

$$\begin{aligned} &-\frac{\partial\hat{\phi}_p}{\partial\tau} + \left(r-\frac{1}{2}\sigma^2\right)\frac{\partial\hat{\phi}_p}{\partial X} + \frac{1}{2}\sigma^2\frac{\partial^2\hat{\phi}_p}{\partial X^2} = 0 \\ \implies &-\mathbf{v}_1 A\mathbf{z}_2^\top + \left(r-\frac{1}{2}\sigma^2\right)\mathbf{z}_1 A\mathbf{v}_2^\top - \frac{1}{2}\sigma^2\mathbf{z}_3 A\mathbf{v}_2^\top + \left(r-\frac{1}{2}\sigma^2\right)\frac{p\pi}{b-a}\cos\left(p\pi\frac{x-a_1}{b_1-a_1}\right) \\ &-\frac{1}{2}\sigma^2\left(\frac{p\pi}{b-a}\right)^2\sin\left(p\pi\frac{x-a_1}{b_1-a_1}\right) = 0 \\ \iff &\mathbf{v}_1 A\mathbf{z}_2^\top - \left(\left(r-\frac{1}{2}\sigma^2\right)\mathbf{z}_1 - \frac{1}{2}\sigma^2\mathbf{z}_3\right)A\mathbf{v}_2^\top = \left(r-\frac{1}{2}\sigma^2\right)\frac{p\pi}{b-a}\cos\left(p\pi\frac{x-a_1}{b_1-a_1}\right) \\ &-\frac{1}{2}\sigma^2\left(\frac{p\pi}{b-a}\right)^2\sin\left(p\pi\frac{x-a_1}{b_1-a_1}\right), \end{aligned} \tag{4.22}$$

where the vectors are given by

$$\mathbf{v}_1 = \left(\sin\left(\pi \tfrac{x-a_1}{b_1-a_1}\right) \quad \cdots \quad \sin\left(N\pi \tfrac{x-a_1}{b_1-a_1}\right) \right),$$
$$\mathbf{v}_2 = \left(1/2\tau \quad \tfrac{b_2-a_2}{\pi} \sin\left(\pi \tfrac{\tau-a_2}{b_2-a_2}\right) \quad \cdots \quad \tfrac{b_2-a_2}{(N-1)\pi} \sin\left((N-1)\pi \tfrac{\tau-a_2}{b_2-a_2}\right) \right),$$
$$\mathbf{z}_1 = \left(\tfrac{\pi}{b_1-a_1} \cos\left(\pi \tfrac{x-a_1}{b_1-a_1}\right) \quad \cdots \quad \tfrac{N\pi}{b_1-a_1} \cos\left(N\pi \tfrac{x-a_1}{b_1-a_1}\right) \right),$$
$$\mathbf{z}_2 = \left(1/2 \quad \cos\left(\pi \tfrac{\tau-a_2}{b_2-a_2}\right) \quad \cdots \quad \cos\left((N-1)\pi \tfrac{\tau-a_2}{b_2-a_2}\right) \right),$$
$$\mathbf{z}_3 = \left(\left(\tfrac{\pi}{b_1-a_1}\right)^2 \sin\left(\pi \tfrac{x-a_1}{b_1-a_1}\right) \quad \cdots \quad \left(\tfrac{N\pi}{b_1-a_1}\right)^2 \sin\left(N\pi \tfrac{x-a_1}{b_1-a_1}\right) \right).$$

Given the above formula, we wish to solve it in order to find the matrix A (containing the unknown coefficients) that satisfies the equation. In order to do that, a grid with combinations of values of x and τ needs to be defined. We choose $M \times M$ training points, with $M = N$ to prevent overfitting, as discussed in Chapter 3. This means that we assume M training points for each dimension. Let x_m be the m-th training point in the log-asset dimension, for $m = 1, ..., M$, and τ_ℓ the ℓ-th training point in the time dimension, for $l = 0, ..., M-1$.

Subsequently, we define matrices out of the vectors previously defined, with M rows, one for each training point, and N columns, as follows

$$\mathbf{V}_1[m,:] = \left(\sin\left(\pi \tfrac{x_m-a_1}{b_1-a_1}\right) \quad \cdots \quad \sin\left(N\pi \tfrac{x_m-a_1}{b_1-a_1}\right) \right),$$

and equivalently for matrices $\mathbf{V}_2, \mathbf{Z}_1, \mathbf{Z}_2, \mathbf{Z}_3$. Here $\mathbf{V}_1[m,:]$ stands for the m-th row of matrix $\mathbf{V}_1$.

Then, the pricing PDE evaluated at point (x_m, τ_ℓ) becomes

$$\begin{aligned} &\mathbf{V}_1[m,:] A \mathbf{Z}_2[\ell,:]^\top - \left(\left(r - \frac{1}{2}\sigma^2\right)\mathbf{Z}_1[m,:] - \frac{1}{2}\sigma^2 \mathbf{Z}_3[m,:]\right) A \mathbf{V}_2[\ell,:]^\top \\ &= \left(r - \frac{1}{2}\sigma^2\right) \frac{p\pi}{b_1-a_1} \cos\left(p\pi \frac{x_m-a_1}{b_1-a_1}\right) - \frac{1}{2}\sigma^2 \left(\frac{p\pi}{b_1-a_1}\right)^2 \sin\left(p\pi \frac{x_m-a_1}{b_1-a_1}\right). \end{aligned} \tag{4.23}$$

Before solving the linear system for A, note that (4.23) is not a standard linear system of the form $My = b$, which has to be solved for the unknown vector y. Instead, the system can be seen as a matrix equation, in which the unknown matrix A has to be solved. A previous thesis done at FF Quant [58] showed how to transform (4.23) into a equation of the form $My = b$ by vectorizing the matrix $A \in \mathbb{R}^{N\times N}$ into a vector $\text{vec}(A) \in \mathbb{R}^{N^2}$. We shall consider the vectorization which stacks all the columns of A vertically in order,

$$\text{vec}(A) = \begin{pmatrix} A[:,1] \\ A[:,2] \\ \vdots \\ A[:,N] \end{pmatrix}_{N^2\times 1} \tag{4.24}$$

Now, consider the matrix-vector products in (4.23), where $\mathbf{V}_1[m,:] \in \mathbb{R}^{1\times N}$, $A \in \mathbb{R}^{N\times N}$, $\mathbf{Z}_2[\ell,:]^\top \in \mathbb{R}^{N\times 1}$, and thus,

$$\mathbf{V}_1[m,:]A\mathbf{Z}_2[\ell,:]^\top = \sum_{k_1=1}^{N}\sum_{n=0}^{N-1}\mathbf{V}_1[m,k]A[k,n]\mathbf{Z}_2[n,\ell]\,. \tag{4.25}$$

Applying $\text{vec}(\mathbf{ab}^T) = \mathbf{b}\otimes\mathbf{a}$, where $\otimes$ denotes the Kronecker product, and the linearity of the $\text{vec}(\cdot)$ operator, we have

$$\begin{aligned}\text{vec}(\mathbf{V}_1[m,:]A\mathbf{Z}_2[\ell,:]^\top) &= \sum_{k_1=1}^{N}\sum_{n=0}^{N-1}A[k,n]\mathbf{Z}_2[\ell,:](:,n)\otimes\mathbf{V}_1[m,:](:,k)\\ &= (\mathbf{Z}_2[\ell,:]\otimes\mathbf{V}_1[m,:])\text{vec}(A)\,.\end{aligned} \tag{4.26}$$

In this way, we are able to represent (4.23) in vectorized format,

$$\begin{aligned}&\left[(\mathbf{Z}_2[\ell,:]\otimes\mathbf{V}_1[m,:]) - \left(\mathbf{V}_2[\ell,:]\otimes\left(\left(r-\frac{1}{2}\sigma^2\right)\mathbf{Z}_1[m,:] - \frac{1}{2}\sigma^2\mathbf{Z}_3[m,:]\right)\right)\right]\text{vec}(A)\\ &= \left(r-\frac{1}{2}\sigma^2\right)\frac{p\pi}{b-a}\cos\left(p\pi\frac{x_m-a}{b-a}\right) - \frac{1}{2}\sigma^2\left(\frac{p\pi}{b-a}\right)^2\sin\left(p\pi\frac{x_m-a}{b-a}\right),\ \text{for fixed } p.\end{aligned} \tag{4.27}$$

Thus, we construct a matrix whose rows are given by

$$\mathbf{Z}_2[\ell,:]\otimes\mathbf{V}_1[m,:] - \mathbf{V}_2[\ell,:]\otimes\left(\left(r-\frac{1}{2}\sigma^2\right)\mathbf{Z}_1[m,:] - \frac{1}{2}\sigma^2\mathbf{Z}_3[m,:]\right),$$

and the elements of the RHS vector are given by

$$\left(r-\frac{1}{2}\sigma^2\right)\frac{p\pi}{b_1-a_1}\cos\left(p\pi\frac{x_m-a_1}{b_1-a_1}\right) - \frac{1}{2}\sigma^2\left(\frac{p\pi}{b_1-a_1}\right)^2\sin\left(p\pi\frac{x_m-a_1}{b_1-a_1}\right),$$

for each pair (x_m,τ_ℓ).

For a more intuitive visualization, consider the following representation of the matrix

$$\begin{array}{c}(\tau_0,x_1):\\(\tau_0,x_2):\\\vdots\\(\tau_0,x_M):\\(\tau_1,x_1):\\\vdots\\(\tau_{M-1},x_M):\end{array}\begin{pmatrix}\mathbf{Z}_2[:,0]\otimes\mathbf{V}_1[:,1]-\mathbf{V}_2[:,0]\otimes\left(\left(r-\frac{1}{2}\sigma^2\right)\mathbf{Z}_1[:,1]-\frac{1}{2}\sigma^2\mathbf{Z}_3[:,1]\right)\\ \mathbf{Z}_2[:,0]\otimes\mathbf{V}_1[:,2]-\mathbf{V}_2[:,0]\otimes\left(\left(r-\frac{1}{2}\sigma^2\right)\mathbf{Z}_1[:,2]-\frac{1}{2}\sigma^2\mathbf{Z}_3[:,2]\right)\\ \vdots\\ \mathbf{Z}_2[:,0]\otimes\mathbf{V}_1[:,M]-\mathbf{V}_2[:,0]\otimes\left(\left(r-\frac{1}{2}\sigma^2\right)\mathbf{Z}_1[:,M]-\frac{1}{2}\sigma^2\mathbf{Z}_3[:,M]\right)\\ \mathbf{Z}_2[:,1]\otimes\mathbf{V}_1[:,1]-\mathbf{V}_2[:,1]\otimes\left(\left(r-\frac{1}{2}\sigma^2\right)\mathbf{Z}_1[:,1]-\frac{1}{2}\sigma^2\mathbf{Z}_3[:,1]\right)\\ \vdots\\ \mathbf{Z}_2[:,M-1]\otimes\mathbf{V}_1[:,M]-\mathbf{V}_2[:,M-1]\otimes\left(\left(r-\frac{1}{2}\sigma^2\right)\mathbf{Z}_1[:,M]-\frac{1}{2}\sigma^2\mathbf{Z}_3[:,M]\right)\end{pmatrix}$$

and for the RHS vector,

$$\begin{array}{c} (\tau_0, x_1): \\ (\tau_0, x_2): \\ \vdots \\ (\tau_0, x_M): \\ (\tau_1, x_1): \\ \vdots \\ (\tau_{M-1}, x_M): \end{array} \begin{pmatrix} \left(r-\frac{1}{2}\sigma^2\right)\frac{p\pi}{b-a}\cos\left(p\pi\frac{x_1-a}{b-a}\right)-\frac{1}{2}\sigma^2\left(\frac{p\pi}{b-a}\right)^2\sin\left(p\pi\frac{x_1-a}{b-a}\right) \\ \left(r-\frac{1}{2}\sigma^2\right)\frac{p\pi}{b-a}\cos\left(p\pi\frac{x_2-a}{b-a}\right)-\frac{1}{2}\sigma^2\left(\frac{p\pi}{b-a}\right)^2\sin\left(p\pi\frac{x_2-a}{b-a}\right) \\ \vdots \\ \left(r-\frac{1}{2}\sigma^2\right)\frac{p\pi}{b-a}\cos\left(p\pi\frac{x_M-a}{b-a}\right)-\frac{1}{2}\sigma^2\left(\frac{p\pi}{b-a}\right)^2\sin\left(p\pi\frac{x_M-a}{b-a}\right) \\ \left(r-\frac{1}{2}\sigma^2\right)\frac{p\pi}{b-a}\cos\left(p\pi\frac{x_1-a}{b-a}\right)-\frac{1}{2}\sigma^2\left(\frac{p\pi}{b-a}\right)^2\sin\left(p\pi\frac{x_1-a}{b-a}\right) \\ \vdots \\ \left(r-\frac{1}{2}\sigma^2\right)\frac{p\pi}{b-a}\cos\left(p\pi\frac{x_M-a}{b-a}\right)-\frac{1}{2}\sigma^2\left(\frac{p\pi}{b-a}\right)^2\sin\left(p\pi\frac{x_M-a}{b-a}\right) \end{pmatrix}$$

4

CHOICE OF TRAINING POINTS

The accuracy of the solution improves with a greater number of expansion terms. In our case, since $N = M$, it is necessary to select a high number of training points. However, from the analysis in Chapter 3, we were unable to determine the optimal number of training points.

When pinpointing the best location of the training points, two distinct factors must be accounted for: representativeness of the training points and the limitations arising from directly solving the linear system. The representativeness of the training points refers to choosing the best point allocation by taking into account areas of the domain where the function might exhibit bigger fluctuations (e.g. larger absolute gradient values). Intuitively one would concentrate more points in those areas (namely closer to the barrier level) to produce an accurate approximation. But we also need to consider that the location of the training points can significantly impact the stiffness of the resulting system of equations.

Numerical tests seemed to suggest that the optimal choice is an equidistant grid. For unevenly distributed points, the matrix can become ill-conditioned, which leads to inaccurate solutions by directly solving the linear system. On the other hand, however, numerical tests conducted on equally-spaced points with random perturbations yielded results that closely align with those obtained using strictly equally-spaced points, showing only minor disparities. This means that there is potential for improving the trade-off between the system stability and best point allocation. Even though we will use equally-spaced training points, there is room for future research on this matter.

By the formula for $T_N\hat{\phi}_p$, the boundary conditions and the initial condition are fulfilled regardless of the value of the coefficients A_{k_1,k_2}. Hence, including the points $x = a_1, x = b_1$ and $\tau = a_2 = 0$ in the set of training will not bring any new information to the system. Therefore, we define $x_1 > a_1$, $x_M < b_1$, $\tau_0 > a_2$ and $\tau_{M-1} = b_2$. Since the PDE is valid for any $0 < \tau < T$, we can choose any maturity $T \equiv b_2$ that is adequate for the type of options that we wish to price.

Consider, for instance, a scenario with $M = 64$ evenly-distributed training points for each dimension. The matrix generated by this setup is visually depicted in Figure 4.1. Unfortunately, no regularity pattern nor interesting properties such as symmetry and positive definiteness were identified in the resulting matrix. This is mainly due to the

fact that we consider a trigonometric expansion for $\hat{\phi}_p$ that contains a τ-term for $A_{k_1,0}$ (i.e. when $k_2 = 0$), instead of a Fourier series.

As a result, we opted for a direct solver built in Python to solve the linear system. The direct solver we use is `scipy.linalg.solve()`. The manual reads that the computational complexity is $\mathcal{O}(n^3)$, for a matrix of size $n \times n$. However, testing results suggest that is of order $\mathcal{O}(n^2)$. In our case, dealing with a matrix of size $N^2 \times N^2$, where N represents the number of expansion terms per dimension, the computational complexity for solving the linear system can escalate to $\mathcal{O}(N^4)$. With increasing values of N, this leads to greater CPU time.

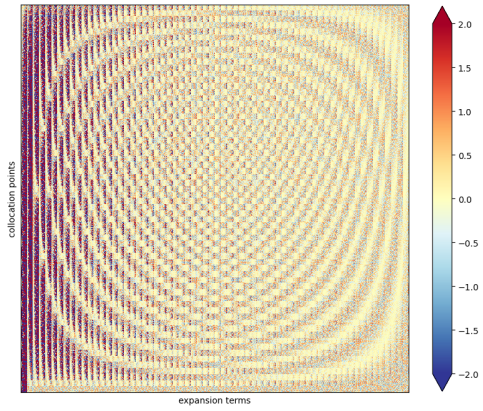

Figure 4.1: Visual representation of the matrix values for $N = M = 64$ expansion terms and training points in all dimensions.

Note that there are values well above 2 and well below -2, but for a better visualization of the values overall in the matrix, this was the chosen range for the color scale.

4.5. RESULTS

This section presents some illustrative examples of the accuracy of the approach developed in previous sections for pricing up-and-out barrier options. Namely, we compare $\hat{\phi}_p$ to the benchmark established in Section 4.2, compare the resulting price to the analytical solution provided by equation (2.5), and also calculate the option's Greeks with respect to the asset price.

However, before we delve into that, it is important to acknowledge a fundamental assumption made when we choose a trigonometric expansion (4.21) to approximate $\hat{\phi}_p$. We assume that this approximation perfectly describes the function $\hat{\phi}_p$ and its partial derivatives. Therefore, we assume that the original functions are smooth and continuous in the entire domain. As a consequence, the coefficients we obtain from this PDE approach represent those of a perfect replication of an entire smooth function.

As a result, $\hat{\phi}_p$ and its partial derivatives, computed with the approximated coefficients via our PDE approach, do not exhibit discontinuities or Dirac deltas. This will be reflected in the results for the option price and its Greeks.

4.5.1. SURVIVAL CH.F.

Using the results derived in Section 4.2, we are able to benchmark $\hat{\phi}_p$ obtained via our approach. Notice that the benchmark itself is also a series approximation, meaning that its accuracy will not be as good as that of a closed-form solution. One should keep that in mind when comparing the results for $\hat{\phi}_p$ under our approach against that benchmark.

Since we anticipate the τ-dimension to be expressed as an exponential-type function, it is reasonable to expect that, as p increases, the approximations for $\hat{\phi}_p$ will worsen, taking into account the analysis performed in Section 3.2.1.

In Figure 4.2, we plot the relative error between $\hat{\phi}_p$ obtained via the alternative series formulation from Section 4.2 (the benchmark) and via our approach, for $N = M = 64$ and different values of p. We use use the set of training points to compute the error and for benchmark values below 10^{-5}, the absolute error is computed instead.

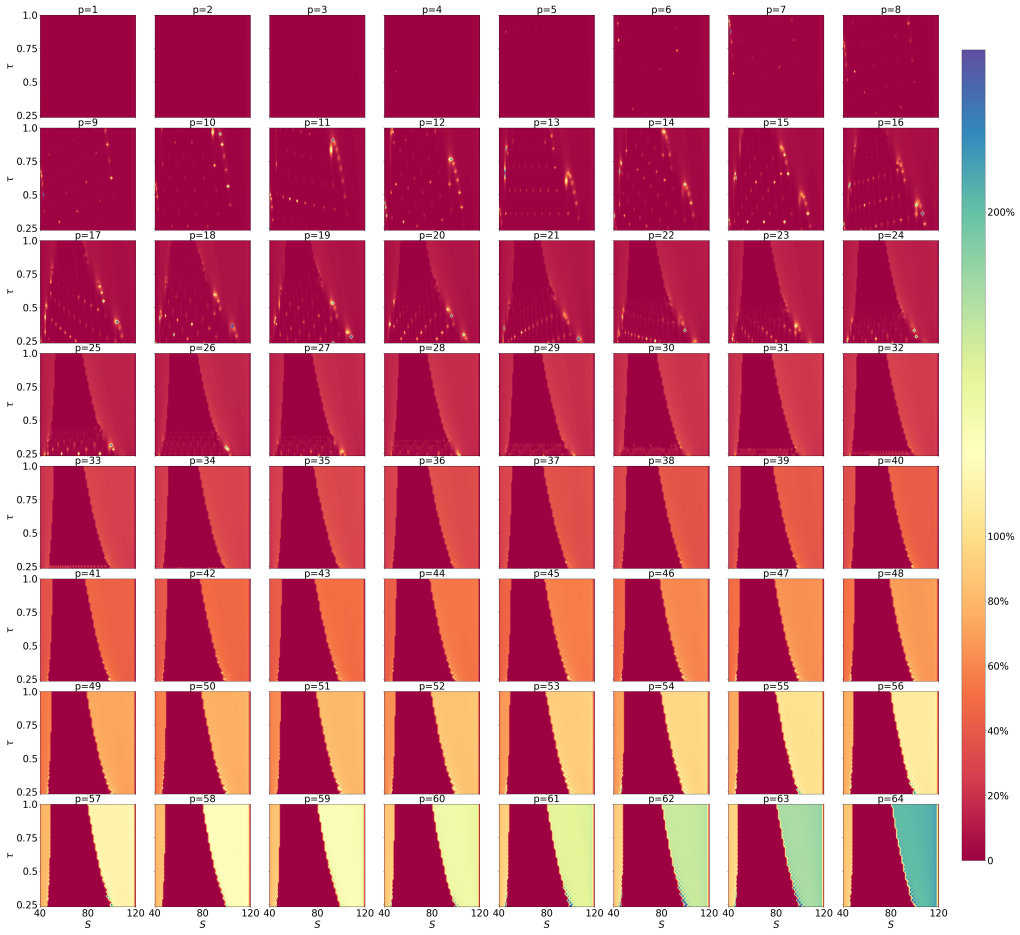

Figure 4.2: Relative error of $\hat{\phi}_p$ obtained via benchmark vs. our approach, for p between 1 and 64.

Notice that for higher values of p, there is an evident error increase closer to the extremes of the asset price domain $S \in [40, 120]$.

Table 4.1 below evidences the convergence regarding the error of $\hat{\phi}_p$, for $S = 110$, varying time to maturity values τ and distinct values of p. In addition, Figure 4.3 shows the L^∞-norm error between the approximated $\hat{\phi}_p$ and the benchmark, computed for the set of training points. Note that the results demonstrate once again that the error tends to increase as the value of p becomes larger.

		Number of expansion terms (N)							
		16		32		64		128	
τ	p	abs error	% error	abs error	% error	abs error	% error	abs error	% error
1	1	5.26e-03	6.55	1.27e-03	1.58	3.10e-04	0.39	7.64e-05	0.09
	5	2.09e-02	10.39	4.91e-03	2.44	1.117e-03	0.58	2.89e-04	0.14
	10	2.68e-02	38.32	5.08e-03	7.26	1.17e-03	1.68	2.86e-04	0.40
	15	3.26e-02	168.61	3.93e-03	20.34	8.55e-04	4.43	2.05e-04	1.06
0.5	1	5.11e-03	3.78	1.28e-03	0.95	3.103-04	0.23	7.65e-05	0.06
	5	2.38e-02	5.76	5.72e-03	1.38	1.37e-03	0.33	3.37e-04	0.08
	10	4.05e-02	20.32	8.21e-03	4.12	1.903-03	0.95	4.64e-04	0.23
	15	6.27e-02	122.50	7.94e-03	15.51	1.74e-03	3.39	4.18e-04	0.82
0.25	1	2.59e-03	1.43	7.13e-04	0.39	1.69e-04	0.09	4.20e-05	0.02
	5	1.32e-02	2.10	3.48e-03	0.55	8.21e-04	0.13	2.04e-04	0.03
	10	2.42e-02	6.50	5.98e-03	1.60	1.37e-03	0.37	3.37e-04	0.09
	15	3.79e-02	60.37	6.28e-03	10.02	1.37e-03	2.18	3.30e-04	0.52

Table 4.1: Absolute and relative error convergence for $\hat{\phi}_p$ obtained via our approach vs. alternative series formulation (benchmark), for $S = 110$ and different values of τ.

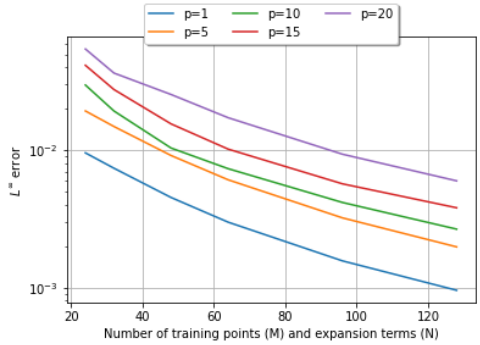

Figure 4.3: L^∞-norm error for $\hat{\phi}_p$ using our approach vs. alternative series formulation (benchmark), for different values of p.

4.5.2. OPTION PRICES

Now we compute the price of an up-and-out call option with parameters $(r, \sigma, K, B) = (0.1, 0.1, 90, 120)$. To obtain the value of the option via our approach, $N = 64$ expansion terms were used. The respective result is benchmarked against the closed-form solution from equation (2.5) and the results are depicted in Figure 4.4.

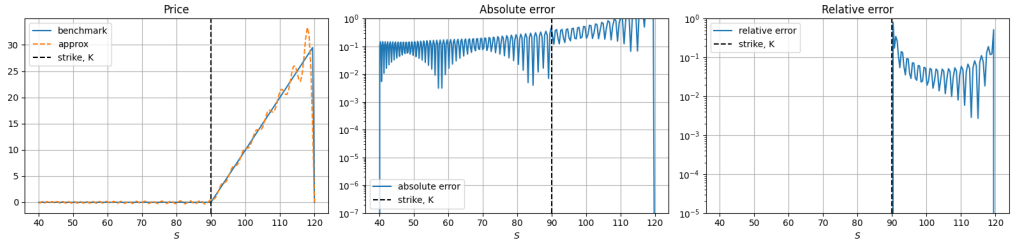

(a) Payoff at maturity level ($\tau = 0$) alongside the absolute and relative errors.

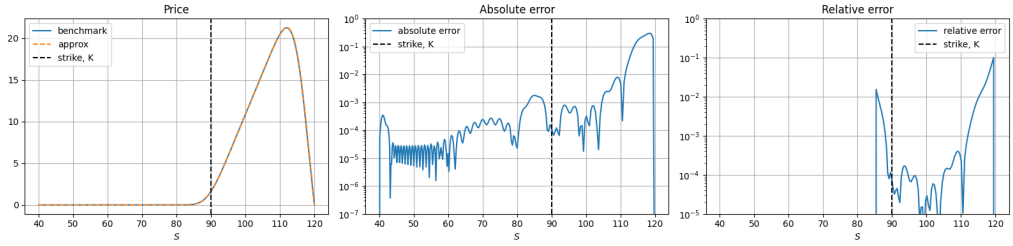

(b) Price, absolute and relative errors for $\tau = 0.1$.

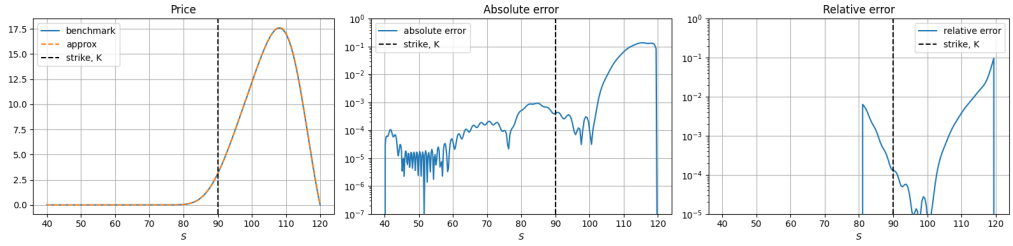

(c) Price, absolute and relative errors for $\tau = 0.25$.

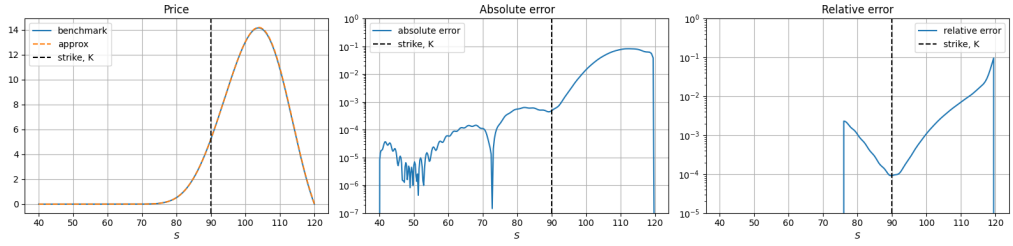

(d) Price, absolute and relative errors for $\tau = 0.5$.

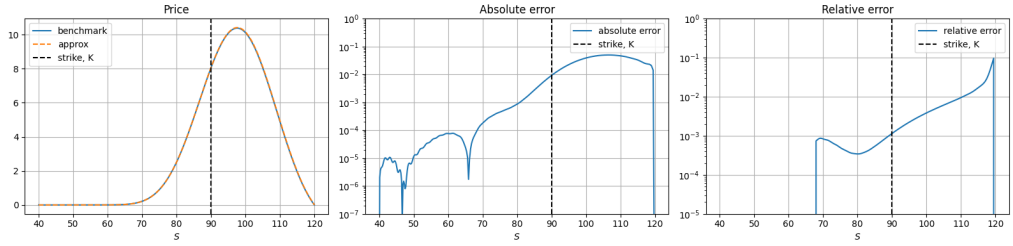

(e) Price, absolute and relative errors for $\tau = 1$.

Figure 4.4: Price and respective errors for different values of τ, using our approach vs. closed-form solution.

For an option at maturity level ($\tau = 0$), its value is just the payoff function, which exhibits a sharp corner at the strike level K, and a jump at the barrier level B. For that reason, the value of the option as approximated by (4.12), exhibits Gibbs phenomenon. That is, there are oscillations in the whole domain and, particularly, in those points.

However, as the maturity increases, the value function becomes smoother and, hence, formula (4.12) is able to recover better the true shape of this function, as shown in the plots above.

To better understand the error level for the price of all training points (τ_ℓ, x_m) against a set of non-training points, we compare the respective errors in Figure 4.5 below. There the relative error is computed for both sets of points separately. The possible values for τ are set above 0.01. This is because lower values tend to yield larger errors, due to the previously discussed limitation of the sine pricing formula.

Overall the relative error exhibits very similar behaviour in the two sets, since we are using a global approximation formulation for $\hat{\phi}_p$. Nonetheless, the error is lower for the training points as these were used to recover the coefficients of $T_N\hat{\phi}_p$.

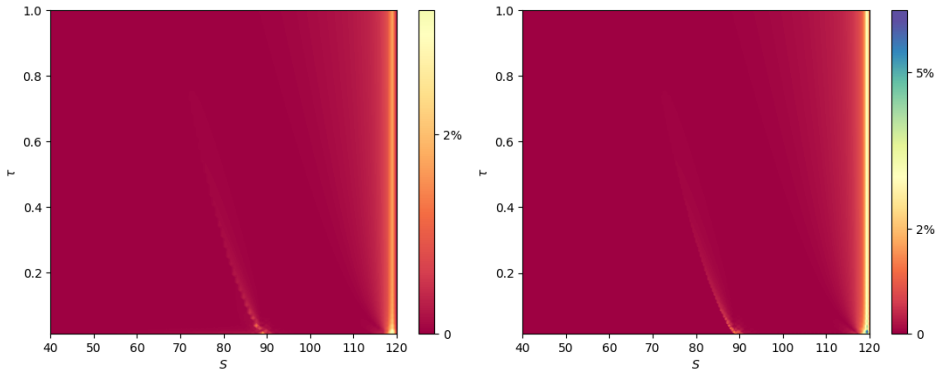

(a) Set of training points.

(b) Set of non-training points.

Figure 4.5: Relative error between the closed-form price and the approximated option price using our approach, for multiple asset prices and maturities.

Notice that for both sets of points, the error is bigger for smaller maturities and closer to the barrier level, $B = 120$. The reason for both these phenomena lies on the fact that very close to the barrier level, the price function exhibits steep skew (as a function of x), especially for smaller maturities. To exemplify this, we plot in Figure 4.6 the pricing function of an up-and-out call option for $\tau = 0.1$ and $\tau = 1$. Notice that for values of x in $[4.6, 4.8]$, the price function decreases by 10, when $\tau = 1$. When $\tau = 0.1$,the price function decreases by 20 for x in $[4.7, 4.8]$.

Therefore, the results observed in Figures 4.4 and 4.5 come as no surprise, since we have seen in Chapter 3 - when analysing the best series approximation for an exponential function - that cosine or sine series have the limitation that a very high number of expansion terms is needed for a converging approximation to a steep smooth function. Consequently, the relative error is bigger for smaller maturities and closer to the barrier level. In light of this, some improvements to the method will be introduced in Chapter 6.

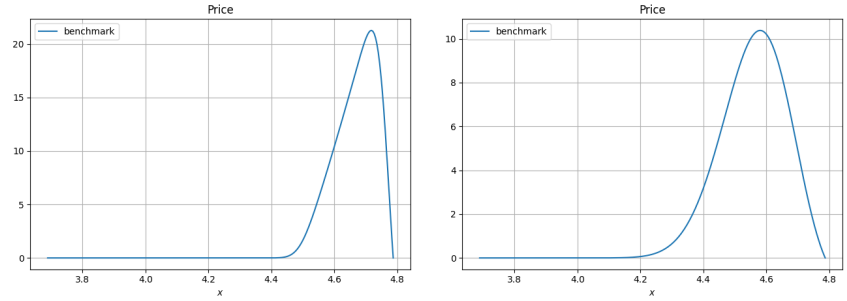

Figure 4.6: Option prices as a function of x for $\tau = 0.1$ (left) and $\tau = 1$ (right), using the closed-form solution.

Finally, table 4.2 presents convergence test results for a fixed asset price of $S = 110$ and different values of τ. All other parameters remain consistent with previous settings. Even though the error decreases as N increases, a very slow convergence rate is observed.

	Number of expansion terms (N)							
	16		32		64		128	
τ	abs error	% error	abs error	% error	abs error	% error	abs error	% error
1	7.16e-01	14.62	1.86e-01	3.80	4.66e-02	0.95	1.17e-02	0.24
0.5	9.54e-01	8.79	2.96e-01	2.73	7.72e-02	0.71	1.97e-02	0.18
0.25	5.00e-01	2.94	2.23e-01	1.31	6.48e-02	0.38	1.74e-02	0.10
0.1	8.80e-01	4.29	1.67e-02	0.08	5.16e-03	0.03	7.48e-04	0.003

Table 4.2: Absolute and relative error convergence for the option price obtained via our approach vs. closed-form solution, for $S = 110$ and different values of τ.

4.5.3. OPTION DELTA AND GAMMA

The Delta of a barrier option can jump near the barrier, producing a discontinuity at the barrier level, as illustrated by the example in Figure 4.7. Hence, near the barrier, the Gamma can be very large and at the barrier level it turns into a Dirac delta. On top of this, Gamma can actually change sign around the barrier.

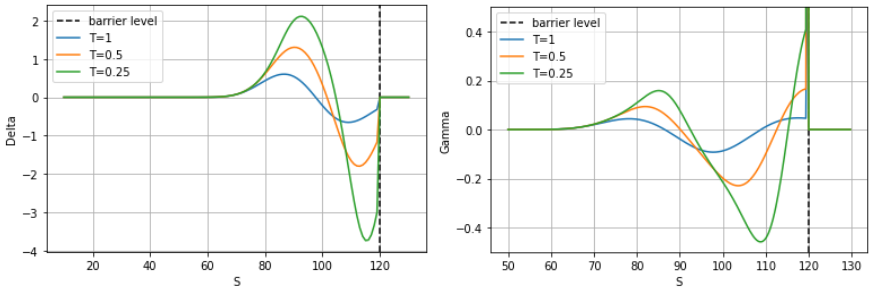

(a) Delta. (b) Gamma.

Figure 4.7: Example of Greeks' profile of an up-and-out call option, for $r = 0.1$, $\sigma = 0.1$, $K = 90$, $B = 120$ and different maturities.

From equation (4.12), the Delta and Gamma of a barrier option can be computed using the derivatives of $\hat{\phi}_p$ through the following equations

$$\frac{\partial V}{\partial S} = \frac{1}{S}\frac{\partial V}{\partial X} = e^{-r(T-t)} \sum_{p=1}^{N} \frac{\partial \hat{\phi}_p}{\partial X}(t,x)\frac{V_p}{S} = e^{-r(T-t)} \sum_{p=1}^{N} \mathrm{Im}\left\{ \frac{\partial \phi}{\partial X}\left(\frac{p\pi}{b-a}, t; x\right) e^{-ip\pi\frac{a}{b-a}} \right\} \frac{V_p}{S}, \tag{4.28}$$

$$\begin{aligned} \frac{\partial^2 V}{\partial S^2} &= \frac{1}{S^2}\left(\frac{\partial^2 V}{\partial X^2} - \frac{\partial V}{\partial X}\right) \\ &= e^{-r(T-t)} \sum_{p=1}^{N} \left(\frac{\partial^2 \hat{\phi}_p}{\partial X^2}(t,x) - \frac{\partial \hat{\phi}_p}{\partial X}(t,x) \right) \frac{V_p}{S^2} \\ &= e^{-r(T-t)} \sum_{p=1}^{N} \mathrm{Im}\left\{ \left[\frac{\partial^2 \phi}{\partial X^2}\left(\frac{p\pi}{b-a}, t; x\right) - \frac{\partial \phi}{\partial X}\left(\frac{p\pi}{b-a}, t; x\right) \right] e^{-ip\pi\frac{a}{b-a}} \right\} \frac{V_p}{S^2}, \end{aligned} \tag{4.29}$$

which means that the derivative of V with respect to X is passed onto the derivative of $\hat{\phi}_p$ with respect to X and the same for the second order derivative. In turn, the derivatives of $\hat{\phi}_p$ are passed onto the derivatives of the survival ch.f., and thus, of the respective survival pdf.

Given that the Delta and Gamma of an option can be obtained as in equation (4.28) and (4.29), respectively, another benefit of our approach is also clear: we are able to retrieve the Delta and Gamma of a barrier option easily in series format, once we obtain the approximation for $\hat{\phi}_p$ from formula (4.21). Figures 4.8-4.10 illustrate these Greeks obtained for different maturities using $T_N\hat{\phi}_p$ with $N = 64$ expansion terms.

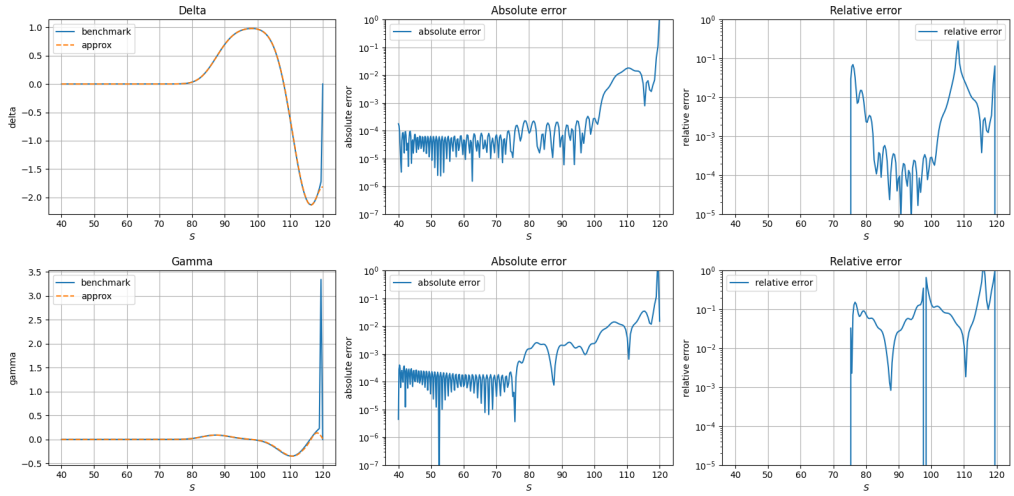

Figure 4.8: Greeks computed using our approach for maturity $\tau = 0.25$.

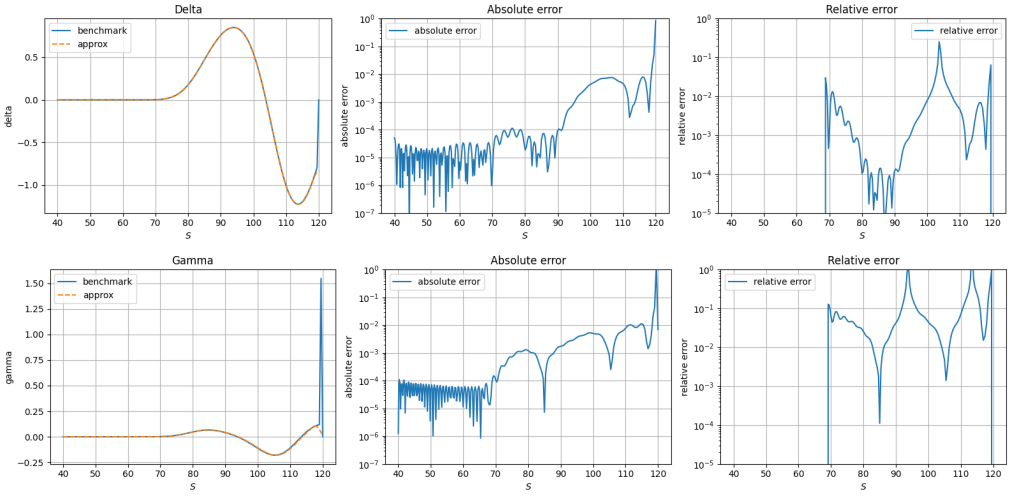

Figure 4.9: Greeks computed using our approach for maturity $\tau = 0.5$.

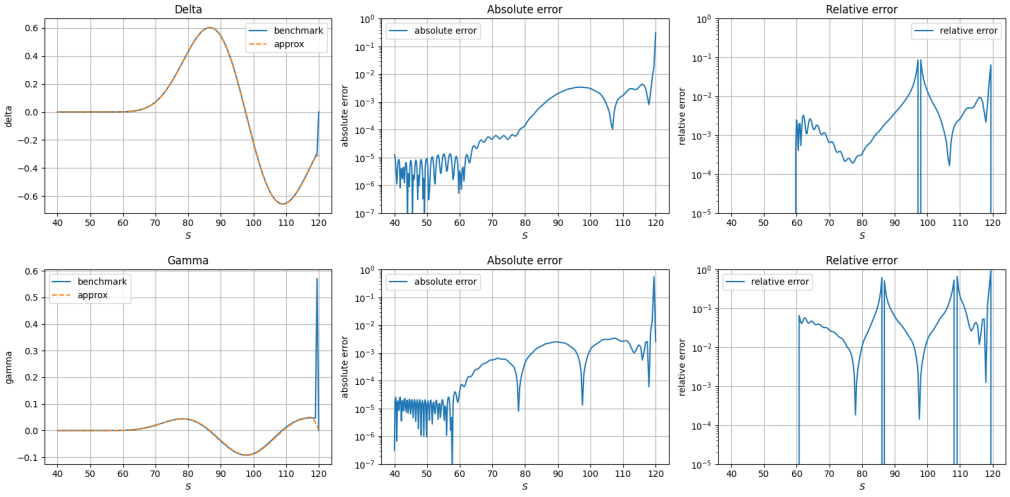

Figure 4.10: Greeks computed using our approach for maturity $\tau = 1$.

Notice that, in the benchmark plots, the sudden peak for Gamma at $x = a$ is a Dirac delta.

As mentioned in the beginning of this section, this approach does not inherently account for $\frac{\partial V}{\partial X}(a) = \frac{\partial V}{\partial X}(b) = 0$, as this only happens because there is a discontinuity at those points. The approximation obtained for $\frac{\partial \hat{\phi}_p}{\partial X}$ is continuous at those points, implying that $\frac{\partial V}{\partial X}$ is also continuous at those points (refer to Figures 4.8, 4.9 and 4.10). To enforce a Delta value of 0 at $x = a$ and b, we could include constraints on the first deriva-

tive of $\hat{\phi}_p$ in the system, but that would lead to a Delta function that continuously approaches 0 at $x = a$ and $x = b$ nonetheless.

Finally, our approximation of Gamma fails to capture the Dirac delta at the barrier level. This discrepancy arises because $\frac{\partial^2 \hat{\phi}_p}{\partial X^2}$ is also continuous in the entire domain $[a, b]$.

5

OUR APPROACH: PRICING BARRIER OPTIONS VIA TRIGONOMETRIC EXPANSION UNDER HESTON'S MODEL

In this chapter, we introduce our novel approach for pricing up-and-out barrier options, under the Heston's stochastic volatility model. Following the same steps as in the GBM case, we start by deriving a formula for the valuation of a barrier option that contains a one-dimensional integral. Its integrand involves a density function that captures the barrier condition, which we refer to as the survival density function. This constitutes one of the key insights of this thesis, facilitating the direct application of the COS pricing method by Fang and Oosterlee [22].

Thereafter, we approximate the sine series coefficients of the survival pdf using a second series expansion. The selection of basis functions in the approximation series is pivotal, and will be analysed in detail, taking into consideration the specific constraints of our research problem. The coefficients of this series are computed from solving the corresponding PDE, derived from the pricing PDE under the Heston's model.

Finally, numerical results are presented in the last section, whereby we compare the resulting option prices with MC simulations.

5.1. THE PRICING PDE

Let S_t be a stochastic process describing the asset price at time t, which will be the underlying for the financial derivative contract. $V(t,S)$ is the value of the contract at time t. Recall that under the risk-neutral measure $\mathbb{Q}$, the stock dynamics and the variance

process v_t are described by the following SDEs, in the Heston's model,

$$\begin{cases} dS_t = & rS_t dt + \sqrt{v_t} S_t d\widetilde{W}_1^{\mathbb{Q}}, \\ dv_t = & \kappa(\bar{v} - v_t)dt + \gamma\sqrt{v_t}\left(\rho d\widetilde{W}_1^{\mathbb{Q}} + \sqrt{1-\rho^2} d\widetilde{W}_2^{\mathbb{Q}}\right), \end{cases} \tag{5.1}$$

with $\widetilde{W}_1^{\mathbb{Q}}$ and $\widetilde{W}_2^{\mathbb{Q}}$ being two independent Brownian motions. Parameters ρ, κ, $\bar{v}$ and γ correspond to the correlation, the speed of mean reversion, the long-term mean of the variance process and the volatility of the volatility, respectively.

The price of an option is given by the discounted expected payoff at time $t < T$ (maturity), i.e.

$$V(t,S,v) = e^{-r(T-t)}\mathbb{E}(V(T,v,S)|\mathscr{F}_t).$$

Applying the Feynman-Kac theorem, it can be shown that the value of the option is the solution to the following pricing PDE:

$$\begin{cases} \frac{\partial V}{\partial t} + rS\frac{\partial V}{\partial S} + \kappa(\bar{v} - v)\frac{\partial V}{\partial v} + \frac{1}{2}vS^2\frac{\partial^2 V}{\partial S^2} + \rho\gamma Sv\frac{\partial^2 V}{\partial S \partial v} + \frac{1}{2}\gamma^2 v\frac{\partial^2 V}{\partial v^2} - rV = 0, \\ V(T,S,v) = f(S_T), \end{cases} \tag{5.2}$$

where $0 \le t \le T$ and $f(\cdot)$ stands for the payoff function. The derivation of this pricing PDE can be done using a martingale approach or a replication and hedging approach, following exactly the same rationale as in Section 2.2 for the BS equation.

Applying a log-transformation of the asset price, $S_t \mapsto X_t := \ln S_t$, the resulting PDE reads

$$\begin{cases} \frac{\partial V}{\partial t} + \left(r - \frac{1}{2}v\right)\frac{\partial V}{\partial X} + \kappa(\bar{v} - v)\frac{\partial V}{\partial v} + \frac{1}{2}v\frac{\partial^2 V}{\partial X^2} + \rho\gamma v\frac{\partial^2 V}{\partial X \partial v} + \frac{1}{2}\gamma^2 v\frac{\partial^2 V}{\partial v^2} - rV = 0, \\ V(T,X,v) = f(X_T), \end{cases} \tag{5.3}$$

where $0 \le t \le T$.

5.1.1. VALUATION OF BARRIER OPTIONS

Let us consider once again an up-and-out barrier option, where $\tau_B := \inf\{\tilde{t} \ge t : S_{\tilde{t}} \ge B \Leftrightarrow X_{\tilde{t}} \ge b\}$, with $b = \ln B$, is the first time that the process S_t hits the upper boundary B. The payoff of an up-and-out barrier option is then given by $f(X_T)\mathbb{1}_{\{\tau_B > T\}}$, where $f(\cdot)$ is the payoff function of an European option. The value of such an option can be written as

$$\begin{aligned} V(t,x,v) &= e^{-r(T-t)}\mathbb{E}^{\mathbb{Q}}\left(f(X_T)\mathbb{1}_{\{\tau_B > T\}}|\mathscr{F}_t\right) \\ &= e^{-r(T-t)}\mathbb{E}^{\mathbb{Q}}\left(f(X_T)\mathbb{1}_{\{\tau_B > T\}}|X_t = x, v_t = v\right) \\ &= e^{-r(T-t)}\mathbb{E}^{\mathbb{Q}}\left[\mathbb{E}^{\mathbb{Q}}\left(f(X_T)\mathbb{1}_{\{\tau_B > T\}}|X_t = x, v_t = v, \mathbb{1}_{\{\tau_B > T\}}\right)\right] \\ &= 0 \cdot \mathbb{P}(\tau_B \le T|X_t = x, v_t = v) \\ &\quad + e^{-r(T-t)}\mathbb{E}^{\mathbb{Q}}[f(X_T)|X_t = x, v_t = v, \tau_B > T] \cdot \mathbb{P}(\tau_B > T|X_t = x, v_t = v) \\ &= e^{-r(T-t)}\left(\int_{\mathbb{R}} f(y)p(y|x,v,\tau_B > T)dy\right) \cdot \mathbb{P}(\tau_B > T|x,v) \\ &= e^{-r(T-t)}\int_{\mathbb{R}} f(y)\underbrace{p(y,\tau_B > T|x,v)}_{=\int_0^\infty p(y,u,\tau_B > T|x,v)du} dy, \end{aligned} \tag{5.4}$$

where $p(y, \tau_B > T|x, v)$ is the joint transition density function such that the realized path does not cross the barrier B (from below) before maturity T.

Just as in the GBM case, the derivations in (5.4) show that the value of the option can be represented by a one-dimensional expectation, where the density function captures the barrier condition. For that reason, the COS pricing formula from [22] can be directly applied under the Heston's model for barrier options as well, once the survival ch.f. is available. Furthermore, since the payoff function is identical to that of a European option, the payoff coefficients for the COS pricing formula remain the same, and a closed-form formula exists.

THE PRICING PDE FOR BARRIER OPTIONS

We proceed as in the GBM case. Take $b = \ln B$ and a as low as possible, such that X_t can be considered close enough to $-\infty$. For the Heston's model, we need to consider the multivariate version of the localized Feynman-Kac theorem.

Theorem 5.1.1 (Localized Feynman-Kac for Heston's model)**.** *Consider processes (X_t, v_t) whose dynamics are ruled by the Heston's model and take $\tau_{a\vee b} := \inf\{\tilde{t} \geq t : X_{\tilde{t}} \leq a \vee X_{\tilde{t}} \geq b\}$ to be the first time that the process X_t exits the interval (a, b). Let $f : [a, b] \times [0, +\infty) \to \mathbb{R}$ be a continuous payoff function. It follows that*

$$\begin{aligned} V(t, x, v) &= e^{-r(T-t)}\mathbb{E}^{\mathbb{Q}}[f(X_T)\mathbb{1}_{\{\tau_{a\vee b}>T\}}|\mathcal{F}_t] \\ &= e^{-r(T-t)}\mathbb{E}^{\mathbb{Q}}[f(X_T)\mathbb{1}_{\{\tau_{a\vee b}>T\}}|X_t = x, v_t = v] \end{aligned}$$

is the unique, bounded solution of the Heston pricing PDE

$$\frac{\partial V}{\partial t} + \left(r - \frac{1}{2}v\right)\frac{\partial V}{\partial X} + \kappa(\bar{v} - v)\frac{\partial V}{\partial v} + \frac{1}{2}v\frac{\partial^2 V}{\partial X^2} + \rho\gamma v\frac{\partial^2 V}{\partial X \partial v} + \frac{1}{2}\gamma^2 v\frac{\partial^2 V}{\partial v^2} - rV = 0, \text{ for } a < X < b, \tag{5.5}$$

with boundary and terminal conditions

$$\begin{aligned} &V(t, a, v) = 0, \text{ for } 0 \leq t \leq T, 0 < v < +\infty, \\ &V(t, b, v) = 0, \text{ for } 0 \leq t \leq T, 0 < v < +\infty, \\ &\frac{\partial V}{\partial t}\Big|_{v=0} + r\frac{\partial V}{\partial X}\Big|_{v=0} + \kappa\bar{v}\frac{\partial V}{\partial v}\Big|_{v=0} - rV\Big|_{v=0} = 0, \text{ for } 0 \leq t \leq T, a < X < b, \\ &V(T, X, v) = f(X_T), \text{ for } a < X_T < b, 0 < v < +\infty. \end{aligned}$$

Proof. Same as for GBM but applied to the Heston pricing PDE. □

The boundary conditions for $x = a$ and $x = b$ are the same as for the GBM case. As for the boundary condition when $v = 0$, it was established according to Heston's original paper [10], where he substitutes $v = 0$ in the original PDE.

5.2. THE PDE FOR THE SURVIVAL CH.F.

Again we employ the sine formulation for the price of a barrier option (2.32),

$$V(t, x, v) \approx e^{-r(T-t)}\sum_{p=1}^{N}\text{Im}\left\{\phi\left(\frac{p\pi}{b-a}, t; x, v\right)e^{-ip\pi\frac{a}{b-a}}\right\}V_p, \tag{5.6}$$

where ϕ is the survival ch.f. corresponding to $p(y,u,\tau_B > T|x,v)$ and the series coefficients V_p for European (and barrier) options are provided by

$$V_p := \frac{2}{b-a}\int_a^b V(T,y)\sin\left(p\pi\frac{y-a}{b-a}\right)dy, \tag{5.7}$$

where $V(T,y)$ is the value at maturity T, i.e. the payoff function.

Let us denote by $\hat{\phi}_p(t,x,v) := \text{Im}\left\{\phi\left(\frac{p\pi}{b-a},t;x,v\right)e^{-ip\pi\frac{a}{b-a}}\right\}$ the sine series coefficients for the survival pdf. Plugging formula (5.6) into the pricing PDE, we obtain

$$\begin{aligned}
&\frac{\partial V}{\partial t}+\left(r-\frac{1}{2}v\right)\frac{\partial V}{\partial X}+\kappa(\bar{v}-v)\frac{\partial V}{\partial v}+\frac{1}{2}v\frac{\partial^2 V}{\partial X^2}+\rho\gamma v\frac{\partial^2 V}{\partial X\partial v}+\frac{1}{2}\gamma^2 v\frac{\partial^2 V}{\partial v^2}-rV=0\\
\iff& rV+e^{-r(T-t)}\sum_{p=1}^{N}\frac{\partial\hat{\phi}_p}{\partial t}V_p+\left(r-\frac{1}{2}v\right)e^{-r(T-t)}\sum_{p=1}^{N}\frac{\partial\hat{\phi}_p}{\partial X}V_p\\
&+\kappa(\bar{v}-v)e^{-r(T-t)}\sum_{p=1}^{N}\frac{\partial\hat{\phi}_p}{\partial v}V_p+\frac{1}{2}ve^{-r(T-t)}\sum_{p=1}^{N}\frac{\partial^2\hat{\phi}_p}{\partial X^2}V_p\\
&+\rho\gamma ve^{-r(T-t)}\sum_{p=1}^{N}\frac{\partial^2\hat{\phi}_p}{\partial X\partial v}V_p+\frac{1}{2}\gamma^2 ve^{-r(T-t)}\sum_{p=1}^{N}\frac{\partial^2\hat{\phi}_p}{\partial v^2}V_p-rV=0\\
\iff&\sum_{p=1}^{N}\left(\frac{\partial\hat{\phi}_p}{\partial t}+\left(r-\frac{1}{2}v\right)\frac{\partial\hat{\phi}_p}{\partial X}+\kappa(\bar{v}-v)\frac{\partial\hat{\phi}_p}{\partial v}+\frac{1}{2}v\frac{\partial^2\hat{\phi}_p}{\partial X^2}+\rho\gamma v\frac{\partial^2\hat{\phi}_p}{\partial X\partial v}+\frac{1}{2}\gamma^2 v\frac{\partial^2\hat{\phi}_p}{\partial v^2}\right)V_p=0\\
\implies&\frac{\partial\hat{\phi}_p}{\partial t}+\left(r-\frac{1}{2}v\right)\frac{\partial\hat{\phi}_p}{\partial X}+\kappa(\bar{v}-v)\frac{\partial\hat{\phi}_p}{\partial v}+\frac{1}{2}v\frac{\partial^2\hat{\phi}_p}{\partial X^2}+\rho\gamma v\frac{\partial^2\hat{\phi}_p}{\partial X\partial v}+\frac{1}{2}\gamma^2 v\frac{\partial^2\hat{\phi}_p}{\partial v^2}=0,
\end{aligned} \tag{5.8}$$

for every $p\in\mathbb{N}$, whereby the last equation follows from the same reasoning as in the GBM case.

The Feynman-Kac formula 5.1.1 states that $V(t,a,v)=V(t,b,v)=0$, which yields $\hat{\phi}_p(t,a,v)=\hat{\phi}_p(t,b,v)=0$. For the terminal condition, we have that $\sum_{p=1}^{N}\hat{\phi}_p(T,x,v)V_p$ corresponds to the sine series expansion of $V(T,x,v)$, $\sum_{p=1}^{N}\sin\left(p\pi\frac{x-a}{b-a}\right)V_p$. Hence, it follows that $\hat{\phi}_p(T,x,v)=\sin\left(p\pi\frac{x-a}{b-a}\right)$.

Finally, let us set $\tau := T-t$, such that the terminal condition for $\hat{\phi}_p$ becomes an initial condition, i.e. $\hat{\phi}_p(0,x,v)=\sin\left(p\pi\frac{x-a}{b-a}\right)$ and $\frac{\partial\hat{\phi}_p}{\partial t}=-\frac{\partial\hat{\phi}_p}{\partial\tau}$.

To sum up, now we have formulated the following IVBP for the barrier option price under Heston's model

$$\begin{cases}
-\frac{\partial\hat{\phi}_p}{\partial\tau}+\left(r-\frac{1}{2}v\right)\frac{\partial\hat{\phi}_p}{\partial X}+\kappa(\bar{v}-v)\frac{\partial\hat{\phi}_p}{\partial v}+\frac{1}{2}v\frac{\partial^2\hat{\phi}_p}{\partial X^2}+\rho\gamma v\frac{\partial^2\hat{\phi}_p}{\partial X\partial v}+\frac{1}{2}\gamma^2 v\frac{\partial^2\hat{\phi}_p}{\partial v^2}=0, a<X<b,\\
\hat{\phi}_p(\tau,a,v)=0,\\
\hat{\phi}_p(\tau,b,v)=0,\\
\hat{\phi}_p(0,x,v)=\sin\left(p\pi\frac{x-a}{b-a}\right).
\end{cases} \tag{5.9}$$

5.3. APPROXIMATION FOR SURVIVAL CH.F.

A closed-form solution for $\hat{\phi}_p$ does not exist. Therefore, our goal is to find a formula for $\hat{\phi}_p$ by solving the respective PDE.

The PDE (5.9) shares the characteristics of linearity and homogeneity, similar to the conditions we encountered in Chapter 4. Following the same reasoning as before, we opt to approximate $\hat{\phi}_p$ using a series expansion based on trigonometric basis functions. $\hat{\phi}_p$ is now a function of x, τ, and v, and thus, we employ the same expansion construction as in the GBM case for x and τ. Thus, our focus for Heston's model lies in determining the most suitable expansion choice for the v-dimension.

5.3.1. v-DIMENSION

Regarding the v-dimension, notice that assuming a sine series expansion on an interval $[a_3, b_3]$ is not suitable: it would imply that $\hat{\phi}_p(\tau, x, v) = 0$ for $v = a_3$ and $v = b_3$, with $a_3 = 0$ and b_3 sufficiently big (such that the density function value at b_3 is of a very small magnitude), whereas it is not true that $\hat{\phi}_p$ is exactly zero on the two boundaries. Additionally, Heston's paper [10] does not provide the option valuation formula for $v = 0$. Since some extra efforts are needed to find this boundary condition, we opt to assume that value of an option for $v = 0$ is not known, and hence, the value of $\hat{\phi}_p$ at those points also cannot be extrapolated from the respective option value.

It is not a good choice to employ cosine series expansion, either. The reason is that it forces the first derivative with respect to v to be equal to 0 on the boundaries of the interval $[a_3, b_3]$, and we do not know anything about the derivative evaluated on those points.

One idea to circumvent this issue is to use a cosine series expansion on a wider interval, i.e. $[a_3 - \varepsilon, b_3 + \varepsilon]$, instead of $[a_3, b_3]$, for $\varepsilon > 0$ big enough. We have seen in Chapter 3 that this does not work for the τ-dimension because the coefficients of the function with respect to τ depend on the expansion terms for x. However, the Heat equation obtained from applying changes of variables on the Heston pricing PDE in [59] suggests that the function with respect to v does not have any dependencies on the expansion terms for x.

To better visualize this idea, let us emphasize on this dimension by expressing it as a function of v, $f_3(v)$. Let $S_N f_3(v)$ denote the cosine series expansion of f_3 truncated at level $N-1$ with basis functions defined on the domain $[a_3 - \varepsilon, b_3 + \varepsilon]$. That is,

$$\begin{aligned} f_3(v) \approx S_N f_3(v) &= {\sum_{k_3=0}^{N-1}}' A_{k_3} \cos\left(k_3\pi \frac{v - a_3 + \varepsilon}{b_3 - a_3 + 2\varepsilon}\right), \text{ with } a_3 \le v \le b_3 \\ \implies (S_N f_3)'(v) &= -{\sum_{k_3=0}^{N-1}}' A_{k_3} \frac{k_3\pi}{b_3 - a_3 + 2\varepsilon} \sin\left(k_3\pi \frac{v - a_3 + \varepsilon}{b_3 - a_3 + 2\varepsilon}\right). \end{aligned} \tag{5.10}$$

This way, the derivative on the extremes $a_3 - \varepsilon$ and $b_3 + \varepsilon$ is 0, but not on points $v = a_3$ and $v = b_3$.

5.3.2. TRIGONOMETRIC EXPANSION

Following the same reasoning as for the GBM case, we choose to expand the partial derivative of $\hat{\phi}_p$ with respect to τ as a 3D Fourier series, i.e.

$$\frac{\partial \hat{\phi}_p}{\partial \tau}(\tau,x,v) \approx \sum_{k_1=1}^{N} {\sum_{k_2=0}^{N-1}}' {\sum_{k_3=0}^{N-1}}' A_{k_1,k_2,k_3} \sin\left(k_1\pi\frac{x-a_1}{b_1-a_1}\right)\cos\left(k_2\pi\frac{\tau-a_2}{b_2-a_2}\right)\cos\left(k_3\pi\frac{v-a_3+\varepsilon}{b_3-a_4+2\varepsilon}\right), \tag{5.11}$$

where $a_1 = a$, $b_1 = b$, $a_2 = 0$ and $a_3 = 0$ since 0 is the minimum value that the variance v can take in the settings of our IVBP (5.9). Then, by integrating with respect to time, we obtain a trigonometric expansion for $\hat{\phi}_p$,

$$\begin{aligned}
\hat{\phi}_p(\tau,x,v) &\approx T_N\hat{\phi}_p(\tau,x,v)\\
&= \int_0^\tau \frac{\partial \hat{\phi}_p}{\partial s}(s,x,v)\,ds + \hat{\phi}_p(0,x,v) \text{ by the FTC}\\
&= \sum_{k_1=1}^{N} {\sum_{k_2=1}^{N-1}} {\sum_{k_3=0}^{N-1}}' A_{k_1,k_2,k_3} \sin\left(k_1\pi\frac{x-a_1}{b_1-a_1}\right)\frac{b_2-a_2}{k_2\pi}\sin\left(k_2\pi\frac{\tau-a_2}{b_2-a_2}\right)\cos\left(k_3\pi\frac{v-a_3+\varepsilon}{b_3-a_3+2\varepsilon}\right)\\
&\quad + \sum_{k=1}^{N} {\sum_{k_3=0}^{N-1}}' \frac{1}{2} A_{k_1,0,k_3}\,\tau \sin\left(k_1\pi\frac{x-a_1}{b_1-a_1}\right)\cos\left(k_3\pi\frac{v-a_3+\varepsilon}{b_3-a_3+2\varepsilon}\right) + \sin\left(p\pi\frac{x-a_1}{b_1-a_1}\right).
\end{aligned} \tag{5.12}$$

In other words, we start with a 3D Fourier series representation of $\frac{\partial \hat{\phi}_p}{\partial \tau}$, not a Fourier series expansion for $\hat{\phi}_p$. We will refer to this construction $T_N\hat{\phi}_p$ as a 3D trigonometric expansion for the function $\hat{\phi}_p$, since the end result is a linear combination of cosine and since functions but not in the format of a Fourier series expansion.

The boundary conditions $\hat{\phi}_p(\tau,a,v) = \hat{\phi}_p(\tau,b,v) = 0$ are automatically fulfilled for any coefficients A_{k_1,k_2,k_3} and, thanks to our construction of the trigonometric expansion, the same for the initial condition. Worth noting that, this construction is a global decomposition of $\hat{\phi}_p$, thus suitable for any τ, x and v, and in particular, we obtain accurate local approximations for the boundaries and initial time.

Furthermore, the coefficients are now defined by three-dimensional integrals. They can be stored as a three-order tensor $\mathscr{A} \in \mathbb{R}^{N\times N\times N}$ with elements given by $\mathscr{A}[k_1,k_2,k_3] = A_{k_1,k_2,k_3}$. In this thesis, we shall consider that the index k_1 is relative to the row fibers, k_2 to the column fibers and k_3 to the tube fibers (see Section 2.5).

After the determination of the expansion form, we insert formula (5.12) evaluated at different training points into the PDE (5.9). Unlike the 2D case, we cannot represent the resulting system as a matrix-vector product. Nonetheless, the underlying concept remains the same, and our goal is to solve the resulting system to determine the unknown coefficients, i.e. the elements of the tensor $\mathscr{A}$.

To achieve this, we define a set with combinations of values of x, τ and v, in which the PDE will be evaluated. To be more precise, we choose $M\times M\times M$ training points, with $M = N$ to prevent overfitting, as discussed in Chapter 3. Let x_m be the m-th training point in the log-asset dimension, for $m = 1,\ldots,M$, τ_ℓ the ℓ-th training point in the time

dimension, for $l = 0, ..., M-1$ and v_n the n-th training point in the variance dimension, for $n = 0, \dots, M-1$.

Subsequently, we define matrices with M rows and N columns that contain the basis functions evaluated at the training points. Matrices $\mathbf{V}_1, \mathbf{V}_2, \mathbf{Z}_1, \mathbf{Z}_2$ and $\mathbf{Z}_3$ are defined as in Chapter 4. We need to define new matrices $\mathbf{V}_3, \mathbf{Z}_4$ and $\mathbf{Z}_5$ as follows

$$
\begin{aligned}
\mathbf{V}_3[n,:] &= \begin{pmatrix} 1/2 & \cos\left(\pi \frac{v_n - a_3 + \varepsilon}{b_3 - a_3 + 2\varepsilon}\right) & \cdots & \cos\left((N-1)\pi \frac{v_n - a_3 + \varepsilon}{b_3 - a_3 + 2\varepsilon}\right) \end{pmatrix}, \\
\mathbf{Z}_4[n,:] &= \begin{pmatrix} 0 & -\frac{\pi}{b_3 - a_3 + 2\varepsilon} \sin\left(\pi \frac{v_n - a_3 + \varepsilon}{b_3 - a_3 + 2\varepsilon}\right) & \cdots & -\frac{(N-1)\pi}{b_3 - a_3 + 2\varepsilon} \sin\left((N-1)\pi \frac{v_n - a_3 + \varepsilon}{b_3 - a_3 + 2\varepsilon}\right) \end{pmatrix}, \\
\mathbf{Z}_5[n,:] &= \begin{pmatrix} 0 & -\left(\frac{\pi}{b_3 - a_3 + 2\varepsilon}\right)^2 \cos\left(\pi \frac{v_n - a_3 + \varepsilon}{b_3 - a_3 + 2\varepsilon}\right) & \cdots & -\left(\frac{(N-1)\pi}{b_3 - a_3 + 2\varepsilon}\right)^2 \cos\left((N-1)\pi \frac{v_n - a_3 + \varepsilon}{b_3 - a_3 + 2\varepsilon}\right) \end{pmatrix},
\end{aligned}
$$

where $\mathbf{V}_3[n,:]$ stands for the n-th row of matrix $\mathbf{V}_3$, with a similar notation for the other matrices.

Just like in the GBM case, the goal is to derive a linear system where the unknowns are the elements of $\mathscr{A}$. To that end, we first vectorize the tensor $\mathscr{A} \in \mathbb{R}^{N \times N \times N}$ by stacking up all the tube fibers of $\mathscr{A}$ vertically in order, as previously illustrated in Section 2.5.

Applying $\text{vec}(\mathbf{a}\mathbf{b}^T) = \mathbf{b} \otimes \mathbf{a}$, where $\otimes$ denotes the Kronecker product, and the linearity of the $\text{vec}(\cdot)$ operator, we have

$$
\begin{aligned}
&\sum_{k_1=1}^{N} \sum_{k_2=0}^{N-1} \sum_{k_3=0}^{N-1} \mathscr{A}[k_1, k_2, k_3] (\mathbf{Z}_2[\ell,:](:,k_2) \otimes \mathbf{V}_3[n,:](:,k_3) \otimes \mathbf{V}_1[m,:](:,k_1)) \\
&= (\mathbf{Z}_2[\ell,:] \otimes \mathbf{V}_3[n,:] \otimes \mathbf{V}_1[m,:]) \text{vec}(\mathscr{A}).
\end{aligned} \tag{5.13}
$$

Then the pricing PDE evaluated at point (τ_ℓ, x_m, v_n) leads to

$$
\begin{aligned}
&(\mathbf{Z}_2[\ell,:] \otimes \mathbf{V}_3[n,:] \otimes \mathbf{V}_1[m,:]) \text{vec}(\mathscr{A}) - \left(r - \frac{1}{2} v_n\right) (\mathbf{V}_2[\ell,:] \otimes \mathbf{V}_3[n,:] \otimes \mathbf{Z}_1[m,:]) \text{vec}(\mathscr{A}) \\
&+ \kappa(\bar{v} - v_n) (\mathbf{V}_2[\ell,:] \otimes \mathbf{Z}_3[n,:] \otimes \mathbf{V}_1[m,:]) \text{vec}(\mathscr{A}) + \frac{1}{2} v_n (\mathbf{V}_2[\ell,:] \otimes \mathbf{V}_3[n,:] \otimes \mathbf{Z}_4[m,:]) \text{vec}(\mathscr{A}) \\
&+ \rho\gamma v_n (\mathbf{V}_2[\ell,:] \otimes \mathbf{Z}_3[n,:] \otimes \mathbf{Z}_1[m,:]) \text{vec}(\mathscr{A}) + \frac{1}{2} \gamma^2 v_n (\mathbf{V}_2[\ell,:] \otimes \mathbf{Z}_5[n,:] \otimes \mathbf{V}_1[m,:]) \text{vec}(\mathscr{A}) \\
&= \left(r - \frac{1}{2} v_n\right) \frac{p\pi}{b_1 - a_1} \cos\left(p\pi \frac{x_m - a_1}{b_1 - a_1}\right) - \frac{1}{2} v_n \left(\frac{p\pi}{b_1 - a_1}\right)^2 \sin\left(p\pi \frac{x_m - a_1}{b_1 - a_1}\right) \\
\iff &\Big[(\mathbf{Z}_2[\ell,:] \otimes \mathbf{V}_3[n,:] \otimes \mathbf{V}_1[m,:]) - \Big(\mathbf{V}_2[\ell,:] \otimes \Big(\left(r - \frac{1}{2} v_n\right) \mathbf{V}_3[n,:] \otimes \mathbf{Z}_1[m,:] \\
&- \kappa(\bar{v} - v_n) \mathbf{Z}_3[n,:] \otimes \mathbf{V}_1[m,:] - \frac{1}{2} v_n \mathbf{V}_3[n,:] \otimes \mathbf{Z}_4[m,:] - \rho\gamma v_n \mathbf{Z}_3[n,:] \otimes \mathbf{Z}_1[m,:] \\
&- \frac{1}{2} \gamma^2 v_n \mathbf{Z}_5[n,:] \otimes \mathbf{V}_1[m,:]\Big)\Big)\Big] \text{vec}(\mathscr{A}) \\
&= \left(r - \frac{1}{2} v_n\right) \frac{p\pi}{b_1 - a_1} \cos\left(p\pi \frac{x_m - a_1}{b_1 - a_1}\right) - \frac{1}{2} v_n \left(\frac{p\pi}{b_1 - a_1}\right)^2 \sin\left(p\pi \frac{x_m - a_1}{b_1 - a_1}\right), \text{for fixed } p.
\end{aligned} \tag{5.14}
$$

CHOICE OF TRAINING POINTS

The range of possible values for v, denoted as $[a_3, b_3]$, corresponds to the specific interval within which we wish to obtain an accurate approximation for the function $\hat{\phi}_p$, but not the interval on which we construct the series expansion (recall Section 5.3.1). The intervals $[a_1, b_1]$ and $[a_2, b_2]$ must adhere to specific boundary conditions (with $[a_1, b_1]$ being equal to $[a, b]$ and a_2 set at 0 due to the initial condition), $[a_3, b_3]$, however, is not constrained by the necessity to satisfy (boundary) conditions of the PDE.

By the formula for $T_N\hat{\phi}_p$, the boundary conditions and the initial condition are fulfilled regardless of the value of the coefficients A_{k_1,k_2,k_3}. Hence, including the points $x = a_1, x = b_1$ and $\tau = a_2 = 0$ in the grid will not bring any new information to the system. Therefore, we define $x_1 > a_1$, $x_M < b_1$, $\tau_0 > a_2$, $\tau_{M-1} = b_2$, $v_0 = a_3 = 0$ and $v_{M-1} = b_3$. Since the PDE is valid for any $0 < \tau < T$, we can choose any maturity $T \equiv b_2$ that is adequate for the type of options that we wish to price. The same rationale holds for b_3.

5

CHOICE FOR PARAMETER ε

There is one free parameter at our disposal, ε. To determine what is the value of ε that minimizes the error, we proceed as follows. We vary the range $[a_3 - \varepsilon, b_3 + \varepsilon]$ for $a_3 = 0$, $b_3 = 0.5$ and different values of ε. We fix $N = M = 32$ for all dimensions in our approach. The set used to compute the errors consists of barrier option values for the training points. The time to maturity is fixed at $\tau = 1$.

To compute the error we use a MC simulation with 100,000 paths and 1,000 time steps as a benchmark. The number of paths was set due to time constraints, as more paths would require longer computational times. Since we are dealing with continuously-monitored barrier options, we deemed as most important to keep the number of time steps high to the detriment of the number of paths. If we consider the configuration of 1,000,000 paths and 1,000 time steps as the one yielding the most accurate results, then 100,000 paths and 1,000 time steps produce results closer to that configuration than 1,000,000 paths and 250 time steps[1].

Taking into account the purpose intended in this section, the choice of number of paths and time steps is deemed enough. In Chapter 7, where comparisons between different models are performed, we chose a larger number of paths for a more accurate comparison.

We adopted multiple metrics for measuring the error, namely L^2-norm, L^∞-norm and mean relative error, with the latter being computed as follows

$$\text{mean relative error} = \frac{1}{M^2}\sum_{m=1}^{M}\sum_{n=1}^{M}\left|\frac{V_{\text{approx}}(\tau_\ell, x_m, v_n) - V_{\text{bench}}(\tau_\ell, x_m, v_n)}{V_{\text{bench}}(\tau_\ell, x_m, v_n)}\right|,$$

where (τ_ℓ, x_m, v_n) stand for training points and ℓ is fixed.

[1] 250 time steps coincides with a daily monitored barrier option.

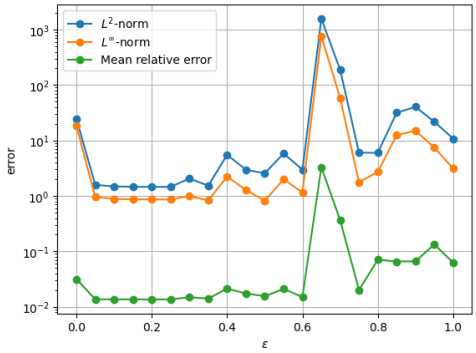

Figure 5.1: Comparison of three error metrics for our approach applied to all training points, while varying ε.

Figure 5.1 indicates that the L^2-norm and the mean relative error are minimized for $\varepsilon = 0.25$. Since these two error metrics take into account the errors at all points and both indicate the same optimal ε, we choose to follow this indication and determine ε in the following way: we set ε as half the length of the support $[a_3, b_3]$, i.e.

$$\varepsilon := \frac{b_3 - a_3}{2},$$

such that the series expansion domain $[a_3 - \varepsilon, b_3 + \varepsilon]$ is double the size of the support of interest $[a_3, b_3]$ for v.

Unfortunately, no regular pattern nor interesting properties such as symmetry and positive definiteness can be identified in the matrix at hand (cf. Figure 5.2). Hence, we recur to a direct solver built in Python to solve the linear system. Since the matrix has size $N^3 \times N^3$, for larger values of N, this corresponds to a significant increase in CPU time and can lead to memory allocation problems.

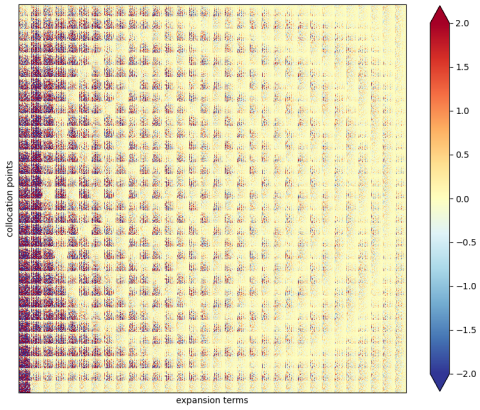

Figure 5.2: Visual representation of the matrix values for $N = M = 32$ expansion terms and training points in all dimensions.

Note that there are values above 2 and below -2, but for a better visualization of the values overall in the matrix, this was the chosen range for the color scale.

5.4. MEMORY AND STABILITY ISSUES

MEMORY ISSUES

The memory requirement to build a $N^3 \times N^3$ matrix and the complexity of the linear system increase substantially with N. This makes the solution computation inadequate for big N on a standard computer.

To tackle these problems, we applied a block iterative method. However, the iteration matrix does not satisfy the condition for convergence of the iterative method [60], regardless of whether we consider Jacobi, Gauss-Seidel or Successive Over-Relaxation. For that reason, the results presented in this thesis are obtained via a direct solver and the tests only go up to $N = M = 32$ for all 3 dimensions. We will focus on improving the results via a different route later in this chapter and in Chapter 6.

STABILITY ISSUES

Numerical computations suggest that as the number of training points increases, the series expansion becomes prone to numerical instability. This issue appears to be intrinsic to our approach, stemming from directly solving a linear system to compute the coefficients. As we increase the number of points along the v-dimension within a fixed interval $[a_3, b_3]$, the training points can approach each other closely. This proximity causes the basis functions to produce similar values, resulting in rows highly similar to each other. For instance, for $[a_3, b_3] = [0, 0.5]$, the condition number of the matrix is of order $\mathcal{O}(10^{17})$, which makes the matrix very ill-conditioned and can lead to inaccurate results.

We employ filters to restore the stability. Let us denote the trigonometric expansion of $\hat{\phi}_p$ with a spectral filter by $T_N^{\varphi}\hat{\phi}_p$, then

$$\begin{aligned} T_N^{\varphi}\hat{\phi}_p = &\sum_{k_1=1}^{N}\sum_{k_2=1}^{N-1}{\sum_{k_3=0}^{N-1}}' A_{k_1,k_2,k_3}\varphi\left(\frac{k_3}{N-1}\right)\sin\left(k_1\pi\frac{x-a_1}{b_1-a_1}\right) \\ &\frac{b_2-a_2}{k_2\pi}\sin\left(k_2\pi\frac{\tau-a_2}{b_2-a_2}\right)\cos\left(k_3\pi\frac{v-a_3+\varepsilon}{b_3-a_3+2\varepsilon}\right) \\ &+\sum_{k=1}^{N}{\sum_{k_3=0}^{N-1}}'\frac{1}{2}A_{k_1,0,k_3}\varphi\left(\frac{k_3}{N-1}\right)\tau\sin\left(k_1\pi\frac{x-a_1}{b_1-a_1}\right)\cos\left(k_3\pi\frac{v-a_3+\varepsilon}{b_3-a_3+2\varepsilon}\right) \\ &+\sin\left(p\pi\frac{x-a_1}{b_1-a_1}\right), \end{aligned} \tag{5.15}$$

where $\varphi(\cdot)$ is the filter of order m.

As discussed in Section 2.3.2, the spectral filter works on the spectral domain, which means that it has influence over the coefficients A_{k_1,k_2,k_3}. In practice, in our approach, when we insert formula (5.15) into the PDE, the filter will actually go alongside the basis functions in the matrix of the linear system and, consequently, the coefficients we obtain are just A_{k_1,k_2,k_3} scaled by a factor of $\varphi\left(\frac{k_3}{N-1}\right)$.

This scaling of the elements of the matrix actually affects the condition number of the matrix[2]. Numerical tests suggest that applying a filter can reduce the condition number by a factor of 10.

Notice that filtering here is not applied for the usual purpose of alleviating the Gibbs phenomenon, since our approach assumes that the solution function is a smooth function (thus, with no discontinuities). It is used as a computationally fast and inexpensive way to precondition the matrix of the linear system in order to improve numerical stability.

Alternative preconditioning methods have been considered. However, it is important to note that the matrix in question is not symmetric positive-definite, making certain preconditioning techniques unsuitable. One alternative is incomplete Cholesky decomposition, but it can be computationally expensive and specially time-consuming. Given that the linear system must be solved for different possible combinations of parameters $(r, \gamma, \bar{v}, \kappa, \rho, B)$, it is crucial to minimize computational time. Diagonal scaling has been tested and found to be ineffective, primarily due to the characteristics of the matrix.

5.5. LOG-VARIANCE

In addition to applying a filter, the numerical stability issue is solved by a transformation from the variance domain to the log-variance domain.

Consider, for example, training points for the v-dimension within the interval $[0.001, 0.5]$. Taking the log-transformation of the variance, the training points for this dimension are now in the interval $[\ln 0.001, \ln 0.5] = [-6.91, -0.69]$, which consists of a bigger range of values. For an increasing number of training points in this interval, the points will not be as close as in the original interval $[0.001, 0.5]$. As a result, the value of the basis functions evaluated at those new training points are also not as close to each other (or even approximately equal), which leads to a better conditioned matrix. In its turn, this produces a more numerically stable linear system. In fact, numerical testing has shown that taking the log-transformation alone allows to reduce the condition number from $\mathcal{O}(10^{17})$ to $\mathcal{O}(10^{7})$. Another benefit of changing to the log-variance domain is a higher convergence speed of the series expansion, since the marginal distribution of the variance is highly skewed whereas that of the log-variance is much more closer to Gaussian. This has been explained and tested in the paper by Fang and Oosterlee [17].

[2] A common way of preconditioning a matrix is through diagonal scaling [60], for example.

5.5.1. APPROXIMATION WITH LOG-VARIANCE

Let us follow the same derivation steps as before, but now we apply one final change of variable $v_t \mapsto u_t := \ln v_t$, and the pricing PDE reads

$$\begin{aligned}
&\frac{\partial V}{\partial t} + \left(r - \frac{1}{2}e^u\right)\frac{\partial V}{\partial X} + \left(\kappa(\bar{v} - e^u) - \frac{1}{2}\gamma^2\right)e^{-u}\frac{\partial V}{\partial u} + \frac{1}{2}e^u\frac{\partial^2 V}{\partial X^2} \\
&+ \rho\gamma\frac{\partial^2 V}{\partial X \partial u} + \frac{1}{2}\gamma^2 e^{-u}\frac{\partial^2 V}{\partial u^2} - rV = 0 \\
\Longrightarrow\ & e^u\frac{\partial V}{\partial t} + \left(r - \frac{1}{2}e^u\right)e^u\frac{\partial V}{\partial X} + \left(\kappa(\bar{v} - e^u) - \frac{1}{2}\gamma^2\right)\frac{\partial V}{\partial u} + \frac{1}{2}e^{2u}\frac{\partial^2 V}{\partial X^2} \\
&+ \rho\gamma e^u\frac{\partial^2 V}{\partial X \partial u} + \frac{1}{2}\gamma^2\frac{\partial^2 V}{\partial u^2} - e^u rV = 0.
\end{aligned} \tag{5.16}$$

The final step was taken in order to cancel out the term e^{-u} present in the first formulation of the PDE, since for very small values of the variance v ($v \approx 0$), we have that e^{-u} approches $+\infty$. The presence of terms e^u and e^{2u} in the final formulation of the PDE are reasonable because the values for the variance (and thus, for u) are never too big.

From this new pricing PDE, and following the same steps as in Section 5.2, we obtain the following problem that $\hat{\phi}_p$ must satisfy

$$\begin{cases}
-e^u\frac{\partial \hat{\phi}_p}{\partial \tau} + \left(r - \frac{1}{2}e^u\right)e^u\frac{\partial \hat{\phi}_p}{\partial X} + \left(\kappa(\bar{v} - e^u) - \frac{1}{2}\gamma^2\right)\frac{\partial \hat{\phi}_p}{\partial u} + \frac{1}{2}e^{2u}\frac{\partial^2 \hat{\phi}_p}{\partial X^2} \\
+\rho\gamma e^u\frac{\partial^2 \hat{\phi}_p}{\partial X \partial u} + \frac{1}{2}\gamma^2\frac{\partial^2 \hat{\phi}_p}{\partial u^2} = 0, a < X < b, \\
\hat{\phi}_p(\tau, a, u) = 0, \\
\hat{\phi}_p(\tau, b, u) = 0, \\
\hat{\phi}_p(0, x, u) = \sin\left(p\pi\frac{x-a}{b-a}\right).
\end{cases} \tag{5.17}$$

To approximate $\hat{\phi}_p$, we construct the same trigonometric expansion as before, only now we have a cosine expansion for u that ranges between $[\ln a_3 - \tilde{\varepsilon}, \ln b_3 + \tilde{\varepsilon}]$.

CHOICE OF PARAMETER $\tilde{\varepsilon}$

Recall that for the variance, we had to choose a free parameter ε. Now that we are working in the log-domain we need to justify the choice of parameter $\tilde{\varepsilon}$ as well. Applying the same reasoning as before, and choosing $\tilde{\varepsilon}$ such that $[\ln a_3 - \tilde{\varepsilon}, \ln b_3 + \tilde{\varepsilon}]$ is double the length of $[\ln a_3, \ln b_3]$ has been proven not to work through numerical tests, thus, we explore another approach. Consider the following

$$\begin{aligned}
b_3 + \varepsilon = e^{\ln b_3 + \tilde{\varepsilon}} &\Longleftrightarrow \ln\left(b_3 + \frac{b_3 - a_3}{2}\right) = \ln b_3 + \tilde{\varepsilon} \\
&\Longleftrightarrow \tilde{\varepsilon} = \ln\left(\frac{b_3 + \frac{b_3 - a_3}{2}}{b_3}\right) \\
&\Longleftrightarrow \tilde{\varepsilon} = \ln(1 + 0.5), \text{ since } a_3 = 0 \\
&\Longleftrightarrow \tilde{\varepsilon} \approx 0.4.
\end{aligned}$$

Recall that for $a_3 = 0$, the left-end of the domain $[a_3 - \varepsilon, b_3 + \varepsilon]$ is negative. Once we move to the log-domain it is no longer possible to consider negative values. As a consequence, an accurate extension of left-end side of the support $[\ln a_3, \ln b_3]$ is not available. Consequently, the results for a smaller log-variance will be not as accurate as the results for a bigger value of the log-variance. This is illustrated in Section 5.6.

5.6. RESULTS

For the Heston's model, no benchmark survival ch.f. is available. In fact, we explored the possibility of transforming the pricing PDE into the second-order Heat equation, for which there are known solutions (see [49]), in order to ultimately find a benchmark survival ch.f. like in the GBM case. This has been previously done by Dell'Era in [59] and considering all the changes of variables involved, finding an easy and straightforward solution for the resulting second-order Heat equation is not feasible. In particular, to obtain a solution, one would need to constrain the variance domain to a closed interval and know the value of the option at the boundaries of that domain, which, unfortunately, we do not know. Consequently, this approach has proven itself unsuccessful for attaining the desired results. This means that we will not have a survival ch.f. to benchmark our procedure against for the Heston's model case. Therefore, we focus on the testing results for the price of an up-and-out call option only.

5.6.1. OPTION PRICES

We compute the price of an up-and-out call option with parameters $(r, \gamma, \bar{v}, \kappa, \rho, K, B) = (0.1, 0.1, 0.02, 2.0, -0.5, 90, 120)$. To obtain the value of the option via our approach (5.6), $N = 32$ expansion terms were used for all dimensions. The respective result is benchmarked against a MC simulation with 100,000 paths and 1,000 time steps, for the same reason as in Section 5.3.2.

For an option at maturity level ($\tau = 0$), its value is just the payoff function, which exhibits a sharp corner at the strike level K, and a jump at the barrier level B. For that reason, the value of the option as approximated by (5.6), exhibits Gibbs phenomenon. Thus, the approximated value is not perfect and there are oscillations in the whole domain and particularly in those points.

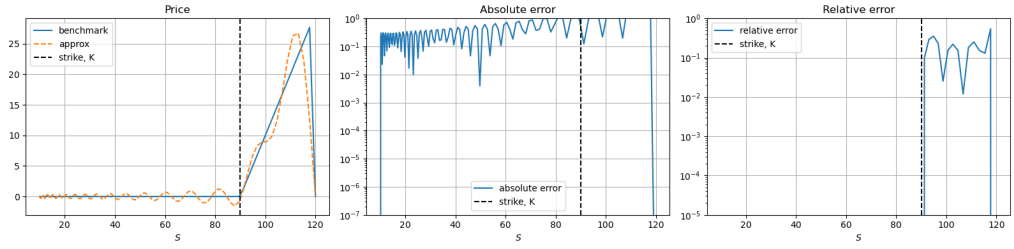

Figure 5.3: Payoff at maturity level ($\tau = 0$) and respective errors, using our approach vs. MC simulation.

However, as the maturity increases, the value function exhibits a smoother graph and, hence, formula (5.6) is able to better match the true shape of this function, as shown in Figures 5.4 and 5.5.

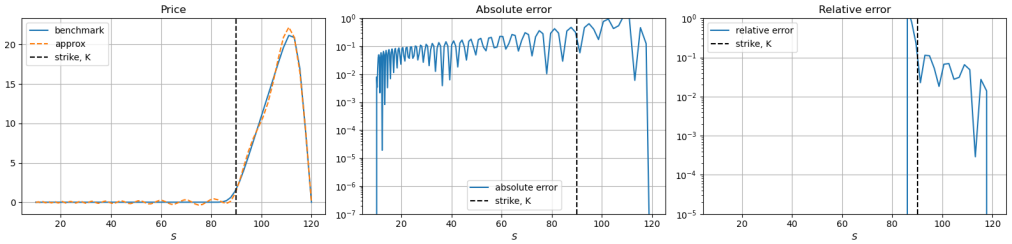

(a) Price, absolute and relative errors for $\tau = 0.1$.

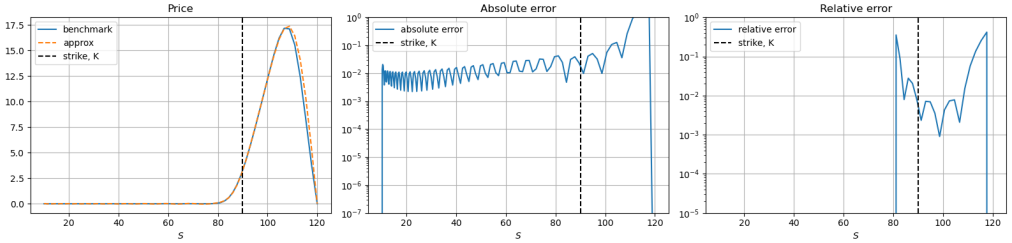

(b) Price, absolute and relative errors for $\tau = 0.25$.

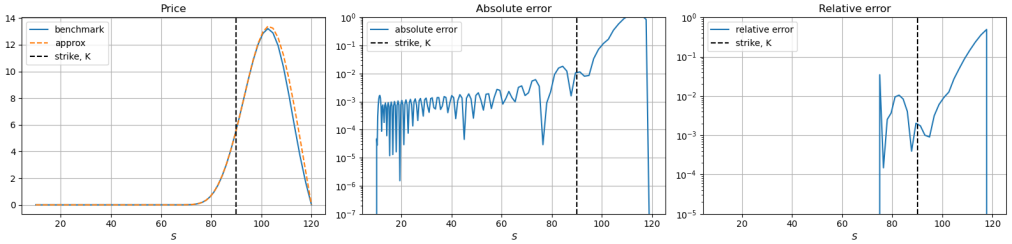

(c) Price, absolute and relative errors for $\tau = 0.5$.

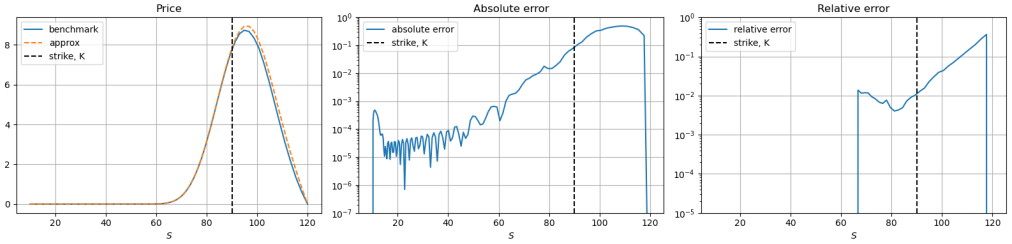

(d) Price, absolute and relative errors for $\tau = 1$.

Figure 5.4: Price and respective errors for $\nu = 0.01$ (volatility $\sigma = 0.1$) and different values of τ, using our approach vs. MC simulation.

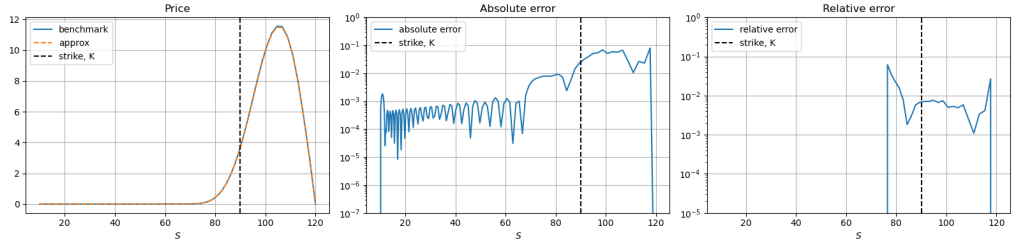

(a) Price, absolute and relative errors for $\tau = 0.1$.

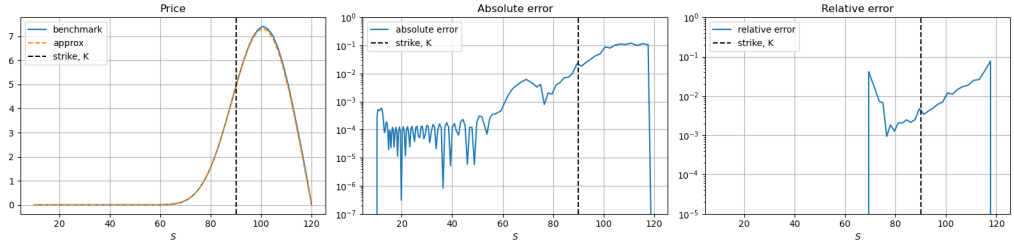

(b) Price, absolute and relative errors for $\tau = 0.25$.

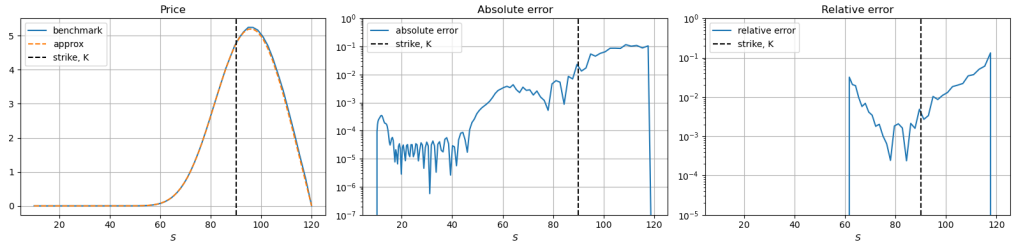

(c) Price, absolute and relative errors for $\tau = 0.5$.

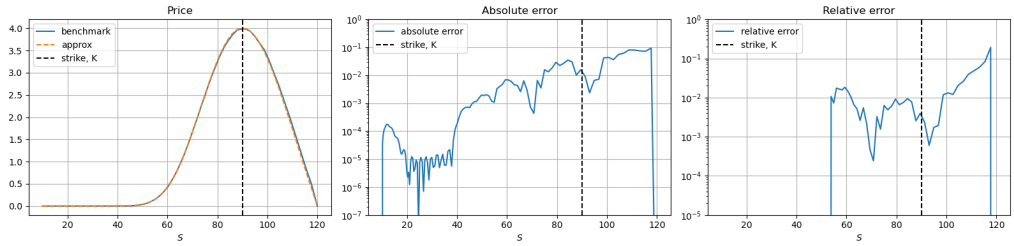

(d) Price, absolute and relative errors for $\tau = 1$.

Figure 5.5: Price and respective errors for $\nu = 0.09$ (volatility $\sigma = 0.3$) and different values of τ, using our approach vs. MC simulation.

Next, the error level for the price of all training points $(\tau_\ell, x_m, \upsilon_n)$ is compared with that for a set of non-training points (see Figure 5.6 below). There the relative error is computed for both sets of points separately.

We observe that overall the relative error exhibits very similar behaviour in the two sets, confirming an uniform level of accuracy for the constructed global approximation of $\hat{\phi}_p$. Nonetheless, the error is lower for the training points, which is also intuitive.

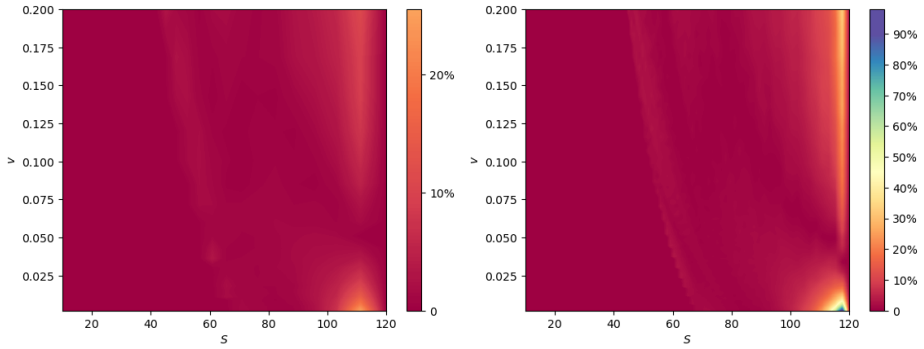

(a) Set of training points.

(b) Set of non-training points.

Figure 5.6: Relative error between the MC simulation price and the approximated option price using our approach, for fixed time to maturity $\tau = 1$, multiple asset prices and variances.

5

Also notice the line between $S = 40$ and $S = 80$ that faintly seems to be separating the colormap in two distinct regions. This is because for benchmark values below 10^{-1}, the absolute error is computed instead, which means that to the left of that line, the absolute error is computed instead of the relative error.

Moreover, just like in the GBM case, the error is bigger closer to the barrier level, $B = 120$. The reason lies on the fact that very close to the barrier level, the price function exhibits steep skew (as a function of x) and the sine series has trouble approximating this well with only $N = 32$ expansion terms. More expansion terms are needed for a more accurate approximation. This is particularly true for smaller variance values and smaller maturities, which is in accordance with Figures 4.5 and 5.6.

Based on the testing results and the discussion above, some improvements to the method will be made in Chapter 6.

6

IMPROVEMENTS TO OUR APPROACH

In light of the results obtained in Chapters 4 and 5, there is room for improvement in the described approach. More specifically, without the need to increase the number of training points and expansion terms, we aim to obtain more accurate prices for the options. That can be achieved by using the asset price process S_t directly, instead of using the log-asset $X_t := \ln S_t$. The specific motivation is presented below.

Just as for any machine learning method, the representativeness of the training points is the key to a fast training procedure. That is, we wish to use the best grid possible that captures the "full information" of the survival pdf (and of $\hat{\phi}_p$) when the number of grid points is fixed. This means that we must have enough points to cover the parts of the function that are more skewed. For an up-and-out barrier, there is a bigger concentration of probability mass closer to the barrier level (see e.g. Figure 6.1).

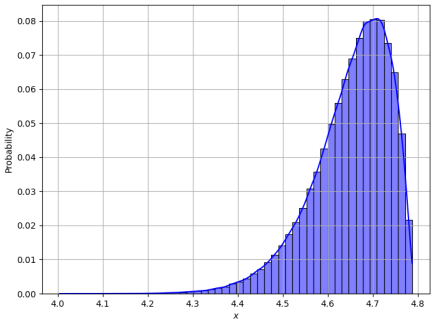

Figure 6.1: Example of probability mass for an up-and-out call option with $B = 120$ ($\ln B = 4.79$), computed using the paths of a MC simulation.

Consider, as an example, $M = 32$ training points in the x-dimension, such that they are evenly spaced between the lower barrier level a and the upper barrier level b. In the log-asset domain, the points are equally spaced, but in the asset domain those exact points will be more concentrated on the left-end of the domain. This means that for

the right-end of the domain, there are not enough points to cover the concentration of density mass and the steep descent of the pdf close to the barrier level.

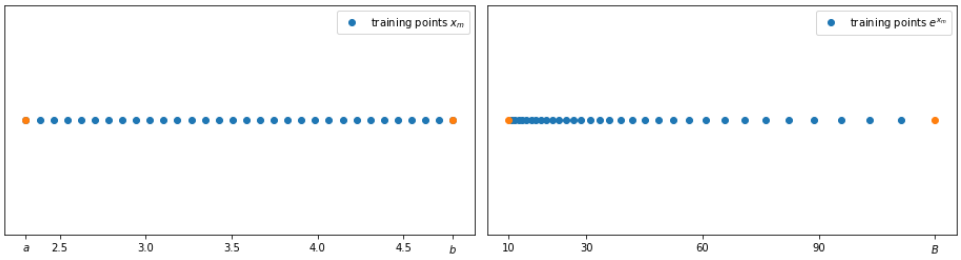

(a) x-domain. (b) s-domain.

Figure 6.2: Equally-spaced training points, x_m, in the x-domain for $M = 32$, and respective points in the s-domain.

One could consider allocating more points closer to the barrier level in the log-asset domain. However, an increase in the number of training points closer to the barrier is only possible when we increase the number of points in the entire log-asset domain, as we need to keep the training points at an equal distance (see Chapter 4). In light of this, a viable option seems to be to work on the asset domain directly instead of the log-asset domain. This is sustained by the grid of points in Figure 6.3: in the range $S \in [90, 120]$, where the density is more concentrated, the number of training points is 10, as opposed to 4 for the equally-spaced points in the log-asset domain in Figure 6.2.

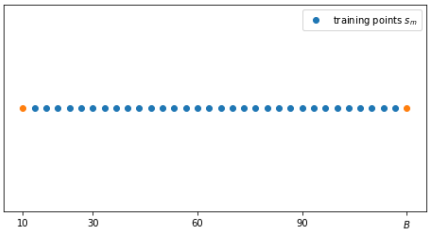

Figure 6.3: Equally-spaced training points, s_m, in the s-domain for $M = 32$.

6.1. APPLICATION TO GBM MODEL

We depart from the pricing PDE for the asset price,

$$\begin{cases} \frac{\partial V}{\partial t} + rS\frac{\partial V}{\partial S} + \frac{1}{2}\sigma^2 S^2 \frac{\partial^2 V}{\partial S^2} - rV = 0, \\ V(T,S) = f(S_T), \end{cases} \tag{6.1}$$

and applying the same derivation steps as in Chapter 4, we arrive at an IVBP that needs to be solved for $\hat{\phi}_p$. Only now, $\hat{\phi}_p$ is a function of τ and s.

$$\begin{cases} -\dfrac{\partial \hat{\phi}_p}{\partial \tau} + rS\dfrac{\partial \hat{\phi}_p}{\partial S} + \dfrac{1}{2}\sigma^2 \dfrac{\partial^2 \hat{\phi}_p}{\partial S^2} = 0, \ a < S < b, \\ \hat{\phi}_p(\tau, a) = 0, \\ \hat{\phi}_p(\tau, b) = 0, \\ \hat{\phi}_p(0, s) = \sin\left(p\pi \frac{s-a}{b-a}\right), \end{cases} \tag{6.2}$$

where a is an appropriate lower bound close to 0 but not equal to 0 (otherwise the PDE is degenerate in that boundary [1]), and $b = B$, the barrier level. The trigonometric expansion for $\hat{\phi}_p$ reads

$$\begin{aligned} T_N \hat{\phi}_p = &\sum_{k_1=1}^{N} \sum_{k_2=1}^{N-1} A_{k_1,k_2} \frac{b_2 - a_2}{k_2 \pi} \sin\left(k_2 \pi \frac{\tau - a_2}{b_2 - a_2}\right) \sin\left(k_1 \pi \frac{s - a_1}{b_1 - a_1}\right) \\ &+ \sum_{k_1=1}^{N} A_{k_1,0} \frac{1}{2} \tau \sin\left(k_1 \pi \frac{s - a_1}{b_1 - a_1}\right) + \sin\left(p\pi \frac{s - a_1}{b_1 - a_1}\right), \end{aligned} \tag{6.3}$$

with $b_1 = b$, $a_1 = a$ and $a_2 = 0$.

Once the coefficients are computed, we obtain an approximation of $\hat{\phi}_p$ and that can be used to price a barrier option using the following sine pricing formula

$$V(t,s) \approx e^{-r(T-t)} \sum_{p=1}^{N} \hat{\phi}_p(t,s) V_p = e^{-r(T-t)} \sum_{p=1}^{N} \operatorname{Im}\left\{\phi\left(\frac{p\pi}{b-a}, t; s\right) e^{-ip\pi \frac{a}{b-a}}\right\} V_p, \tag{6.4}$$

where the coefficients V_p are defined by

$$V_p := \frac{2}{b-a} \int_a^b V(y,T) \sin\left(p\pi \frac{y-a}{b-a}\right) dy, \tag{6.5}$$

with $V(y,T) = (y-K)^+$ in the case of a call option, for instance.

6.1.1. RESULTS

Now we compute the price of an up-and-out call option using exactly the same parameters as before. For the same number of expansion terms (and training points) $N = M = 64$, we see in Figure 6.4 an improvement in the errors for the price against those of Chapter 4.

[1] The BS PDE is degenerated when the stock price approaches zero (see [61]). This degeneracy may affect the accuracy of the numerical method used.

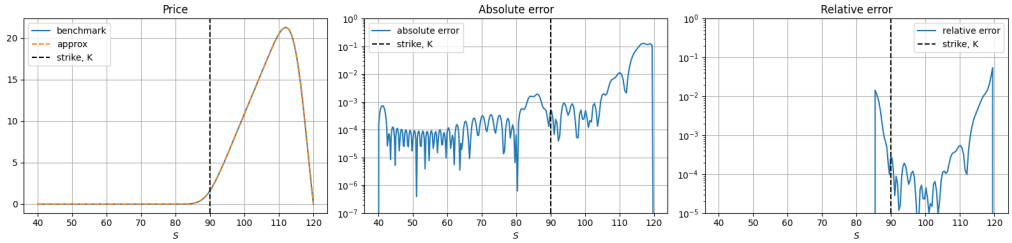

(a) Price, absolute and relative errors for $\tau = 0.1$.

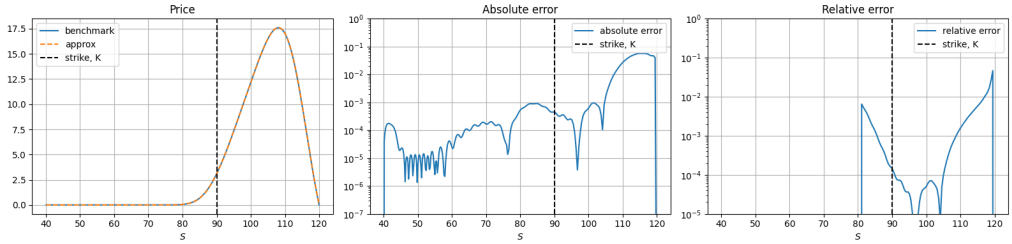

(b) Price, absolute and relative errors for $\tau = 0.25$.

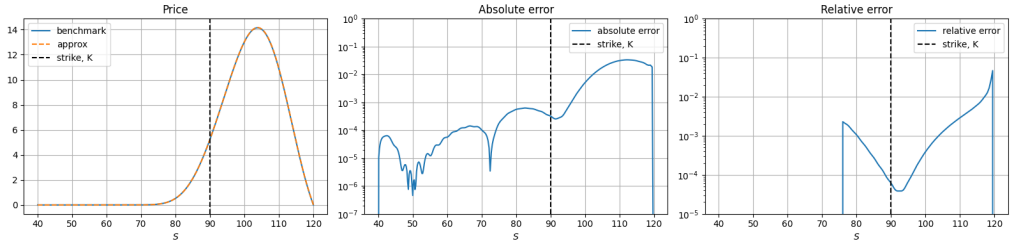

(c) Price, absolute and relative errors for $\tau = 0.5$.

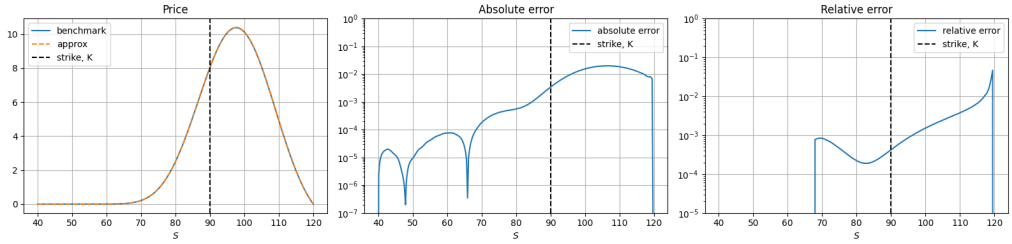

(d) Price, absolute and relative errors for $\tau = 1$.

Figure 6.4: Price and respective errors for different values of τ, using our approach vs. closed-form solution.

As previously mentioned, when the maturity level is set to $\tau = 0$, the presence of the Gibbs phenomenon is a direct result of the inherent characteristics of the payoff function. To mitigate this issue, we apply an order 1 filter to the pricing formula (6.4), with the purpose of eliminating this phenomenon. This filtering process is reflected in the outcomes displayed in Figure 6.5, according to which the oscillations away from the sharp corner $S = K$ and the discontinuity $S = B$ are significantly improved.

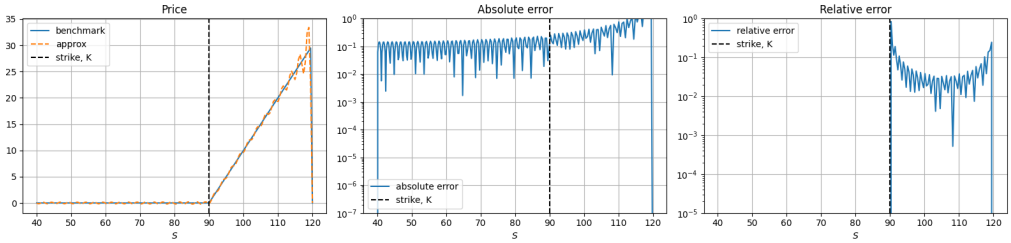

(a) Without filter.

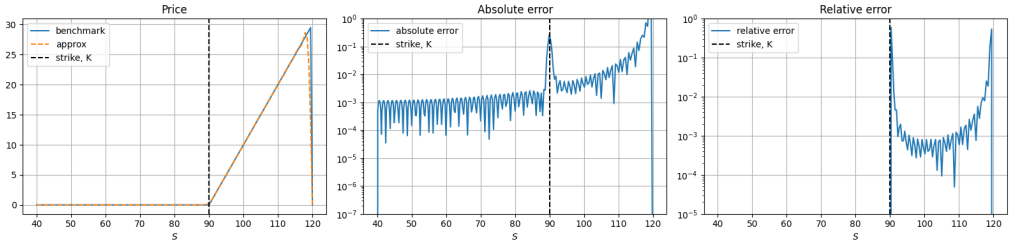

(b) With filter.

Figure 6.5: Price and respective errors for maturity ($\tau = 0$), using our approach vs. closed-form solution.

To better understand the error level for the price of all training points (τ_ℓ, s_m) against a set of non-training points, we compute the relative error for both sets of points separately, in Figure 4.5. Overall the relative error exhibits very similar behaviour to what we have seen in Chapter 4. The set of non-training points is the same as before, but now we observe an improvement in the accuracy.

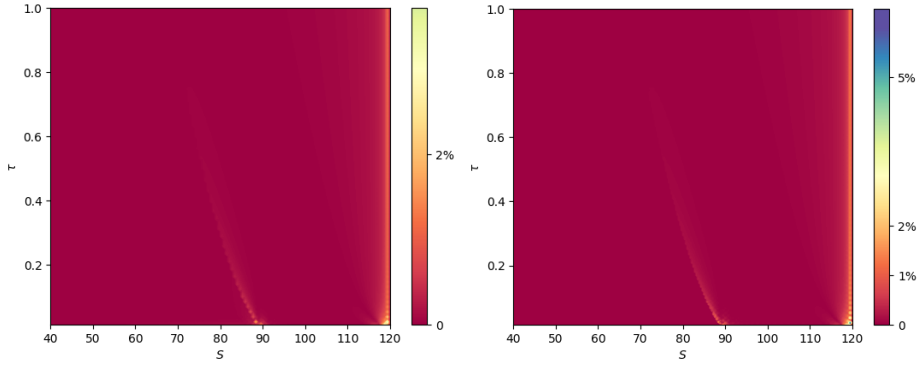

(a) Set of training points.

(b) Set of non-training points.

Figure 6.6: Relative error between the closed-form price and the approximated option price using our approach, for multiple asset prices and maturities.

Table 6.1 presents convergence test results regarding the error in option prices for a fixed asset price of $S = 110$ and different times to maturity values τ. All other parameters

are as in previous settings. While the error diminishes with higher values of N, the rate of convergence is relatively slow. Nonetheless, overall the results exhibit greater accuracy for the same N when compared to those presented in Table 4.2.

	N							
	16		32		64		128	
τ	abs error	% error	abs error	% error	abs error	% error	abs error	% error
1	2.97e-01	6.08	7.40e-02	1.52	1.85e-02	0.38	4.64e-03	0.09
0.5	4.77e-01	2.20	1.24e-01	1.14	3.15e-02	0.29	7.93e-03	0.07
0.25	3.06e-01	1.80	1.02e-01	0.60	2.69e-02	0.16	6.88e-03	0.04
0.1	3.68e-01	1.80	4.74e-02	0.23	1.13e-02	0.05	2.67e-03	0.01

Table 6.1: Absolute and relative error convergence for the option price obtained via our approach vs. closed-form solution, for $S = 110$ and different values of τ.

6.2. APPLICATION TO HESTON'S MODEL

Similar to the GBM case in Section 6.1, we depart from the pricing PDE for the asset price,

$$\begin{cases} \frac{\partial V}{\partial t} + rS\frac{\partial V}{\partial S} + \kappa(\bar{v} - v)\frac{\partial V}{\partial v} + \frac{1}{2}vS^2\frac{\partial^2 V}{\partial S^2} + \rho\gamma Sv\frac{\partial^2 V}{\partial S \partial v} + \frac{1}{2}\gamma^2 v\frac{\partial^2 V}{\partial v^2} - rV = 0, \\ V(T, S, v) = f(S_T), \end{cases} \tag{6.6}$$

and applying the same derivation steps as in Chapter 5, we arrive at an IVBP that needs to be solved for $\hat{\phi}_p$. Only now, $\hat{\phi}_p$ is a function of τ, s and $u := \ln v$.

$$\begin{cases} -e^u\frac{\partial \hat{\phi}_p}{\partial \tau} + rSe^u\frac{\partial \hat{\phi}_p}{\partial S} + \left(\kappa(\bar{v} - e^u) - \frac{1}{2}\gamma^2\right)\frac{\partial \hat{\phi}_p}{\partial u} + \frac{1}{2}e^{2u}S^2\frac{\partial^2 \hat{\phi}_p}{\partial S^2} + \rho\gamma Se^u\frac{\partial^2 \hat{\phi}_p}{\partial S \partial u} \\ \qquad\qquad + \frac{1}{2}\gamma^2\frac{\partial^2 \hat{\phi}_p}{\partial u^2} = 0, \ a < S < b, \\ \hat{\phi}_p(\tau, a, u) = 0, \\ \hat{\phi}_p(\tau, b, u) = 0, \\ \hat{\phi}_p(0, s, u) = \sin\left(p\pi\frac{s-a}{b-a}\right), \end{cases} \tag{6.7}$$

where a is an appropriate lower bound close to 0, and $b = B$. Take $b_1 = b$, $a_1 = a$, $a_2 = 0$, $a_4 := \ln a_3 - \tilde{\varepsilon}$ and $b_4 := \ln b_3 + \tilde{\varepsilon}$, then the constructed trigonometric expansion reads

$$\begin{aligned} T_N\hat{\phi}_p = &\sum_{k_1=1}^{N}\sum_{k_2=1}^{N-1}\sum_{k_3=1}^{N-1}{}' A_{k_1,k_2,k_3}\frac{b_2 - a_2}{k_2\pi}\sin\left(k_2\pi\frac{\tau - a_2}{b_2 - a_2}\right)\sin\left(k_1\pi\frac{s - a_1}{b_1 - a_1}\right)\cos\left(k_3\pi\frac{u - a_4}{b_4 - a_4}\right) \\ &+ \sum_{k_1=1}^{N}\sum_{k_3=1}^{N-1}{}' A_{k_1,0,k_3}\frac{1}{2}\tau\sin\left(k_1\pi\frac{s - a_1}{b_1 - a_1}\right)\cos\left(k_3\pi\frac{u - a_4}{b_4 - a_4}\right) + \sin\left(p\pi\frac{s - a_1}{b_1 - a_1}\right), \end{aligned} \tag{6.8}$$

Once the coefficients are computed, we obtain an approximation of $\hat{\phi}_p$ and that can be used to price a barrier option using the sine version of the one-dimensional COS formula, with the payoff coefficients V_p given in equation (6.5).

6.2.1. RESULTS

Now we compute the price of an up-and-out call option using the exact same parameters as in Chapter 5. Figures 6.7 and 6.8 show that, for the same number of expansion terms (and training points) $N = M = 32$, there is an improvement in the pricing errors against those of Chapter 5, particularly for a smaller variance.

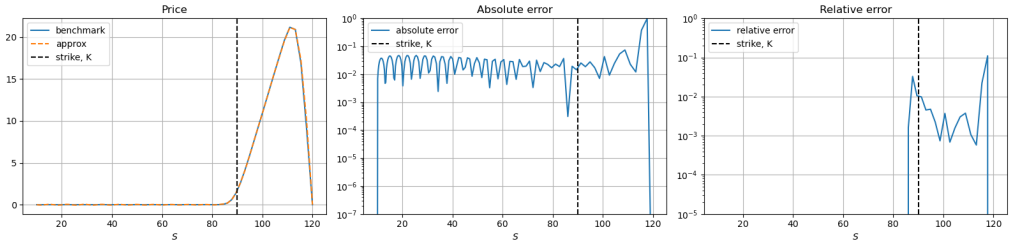

(a) Price, absolute and relative errors for $\tau = 0.1$.

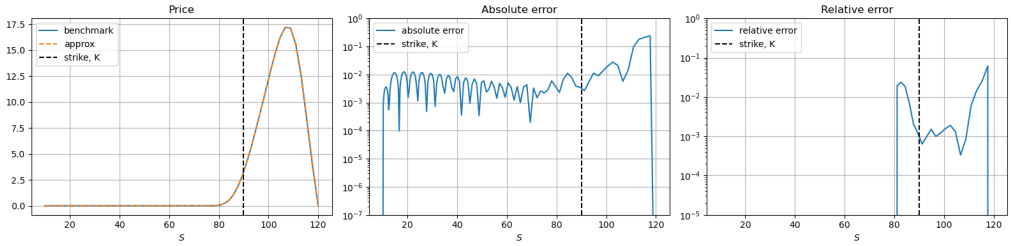

(b) Price, absolute and relative errors for $\tau = 0.25$.

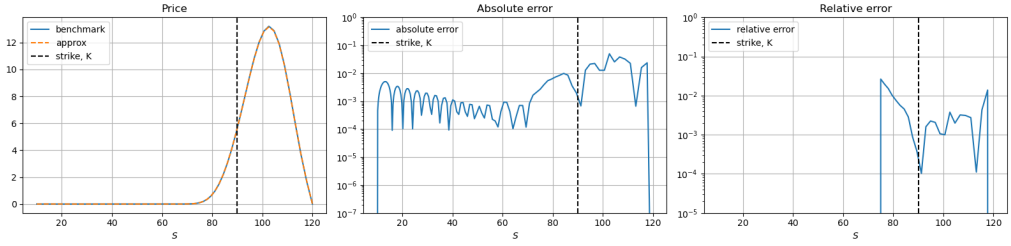

(c) Price, absolute and relative errors for $\tau = 0.5$.

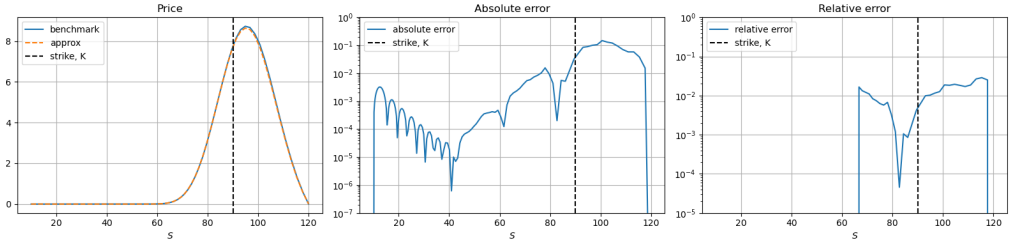

(d) Price, absolute and relative errors for $\tau = 1$.

Figure 6.7: Price and respective errors for $\nu = 0.01$ (volatility $\sigma = 0.1$) and different values of τ, using our approach vs. MC simulation.

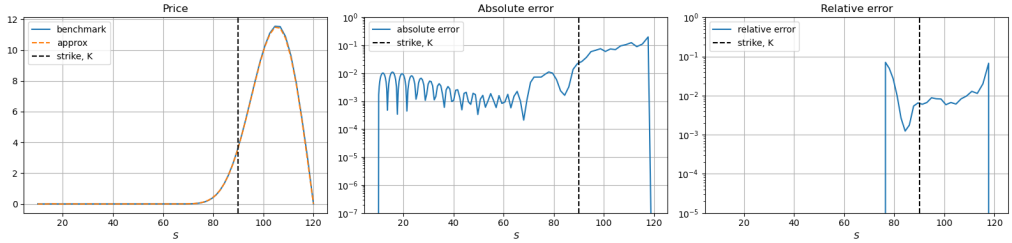

(a) Price, absolute and relative errors for $\tau = 0.1$.

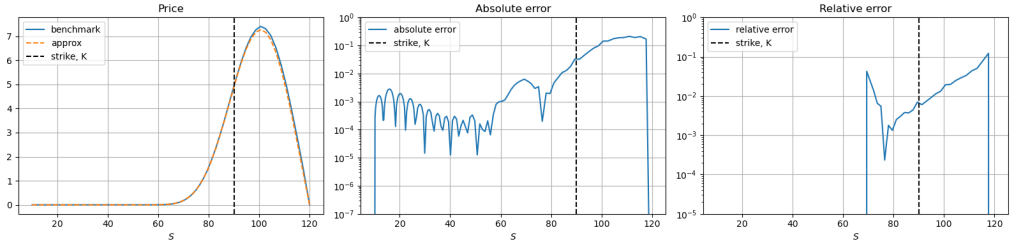

(b) Price, absolute and relative errors for $\tau = 0.25$.

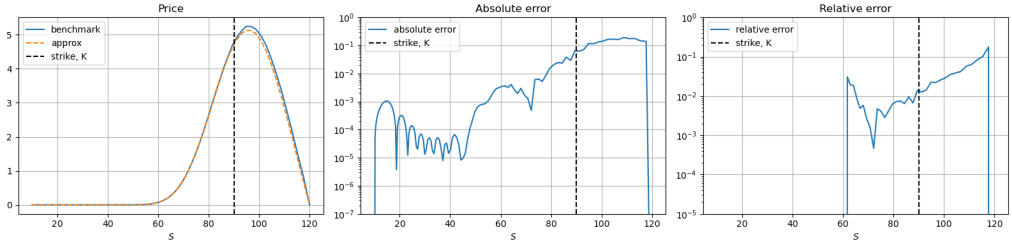

(c) Price, absolute and relative errors for $\tau = 0.5$.

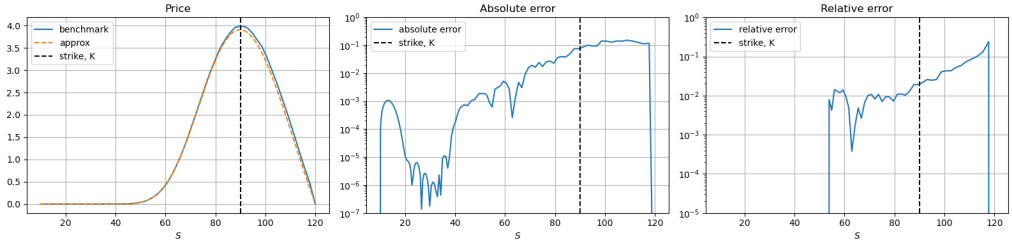

(d) Price, absolute and relative errors for $\tau = 1$.

Figure 6.8: Price and respective errors for $\upsilon = 0.09$ (volatility $\sigma = 0.3$) and different values of τ, using our approach vs. MC simulation.

At maturity level ($\tau = 0$), the Gibbs phenomenon arises due to the characteristics of the payoff function. To address this, we apply a order 1 filter to the pricing formula, which greatly improves the results away from the sharp corner $S = K$ and the discontinuity $S = B$. The comparative results are depicted in Figure 6.9 below. Closer to $S = K$ and $S = B$, the error can be improved by increasing the number of the expansion terms. However, due to memory constraints, it is not done in this thesis but will be tackled in

follow-up theses at FF Quant.

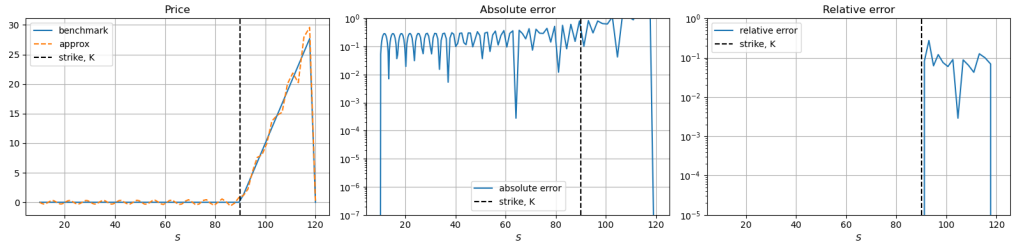

(a) Without filter.

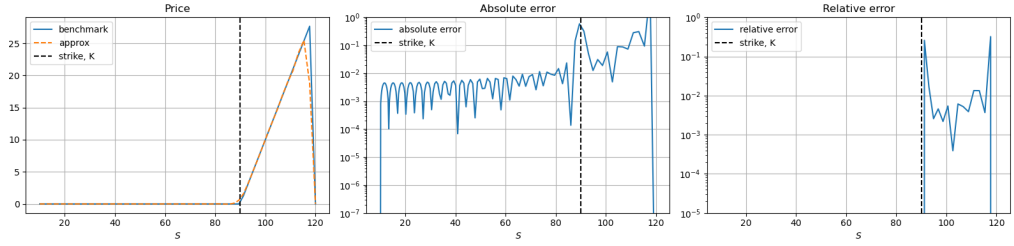

(b) With filter.

Figure 6.9: Price and respective errors for maturity ($\tau = 0$), using our approach vs. MC simulation.

6

In Figure 6.10, the relative error is ploted for the price of all training points (τ_ℓ, x_m, v_n) and a set of non-training points, which aligns with the one used in Section 5.6.

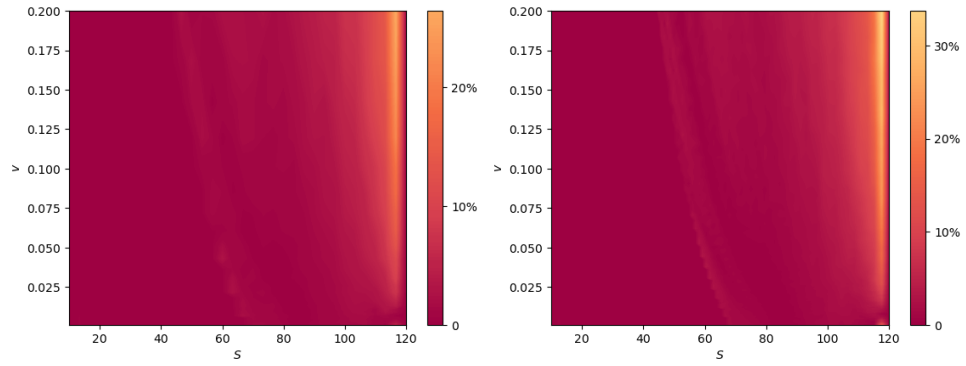

(a) Set of training points.

(b) Set of non-training points.

Figure 6.10: Relative error between the MC simulation price and the approximated option price using our approach, for fixed time to maturity $\tau = 1$, multiple asset prices and variances.

Once again, the error is bigger closer to the barrier level, $B = 120$, due to the fact that very close to the barrier level, the price function exhibits steep behaviour and the sine series has trouble approximating this well with only $N = 32$ expansion terms. More ex-

pansion terms are needed for a more accurate approximation. Nonetheless, we already see a substantial improvement in the accuracy for the set of non-training points as compared to the results in 5.6. For the set of training points, there is no difference compared to what we have seen before, since the error for this set is the intrinsic error associated with our approach. A theoretical discussion on the error is presented in Chapter 8.

Notice that the parameters we used so far satisfy the Feller condition, $2\kappa\bar{\nu} \geq \gamma^2$. However, when the Feller condition is not met, the cumulative distribution of the variance exhibits a near-singular behavior near the origin, i.e. there is an accumulation of probability mass around 0. For $q := 2\kappa\bar{\nu}/\gamma^2 - 1 >> 0$ the density values tend towards zero in both tails. For q smaller and approaching 0, the decay rate of the left-side tail slows down. Near $q = 0$, the left tail stays almost flat. For $q \in [-1, 0]$, the left tail increases drastically in value. For a visual illustration of these observations, we refer to [17].

When the Feller condition is not met, more training points closer to $\nu = 0$ are needed for a better accuracy. Therefore, for each specific parameter set, the interval $[\ln a_3, \ln b_3]$ of possible values of $\ln \nu$ needs to accurately reflect the domain in which the survival ch.f. can take values. Tuning the interval accordingly, our approach also works for the cases where the Feller condition is not satisfied. In Table 6.2, the valuation error is computed for different sets of parameters:

- case 1, where $q >> 0$: $(r, \gamma, \bar{\nu}, \kappa, \rho) = (0.1, 0.1, 0.02, 2.0, -0.5)$
- case 2, where $q \approx 0$: $(r, \gamma, \bar{\nu}, \kappa, \rho) = (0.1, 0.25, 0.21, 0.15, -0.5)$
- case 3, where $q < 0$: $(r, \gamma, \bar{\nu}, \kappa, \rho) = (0.1, 0.35, 0.1, 0.5, -0.9)$
- case 4, where $q \approx -1$: $(r, \gamma, \bar{\nu}, \kappa, \rho) = (0.1, 0.5, 0.05, 0.1, 0.1)$

In all of the cases, we take $K = 90, B = 120, S = 110$ and $\nu = 0.01$.

	case 1		case 2		case 3		case 4	
τ	abs error	% error	abs error	% error	abs error	% error	abs error	% error
1.0	0.0666	1.87	0.0113	0.46	0.0426	2.81	0.8349	13.05
0.5	0.0013	0.01	0.1706	1.96	0.9592	14.22	0.4389	2.82
0.25	0.0903	0.55	0.1197	0.71	0.2686	1.41	0.1000	0.55
0.1	0.0277	0.13	0.0013	0.01	0.1237	0.59	0.2285	1.15

Table 6.2: Absolute and relative error for the option price obtained via our approach vs. MC simulation, for different parameter sets and different values of τ.

Our approach is easily applicable to down-and-out and double barrier options as well. For additional results showcasing the accuracy of the our approach for other types of knock-out barrier, please refer to Appendix A.

Due to the improvement in accuracy by using S_t instead of X_t, we will use construction (6.8) to compare the accuracy of our approach against other existing methods in the literature, in Chapter 7.

7

COMPARISON WITH EXISTING METHODS

In this chapter, we will assess the accuracy of our approach, as described in Chapter 6, by comparing its results and computational efficiency with other existing methods to price barrier options under the Heston's model. These methods can be categorized into two groups: those designed for pricing discretely-monitored barrier options and those for continuously-monitored barrier options.

For the former, a considerably high number of time steps needs to be employed such that the corresponding price converges to the continuous-monitoring case. The COS method for barrier options developed by Fang and Oosterlee [17] falls into this category. In the other category, we find the method developed by He and Lin [29], which provides the price of down-and-out barrier options. Consequently, we will apply our approach with all parameters unchanged, except for the range $[a, b]$ of possible values for the asset price. For this comparison, we set $a = B$, where $B < S$ is the barrier level, and b high enough to be considered close to $+\infty$.

We benchmark these alternative methods and our approach against a MC simulation with 1,000,000 paths, a number consistent with the study by [29]. Although they use 10,000 time steps, our computational resources only allow us to use 1,000 time steps for this assessment, a difference driven by memory allocation constraints. Contrary to previous chapters, we can increase the number of time steps here, given that we will be evaluating the barrier option price for a relatively small number of options.

7.1. METHOD FOR DISCRETELY-MONITORED BARRIER OPTIONS

We start by introducing the COS method for discretely-monitored barrier options by Fang and Oosterlee [17] briefly. Consider the underlying log-asset price process and variance process (S_t, v_t), whose dynamics are under the Heston's model.

Take the log-asset $X_t := \ln S_t$ and the log-variance process $u_t := \ln v_t$. It is assumed that a barrier option is discretely monitored at a fixed set of M times $t_0 < t_1 < \ldots t_m <$

$\ldots < t_M = T$, with $\Delta t := t_{m+1} - t_m$. The pricing of an up-and-out discretely-monitored barrier option problem, with barrier B, is solved backwards in time, with

$$V\left(x_{t_m}, u_{t_m}, t_m\right) = \begin{cases} 0 & \text{when knocked-out,} \\ c\left(x_{t_m}, u_{t_m}, t_m\right) & \text{otherwise,} \end{cases} \tag{7.1}$$

$$V\left(x_{t_M}, u_{t_M}, t_M\right) = \begin{cases} 0 & \text{when knocked-out,} \\ f(x_{t_M}, u_{t_M}, t_M) & \text{otherwise,} \end{cases} \tag{7.2}$$

with $f(\cdot)$ being the payoff function at final time and $c\left(x_{t_m}, u_{t_m}, t_m\right)$ the continuation value at time t_m. The continuation value is given by

$$c\left(x_{t_m}, u_{t_m}, t_m\right) = e^{-r\Delta t}\mathbb{E}^{\mathbb{Q}}_{t_m}\left[v\left(x_{m+1}, u_{m+1}, t_{m+1}\right)\right], \tag{7.3}$$

which can be written as

$$\begin{aligned} c\left(x_{t_m}, u_{t_m}, t_m\right) =& e^{-r\Delta t}\cdot \\ & \int_{\mathbb{R}}\int_{\mathbb{R}} v\left(x_{m+1}, u_{m+1}, t_{m+1}\right) p_{x,\ln v}\left(x_{m+1}, u_{m+1} \mid x_{t_m}, u_{t_m}\right) du_{m+1} dx_{m+1} \\ =& e^{-r\Delta t}\int_{\mathbb{R}}\left[\int_{\mathbb{R}} v\left(x_{m+1}, u_{m+1}, t_{m+1}\right) p_{x|\ln v}\left(x_{m+1} \mid u_{m+1}, x_{t_m}, u_{t_m}\right) dx_{m+1}\right] \\ & p_{\ln v}\left(u_{m+1} \mid u_{t_m}\right) du_{m+1} \\ \approx& e^{-r\Delta t}\int_{a_v}^{b_v}\left[\int_{a}^{b} v\left(x_{m+1}, u_{m+1}, t_{m+1}\right) p_{x|\ln v}\left(x_{m+1} \mid u_{m+1}, x_{t_m}, u_{t_m}\right) dx_{m+1}\right] \\ & p_{\ln v}\left(u_{m+1} \mid u_{t_m}\right) du_{m+1}, \end{aligned} \tag{7.4}$$

where we truncated the integration region by $[a_v, b_v] \times [a, b]$. For more details on how this double integral is computed, we refer to [17].

The inner integral above equals the pricing formula for European options defined between t_m and t_{m+1}, provided that the variance value at the future time point is known. Thus, this method considers at every time interval $[t_m, t_{m+1}]$ a European option with maturity Δt, while checking if the barrier was knocked-out.

Before proceeding with the comparison between this method and our approach, it is important to highlight the differences that make their comparison less straightforward.

Firstly, as mentioned before, this method was developed for discretely-monitored barrier options. Therefore, a substantial number of time points must be considered to enable a meaningful comparison between the two methods. Simultaneously, it is essential to keep in mind that an extremely narrow monitoring interval leads to a highly peaked pdf, resulting in less accurate results. For instance, for a 1-year maturity, the number of monitoring dates is set to 250, which corresponds to daily monitoring.

Secondly, direct comparison of CPU time is not feasible. The COS method computes the price of a barrier option on-the-spot, while our approach involves an initial "offline"

training step to find the coefficients of $\hat{\phi}_p$, followed by the computation of option prices for any strike, maturity, variance, and asset price within the domain used in the computation of the coefficients. Furthermore, it is worth noting that the COS method is implemented in MATLAB whereas our approach is implemented in Python[1]. Hence, we choose to only compare the respective errors, as displayed in Table 7.1[2].

The price corresponds to an up-and-out call option with parameters $(r, \gamma, \bar{v}, \kappa, \rho, S, v, K, B) = (0.1, 0.1, 0.02, 2.0, -0.5, 100, 0.01, 90, 120)$. The ultimate benchmark is the MC simulation with 95% confidence interval. The COS method uses 128 expansion terms and our approach uses 32 expansion terms for all dimensions.

	MC	COS method			our approach		
τ	price	price	abs error	% error	price	abs error	% error
1	7.9965 (±0.017)	8.1101	0.1136	1.42	7.9074	0.0891	1.13
0.8	9.9261 (±0.017)	10.0347	0.1086	1.09	9.8742	0.0519	0.52
0.6	11.9640 (±0.016)	11.7236	0.0051	0.04	11.8850	0.0790	0.66
0.5	12.6225 (±0.015)	12.6671	0.0446	0.35	12.6110	0.0115	0.09
0.3	12.5753 (±0.012)	—	—	—	12.5639	0.0114	0.09
0.1	10.8969 (±0.006)	—	—	—	10.8720	0.0249	0.23

Table 7.1: Comparison of price for an up-and-out barrier option, using MC simulation with 95% confidence interval, COS method for barrier options and our approach. Different times to maturity τ are considered while the other parameters remain unchanged.

Our approach is proven to be more accurate than the COS method for barrier options. This makes sense since the latter was developed for discretely-monitored barrier options. Additionally, the fact that the COS method does not work for any combination of parameters - as demonstrated for example in Table 7.1 -, makes it impractical for a broad application. This limitation is attributed to the method's reliance on the pdf of the variance at current time conditioned on the variance at a previous time. Such a pdf exhibits extreme skewness, namely when the Feller condition is not met.

7.2. METHOD FOR CONTINUOUSLY-MONITORED BARRIER OPTIONS

The method developed by He and Lin [29] provides a formula that needs to be solved via numerical integration for pricing barrier options. In order to perform a comparison between our approach and this method, we shall first briefly introduce the latter. According to this method, the price of a down-and-out barrier option is given by

[1] The results from our approach are generated with a Intel(R) Core(TM) i7-10700F CPU @ 2.90GHz (8 CPU cores), with the code written in Python 3.8.10.

[2] The entries on the table containing "—" correspond to options for which we were not able to compute the price using the respective method.

$$
\begin{aligned}
V(t,x,v) &= \int_0^{+\infty} V(t,x,v|v_T)p(v_T|v_t)dv_T \\
&= \int_0^{+\infty} \left(\frac{1}{2}A_0(v_t,v_T)v + \sum_{k=1}^{\infty} A_k(v_t,v_T)V_k\right) p(v_t|v_T)dv_T,
\end{aligned} \tag{7.5}
$$

with

$$
\begin{aligned}
V_k &= \int_a^b V(t,x|\mathscr{F}_T)\cos\left(k\pi\frac{h_T-a}{b-a}\right)dh_T, \\
A_k(v_t,v_T) &= \frac{2}{b-a}\mathrm{Re}\left\{g\left(\frac{k\pi}{b-a}\middle|v_t,v_T\right)e^{-i\frac{ak\pi}{b-a}}\right\}, \\
h_T &= \int_t^T v_s\,ds,
\end{aligned} \tag{7.6}
$$

where $g(\cdot|v_t,v_T)$ is the ch.f. of h_T and $V(t,x|\mathscr{F}_T)$ is the analytical approximation for barrier option price conditional on knowing the variance at future time T. The analytical expression for $p(v_t|v_T)$ is known. For more details on how this expression is derived, we refer to [29].

Notice that the integral in equation (7.5) does not have an analytical formulation, and for that reason, we need to recur to a numerical integration technique to obtain the price of the option. We use the Clenshaw-Curtis rule with 64 quadrature points. This was deemed as sufficient since our results mirror the paper.

Once again, the CPU time cannot be directly compared since formula (7.5) computes the price of a barrier option on-the-spot, while our approach requires an anterior "offline" training step. Plus, the CPU time of that anterior training step depends strongly on the number of expansion terms used to approximate $\hat{\phi}_p$.

Nonetheless, the results of the comparison are presented in Table 7.2, where the CPU time for our approach refers to the time required to perform the price computation posterior to the computation of the coefficients. The price corresponds to that of a down-and-out call option with parameters $(r,\gamma,\bar{v},\kappa,\rho,S,v,K,B) = (0.1, 0.1, 0.02, 2.0, -0.5, 100, 0.01, 100, 90)$. The ultimate benchmark is the MC simulation with 95% confidence interval. Using formula (7.5), we take 50 expansion terms (as in the paper) and, in our approach, we employ 32 expansion terms for all dimensions.

	MC	He and Lin's approach				our approach			
τ	price	price	time (s)	abs error	% error	price	time (s)	abs error	% error
1	10.7151 (±0.017)	10.9392	78.42	0.2241	2.09	10.7165	0.01344	0.0014	0.0127
0.8	9.0357 (±0.017)	9.1609	78.68	0.1252	1.39	9.0432	0.00047	0.0078	0.0830
0.6	7.2400 (±0.016)	7.2735	78.52	0.0335	0.46	7.2316	0.00063	0.0084	0.1158
0.5	6.2650 (±0.015)	6.2846	78.28	0.0196	0.31	6.2578	0.00047	0.0002	0.0039
0.3	4.1958 (±0.012)	4.2013	78.57	0.0055	0.13	4.1964	0.00069	0.0006	0.0137
0.1	1.8786 (±0.006)	1.8787	78.44	0.0001	0.01	1.9366	0.00050	0.0580	3.0876

Table 7.2: Comparison of price and CPU time for an down-and-out barrier option, using MC simulation with 95% confidence interval, He and Lin's approach and our approach. Different times to maturity τ are considered while the other parameters remain unchanged.

Except for very small maturities, our approach has proven itself consistently more accurate than formula (7.5). Moreover, the step for computing the price, after obtaining the coefficients, showcases superior computational speed compared to the other approach. Our method enables the simultaneous computation of multiple option prices for a vector of different maturities, variances, asset prices and strikes, with minimal impact on CPU time usage (cf. Table 7.3). In contrast, the approach by He and Lin takes on average 78 seconds to compute one price only.

vector of prices	10,000 prices	1,000 prices	100 prices	10 prices	1 price
CPU time (ms)	108.44	10.27	2.28	1.00	0.94

Table 7.3: CPU time (in ms) for computing multiple option prices at the same time using our approach.

8

ERROR ANALYSIS

This chapter is devoted to analysing, from a theoretical point of view, the error convergence behavior and upper bound within the framework outlined in Chapter 4. These results can be readily extended to the approaches described in Chapter 5 and 6. Our analysis commences by identifying the various sources of error, and whenever feasible, we establish theoretical bounds for these errors.

8.1. ERROR SOURCES

In the derivation of our approximation formula for the price of a barrier option, three steps introduce errors: the truncation of the integration range in the risk-neutral valuation formula, the substitution of the survival density by its series expansion truncated on a finite interval and the reconstruction of the truncated trigonometric expansion of $\hat{\phi}_p$. Therefore, the overall error consists of three parts:

1. The truncation of the integration range,

$$V_1(t,x) = e^{-r(T-t)} \int_a^b v(y,T)p(y,\tau_B > T \mid x)\, dy,$$

leads to the error

$$\epsilon_1 := V(t,x) - V_1(t,x) = e^{-r(T-t)} \int_{-\infty}^a v(y,T)p(y,\tau_B > T \mid x) dy.$$

Since, for an up-and-out barrier option, the survival probability above the barrier level b is 0, i.e.

$$V(t,x) = e^{-r(T-t)} \int_{-\infty}^b v(y,T)p(y,\tau_B > T \mid x)\, dy,$$

the integration range truncation error depends solely on the choice of the lower barrier level a.

2. The series truncation,

$$V_2(t,x) = e^{-r(T-t)} \sum_{p=1}^{N} \text{Im}\left\{\phi\left(\frac{p\pi}{b-a}, t; x\right) e^{-ip\pi \frac{a}{b-a}}\right\} V_p,$$

leads to the error

$$\begin{aligned}\epsilon_2 &:= V_1(t,x) - V_2(t,x) \\ &= e^{-r(T-t)} \sum_{p=N+1}^{+\infty} \text{Im}\left\{\phi\left(\frac{p\pi}{b-a}, t; x\right) e^{-ip\pi \frac{a}{b-a}}\right\} V_p \\ &= e^{-r(T-t)} \sum_{p=N+1}^{+\infty} \hat{\phi}_p \cdot V_p,\end{aligned}$$

where ϕ is the survival ch.f. on range $[a,b]$, i.e. $\phi(\omega) = \int_a^b e^{i\omega y} p(y, \tau_B > T \mid x) dy$, and V_p are the Fourier series coefficients of the payoff function, as defined in formula (4.13).

3. The last error comes from approximating $\hat{\phi}_p$ using a trigonometric expansion truncated at level N, for which the coefficients are obtained via solving the linear system resulting from the corresponding PDE. If we assume that $\hat{\phi}_p$ has a spectral series representation, $T\hat{\phi}_p$, given by

$$\begin{aligned}\hat{\phi}_p \approx T\hat{\phi}_p(\tau,x) = &\sum_{k_1=1}^{\infty}\sum_{k_2=1}^{\infty} \alpha_{k_1,k_2} \sin\left(k_1\pi\frac{x-a_1}{b_1-a_1}\right)\frac{b_2-a_2}{k_2\pi}\sin\left(k_2\pi\frac{\tau-a_2}{b_2-a_2}\right) \\ &+ \sum_{k=1}^{\infty}\frac{1}{2}\alpha_{k_1,0}\tau\sin\left(k_1\pi\frac{x-a_1}{b_1-a_1}\right) + \sin\left(p\pi\frac{x-a_1}{b_1-a_1}\right), \text{with } \tau := T-t,\end{aligned} \tag{8.1}$$

then, in practice, we assume that $\hat{\phi}_p$ can be approximated by a trigonometric expansion truncated at level N, $T_N\hat{\phi}_p$, of the following form

$$\begin{aligned}T_N\hat{\phi}_p(\tau,x) = &\sum_{k_1=1}^{N}\sum_{k_2=1}^{N-1} A_{k_1,k_2} \sin\left(k_1\pi\frac{x-a_1}{b_1-a_1}\right)\frac{b_2-a_2}{k_2\pi}\sin\left(k_2\pi\frac{\tau-a_2}{b_2-a_2}\right) \\ &+ \sum_{k=1}^{N}\frac{1}{2}A_{k_1,0}\tau\sin\left(k_1\pi\frac{x-a_1}{b_1-a_1}\right) + \sin\left(p\pi\frac{x-a_1}{b_1-a_1}\right).\end{aligned} \tag{8.2}$$

This will be inserted into the PDE to find the respective coefficients. As a consequence, the error reads,

$$\begin{aligned}\epsilon_3 &:= \hat{\phi}_p(\tau,x) - T_N\hat{\phi}_p(\tau,x) \\ &= \hat{\phi}_p(\tau,x) - \sum_{k_1=1}^{N}\sum_{k_2=1}^{N-1} A_{k_1,k_2} \sin\left(k_1\pi\frac{x-a_1}{b_1-a_1}\right)\frac{b_2-a_2}{k_2\pi}\sin\left(k_2\pi\frac{\tau-a_2}{b_2-a_2}\right) \\ &- \sum_{k=1}^{N}\frac{1}{2}A_{k_1,0}\tau\sin\left(k_1\pi\frac{x-a_1}{b_1-a_1}\right) - \sin\left(p\pi\frac{x-a}{b-a}\right).\end{aligned}$$

It is worth noting that the coefficients V_p are derived analytically, and thus, no error is involved.

8.2. THEORETICAL ERROR BOUNDS

The first two error components are well studied in literature, including the original paper of the COS method [22]. The key to bound the errors lies in the decay rate of the series coefficients, while the convergence rate of the Fourier series depends on the properties of the target-function on the expansion interval.

Error ϵ_2 depends on both $\hat{\phi}_p$ and V_p, i.e. the series coefficients of the survival pdf and those of the payoff, respectively. In finance, we assume that the density is typically smoother than the payoff functions and that $\hat{\phi}_p$ decays faster than V_p. As a consequence, the product of $\hat{\phi}_p$ and V_p converges faster than either $\hat{\phi}_p$ or V_p, and we can establish an upper bound for this product as follows:

$$\left| \sum_{p=N+1}^{\infty} \hat{\phi}_p \cdot V_p \right| \leq C \sum_{p=N+1}^{\infty} \left| \hat{\phi}_p \right|,$$

with C some constant. Hence, error ϵ_2 is dominated by the series truncation error of the survival pdf.

To bound the series truncation error ϵ_2, we can use the theory from Section 2.3.1 to assert that the error converges exponentially in N for a class $C^{\infty}([a_1, b_1] \times [a_2, b_2])$ survival pdf. This results in a upper bound for ϵ_2 given by

$$|\epsilon_2| < Pe^{-N\nu},$$

with $\nu > 0$ and $P > 0$ a term that varies less than exponentially with N. In case the survival pdf has a discontinuity in one of its derivatives, there is algebraic convergence of the Fourier series expansion, for which the error can be bounded as follows:

$$|\epsilon_2| < \frac{P}{N^{\beta-1}},$$

with P being a positive constant and $\beta \geq n \geq 1$(n the algebraic index of convergence of V_p, as defined in Definition 2.3.1). Note that $\beta \geq n$ because the pdf is usually smoother than a payoff function.

The Delta of a barrier option exhibits discontinuities at $x = a$ and $x = b$ and, from equation (4.28), the first derivative of the survival pdf is discontinuous on those points as well. In light of this, from a theoretical point of view, we expect an algebraic convergence of the series for the survival pdf.

In practice, the series approximating the survival pdf in our approach demonstrates algebraic convergence. This is due to the algebraic decay of the series coefficients, $\hat{\phi}_p$, as depicted in Figure 8.1, which suggests that the second error bound should be employed.

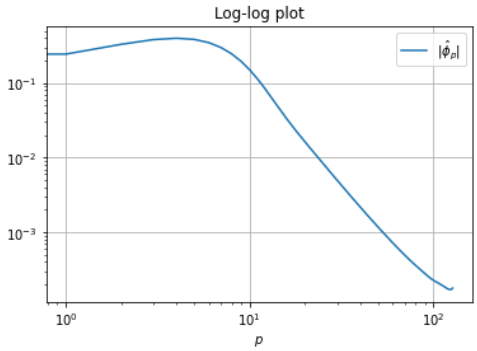

Figure 8.1: Example of log-log plot for $|\hat{\phi}_p(\tau, x)|$, where $x = \ln 100$ and $\tau = 0.5$.

Finally, we turn our attention to error ϵ_3, arising from the determination of coefficients for $T_N\hat{\phi}_p$ through the evaluation of the PDE (4.15) at different training points. As discussed in Section 3.2.2, it is optimal to set the number of training points equal to the number of unknown parameters (the coefficients) for each dimension. This ensures the uniqueness of the linear system, which is subsequently solved using a direct solver, eliminating errors associated with this step.

However, error ϵ_3 inherently comprises three components: the assumption of a trigonometric expansion series for $\hat{\phi}_p$, denoted as $T\hat{\phi}_p$, that belongs to the class C^∞; the truncation of this series at level N, represented as $T_N\hat{\phi}_p$; and the determination of the coefficients through the PDE approach rather than utilizing reference values. To conduct a comprehensive analysis of this error, it is necessary to revisit certain assumptions that we have implicitly or explicitly made.

Recall that there exists no closed-form solution for $\hat{\phi}_p$. However, we have shown that in the context of barrier options, the first derivative of the survival pdf with respect to the variable x exhibits discontinuities at $x = a$ and $x = b$. This implies that the first derivative of $\hat{\phi}_p$ should also possess such discontinuities. Our approach is built upon the assumption that $\hat{\phi}_p$ can be effectively approximated using a trigonometric series expansion, denoted as $T\hat{\phi}_p$, which retains smoothness up to class C^∞. Thus, $T\hat{\phi}_p$ fails to capture these singularities at $x = a$ and $x = b$. Consequently, within this framework, as the truncation level N approaches infinity, the value derived for $T_N\hat{\phi}_p$ using the PDE approach converges more rapidly towards $T\hat{\phi}_p$ than towards $\hat{\phi}_p$.

The series truncation error, i.e. $T\hat{\phi}_p - T_N\hat{\phi}_p$, cannot be dissociated from the use of the PDE to calibrate the coefficients of $T_N\hat{\phi}_p$. The values for the calibrated coefficients A_{k_1,k_2} computed via this approach compensate for the truncation of the series at level N. For $T\hat{\phi}_p$, the coefficients values α_{k_1,k_2} decrease as the number of terms increases, yet they remain non-zero for relatively high indices ($k_1 > N, k_2 > N-1$). This means that for higher-frequency modes within the Fourier series expansion, the amplitudes are non-zero.

Conversely, for $T_N\hat{\phi}_p$, the higher-frequency modes ($k_1 > N, k_2 > N-1$) demonstrate zero amplitudes, while the lower-frequency modes possess larger amplitudes to com-

pensate for this fact. The source of error lies in the fact that emphasizing the lower-frequency modes fails to entirely offset the accuracy loss in the higher-frequency modes. Essentially, the truncation of the series results in a reduction of spectral accuracy for $T_N\hat{\phi}_p$ when compared to the infinite expansion, $T\hat{\phi}_p$. It is worth noting, however, that as the number of expansion terms N increases, A_{k_1,k_2} progressively converges towards α_{k_1,k_2}.

In the scenario where, instead of employing the PDE approach, we were to utilize reference values and a minimization process to ascertain the coefficients of $T_N\hat{\phi}_p$ that yield the most accurate approximation, this compensation phenomenon from the lower modes would not come into play.

Additionally, error ϵ_3 is challenging to quantify as it strongly depends on the index p. The results of the numerical tests presented in Figures 3.10 (for Heat equation) and 4.3 (for GBM) suggest that there is an algebraic error convergence of the truncated approximation $T_N\hat{\phi}_p$ with respect to the benchmark value for $\hat{\phi}_p$. Nevertheless, these are only a numerical tests and further analysis is necessary to confirm the type of convergence of ϵ_3.

9

Conclusions and Future Research

In this thesis, we have formulated, tested and analyzed a novel approach for pricing continuously-monitored barrier options, relying solely on the pricing PDE. This method comprises three main components: determining the most suitable expansion form for getting the survival ch.f. of a knock-out option; determining the coefficients of this expansion through solving a linear system derived from the PDE it satisfies; and applying the one-dimensional COS method for pricing the respective option.

While our primary focus has been the application of this novel approach to up-and-out barrier options, this method is equally applicable to down-and-out or double barrier options. Furthermore, we have applied our methodology to two distinct models, starting with the GBM model, and subsequently Heston's model. Theoretically, this approach is general and can cope with other model dynamics.

The first key insight from this thesis is that the barrier-hitting probability can be absorbed into the so-called survival density function. This result allowed us to leverage on the one-dimensional COS formula, traditionally employed for pricing European options, to value barrier options. Consequently, our main focus was on recovering this survival pdf, specifically aiming the determination of the coefficients of the sine series expansion of the survival pdf, denoted as $\hat{\phi}_p := \text{Im}\left\{\phi\left(\frac{p\pi}{b-a}\right) e^{-ip\pi\frac{a}{b-a}}\right\}$.

Our approach was inspired by the findings of supervised machine learning research conducted at FF Quant [30], which indicated that the Fourier transform of the survival density function, i.e. the survival ch.f., can again be accurately approximated by a Fourier series expansion. Also, the coefficients for this expansion can be derived from a training dataset. Throughout the development of our new method, we gained deeper understanding of the Fourier theory, which led to the second insight: expanding the derivative of the function $\hat{\phi}_p$ into cosine or sine series, rather than the function itself, can significantly enhance the accuracy of the original function approximation. As a result, we concluded that an effective approximation arises from applying a two-dimensional Fourier series expansion to the first-order derivative of $\hat{\phi}_p$ with respect to time. When integrated,

this choice yields a trigonometric series expansion with an additional term alongside the conventional Fourier series, which results in a better fit to $\hat{\phi}_p$ than the Fourier series expansion.

Furthermore, the third pivotal insight of this thesis lies in the fact that applying a change of variables to the solution function can improve convergence by altering the shape of the function to be approximated. We have shown the greater accuracy of expressing $\hat{\phi}_p$ as a function of asset price, maturity, and log-variance.

The main idea underpinning the methodology developed in this thesis revolved around obtaining the coefficients of the trigonometric series expansion of $\hat{\phi}_p$ from the PDE it satisfies, by evaluating it at different training points. In turn, this PDE is derived from the pricing PDE for a barrier option, which contains Dirichlet boundary conditions at the barrier levels. Hence, this approach is particularly advantageous in situations whereby accurate reference values are difficult to obtain or unavailable, as it relies solely on the pricing PDE to produce option prices.

It is noteworthy that the calibration of the coefficients of the series for $\hat{\phi}_p$ can be done "offline" in advance. As long as the model parameters of the underlying do not change, the trained coefficients can be reused. Particularly, since the series expansion provides a global approximation, it is possible to price a large number of options simultaneously for different strikes, maturities, asset prices and variances - all using the same coefficients. The coefficients only need to be updated in the next re-calibration of the underlying process model.

Numerical tests and analyses were performed to verify the robustness and efficiency of this method for different parameter sets. For similar accuracy levels, our approach's computational time greatly outperforms that of MC simulations. Plus, this method has superior computational efficiency and accuracy as compared to other existing methods in the literature.

Nonetheless, there are certain challenges, which stem from the method's dependence on a linear system created through the evaluation of the PDE at specific training points. Further investigations into optimizing the allocation of these training points is pivotal for a successful and broad application of this approach. Additional research may also delve into optimizing the choice of the interval $[a_3, b_3]$ for the v-dimension, particularly when the Feller condition is not met, as larger maturities have exhibited results of varying accuracy.

In summary, this thesis lays the foundation for enhanced pricing accuracy and efficiency in the context of knock-out barrier options under stochastic volatility models. A future research focus could be to extend this approach to other stochastic models, particularly the SABR model, where accurate reference values are often unavailable. Lastly, the method developed in this thesis can also be combined with tensor calculus, such as Canonical Polyadic Decomposition, to free up contract parameters as function variables and reduce computational complexity.

BIBLIOGRAPHY

[1] J. Hakala and U. Wystup, *Foreign Exchange Risk: Models, Instruments and Strategies*. Risk Publications, Feb. 2002, ISBN: 1899332375. [Online]. Available: https://api.semanticscholar.org/CorpusID:153105260.

[2] A. Lipton, *Mathematical Methods for Foreign Exchange: A Financial Engineer's Approach*. World Scientific, Jul. 2001, ISBN: 978-981-02-4615-0. DOI: 10.1142/4694.

[3] A. Lipton and W. McGhee, "Universal barriers," *Risk*, vol. 15, no. 5, pp. 81–85, May 2002.

[4] U. Wystup, *FX Options and Structured Products*. John Wiley & Sons Ltd, 2006, ISBN: 978-0-470-01145-4.

[5] A. Giese, "On the Pricing of Discrete Barrier Options in Models Beyond Black-Scholes," Ph.D. dissertation, TU Berlin, Berlin, 2002.

[6] F. Black and M. Scholes, "The Pricing of Options and Corporate Liabilities," *Journal of Political Economy*, vol. 81, pp. 637–654, 3 1973.

[7] R. C. Merton, "Theory of Rational Option Pricing," *The Bell Journal of Economics and Management Science*, vol. 4, pp. 141–183, 1 1973.

[8] R. Heynen and H. Kat, "Partial Barrier Options," *The Journal of Financial Engineering*, vol. 3, pp. 253–274, 1994.

[9] N. Kunitomo and M. Ikeda, "Pricing Options With Curved Boundaries," *Mathematical Finance*, vol. 2, pp. 275–298, 4 Oct. 1992, ISSN: 0960-1627. DOI: 10.1111/j.1467-9965.1992.tb00033.x.

[10] S. L. Heston, "A Closed-Form Solution for Options with Stochastic Volatility with Applications to Bond and Currency Options," *The Review of Financial Studies*, vol. 6, no. 2, pp. 327–343, 1993.

[11] J. Hull and A. White, "The Pricing of Options on Assets with Stochastic Volatilities," *The Journal of Finance*, vol. 42, pp. 281–300, 2 Jun. 1987, ISSN: 00221082. DOI: 10.1111/j.1540-6261.1987.tb02568.x.

[12] E. M. Stein and J. C. Stein, "Stock Price Distributions with Stochastic Volatility: An Analytic Approach," *Review of Financial Studies*, vol. 4, pp. 727–752, 1991. [Online]. Available: http://rfs.oxfordjournals.org/.

[13] P. Hagan, D. Kumar, A. Lesniewski, and D. Woodward, "Managing Smile Risk," *Wilmott Magazine*, vol. 1, pp. 84–108, Jan. 2002.

[14] K. Ito and J. Toivanen, "Lagrange Multiplier Approach with Optimized Finite Difference Stencils for Pricing American Options under Stochastic Volatility," *SIAM Journal on Scientific Computing*, vol. 31, pp. 2646–2664, 4 Jan. 2009, ISSN: 1064-8275. DOI: 10.1137/07070574X.

[15] Y. Muroi and T. Yamada, "Spectral binomial tree: New algorithms for pricing barrier options," *Journal of Computational and Applied Mathematics*, vol. 249, pp. 107–119, 2013, ISSN: 0377-0427. DOI: https://doi.org/10.1016/j.cam.2012.10.036. [Online]. Available: https://www.sciencedirect.com/science/article/pii/S0377042713000824.

[16] J. C. Cox, S. A. Ross, and M. Rubinstein, "Option pricing: A simplified approach," *Journal of Financial Economics*, vol. 7, no. 3, pp. 229–263, 1979, ISSN: 0304-405X. DOI: https://doi.org/10.1016/0304-405X(79)90015-1. [Online]. Available: https://www.sciencedirect.com/science/article/pii/0304405X79900151.

[17] F. Fang and C. W. Oosterlee, "A Fourier-based Valuation Method of Bermudan and Barrier Options under Heston's Model," *SIAM Journal on Financial Mathematics*, vol. 2, no. 1, pp. 440–463, 2011. DOI: 10.1137/100794158.

[18] M. Ruijter and C. W. Oosterlee, "Two-dimensional Fourier cosine series expansion method for pricing financial options," *SIAM Journal on Scientific Computing*, vol. 34, no. 5, B642–B671, 2012. DOI: 10.1137/120862053.

[19] M. Broadie and Y. Yamamoto, "Application of the fast Gauss transform to option pricing," *Management Science*, vol. 49, no. 8, pp. 1071–1088, Aug. 2003. [Online]. Available: https://www.jstor.org/stable/4133937.

[20] M. Broadie and Y. Yamamoto, "A double-exponential fast Gauss transform for pricing discrete path-dependent options," *Operational Research*, vol. 53, no. 5, pp. 764–779, 2005.

[21] L. Feng and V. Linetsky, "Pricing Discretely Monitored Barrier Options and Defaultable Bonds in LVY Process Models: A Fast Hilbert Transform Approach," *Mathematical Finance*, vol. 18, no. 3, pp. 337–384, Jul. 2008, ISSN: 09601627. DOI: 10.1111/j.1467-9965.2008.00338.x.

[22] F. Fang and C. W. Oosterlee, "A novel pricing method for european options based on fourier-cosine series expansions," *SIAM Journal on Scientific Computing*, vol. 31, no. 2, pp. 826–848, 2008, ISSN: 10648275. DOI: 10.1137/080718061.

[23] A. Ilhan, M. Jonsson, and K. R. Sircar, "Singular Perturbations for Boundary Value Problems Arising from Exotic Options," *SIAM Journal on Applied Mathematics*, vol. 64, no. 4, pp. 1268–1293, 2004. DOI: 10.1137/S0036139902420043.

[24] T. Kato, A. Takahashi, and T. Yamada, "An Asymptotic Expansion Formula for Up-and-Out Barrier Option Price under Stochastic Volatility Model," Feb. 2013. DOI: 10.14495/jsiaml.5.17.

[25] A. Lipton, A. Gal, and A. Lasis, "Pricing of vanilla and first generation exotic options in the local stochastic volatility framework: survey and new results," *Quantitative Finance*, vol. 14, no. 11, pp. 1899–1922, 2014. DOI: 10.1080/14697688.2014.930965.

[26] W. Barger and M. Lorig, "Approximate pricing of European and Barrier claims in a local-stochastic volatility setting," *International Journal of Financial Engineering*, Jun. 2017, ISSN: 2424-7863. DOI: 10.1142/S2424786317500189.

[27] I. Karatzas and S. E. Shreve, *Brownian Motion and Stochastic Calculus*, 2nd ed. Springer-Verlag, 1991, ISBN: 0387976558.

[28] S. E. Shreve, *Stochastic Calculus for Finance II*. Springer New York, 2004, ISBN: 978-1-4419-2311-0. DOI: 10.1007/978-1-4757-4296-1.

[29] X. J. He and S. Lin, "An Analytical Approximation Formula for Barrier Option Prices Under the Heston Model," *Computational Economics*, vol. 60, no. 4, pp. 1413–1425, Dec. 2022, ISSN: 15729974. DOI: 10.1007/s10614-021-10186-7.

[30] L. Klomp, "Pricing Barrier Options under Lévy Processes using Dimension-reduced Cosine Expansion," Aug. 2023. [Online]. Available: http://resolver.tudelft.nl/uuid:a08e7ee1-fef0-4f9e-9e72-abe90f714a13.

[31] C. W. Oosterlee and L. A. Grzelak, *Mathematical Modeling Computation in Finance*. World Scientific Publishing Europe Ltd., 2020, ISBN: 978-1-78634-794-7.

[32] R. L. Karandikar and B. V. Rao, *Introduction to Stochastic Calculus*. Springer Singapore, 2018, ISBN: 978-981-10-8317-4. DOI: 10.1007/978-981-10-8318-1.

[33] D. J. Higham, *An Introduction to Financial Option Valuation: Mathematics, Stochastics and Computation*. Cambridge University Press, 2004, ISBN: 9780511800948. DOI: 10.1017/CBO9780511800948.

[34] H. Föllmer and A. Schied, *Stochastic Finance*. De Gruyter, Jul. 2016, ISBN: 9783110463453. DOI: 10.1515/9783110463453.

[35] J. Cox, J. Ingersoll, and S. Ross, "A theory of the term structure of interest rates," *Econometrica*, vol. 53, pp. 385–407, 1985.

[36] W. Feller, "Two singular diffusion problems," *The Annals of Mathematics*, vol. 54, pp. 173–182, 1951.

[37] A. S. Hurn, K. A. Lindsay, and A. J. Mcclelland, "On the Efficacy of Fourier Series Approximations for Pricing European and Digital Options," *Applied Mathematics*, vol. 5, no. 17, pp. 2786–2807, Oct. 2014. DOI: 10.4236/am.2014.517267.

[38] X.-S. Yang, *Engineering Mathematics with Examples and Applications*. Academic Press, 2017.

[39] J. P. Boyd, *Chebyshev and Fourier Spectral Methods Second Edition*. Courier Corporation, 2000. [Online]. Available: http://www-personal.engin.umich.edu/%E2%88%BCjpboyd/2000.

[40] P. B. Laval, *Integration and Differentiation of Fourier Series*.

[41] C. M. Bender and S. A. Orszag, *Advanced Mathematical Methods for Scientists and Engineers I*. Springer New York, 1999, ISBN: 978-1-4419-3187-0. DOI: 10.1007/978-1-4757-3069-2.

[42] S. Gottlieb, J.-H. Jung, and S. Kim, "A Review of David Gottlieb's Work on the Resolution of the Gibbs Phenomenon," *Communications in Computational Physics*, vol. 9, no. 3, pp. 497–519, Mar. 2011, ISSN: 1815-2406. DOI: 10.4208/cicp.301109.170510s. [Online]. Available: https://www.cambridge.org/core/product/identifier/S1815240600001201/type/journal_article.

9

[43] E. Tadmor, "Filters, mollifiers and the computation of the Gibbs phenomenon," *Acta Numerica*, vol. 16, pp. 305–378, May 2007, ISSN: 09624929. DOI: 10.1017/S0962492906320016.

[44] M. Versteegh, "The Gibbs phenomenon in option pricing methods," Ph.D. dissertation, TU Delft, Delft, Oct. 2012.

[45] R. Russel and L. Shampine, "A collocation method for boundary value problems," *Numerische Mathematik*, vol. 19, pp. 1–28, 1 1972.

[46] J. Wright, *Collocation Methods from Interpolation*, Oct. 2022. [Online]. Available: https://www.jameswright.xyz/post/20220925/collocation-methods-from-interpolation/.

[47] T. G. Kolda and B. W. Bader, "Tensor decompositions and applications," *SIAM Review*, vol. 51, no. 3, pp. 455–500, 2009, ISSN: 00361445. DOI: 10.1137/07070111X.

[48] R. You, Y. Yao, and J. Shi, "Tensor-based ultrasonic data analysis for defect detection in fiber reinforced polymer (FRP) composites," *Chemometrics and Intelligent Laboratory Systems*, vol. 163, pp. 24–30, 2017, ISSN: 0169-7439. DOI: https://doi.org/10.1016/j.chemolab.2017.02.007. [Online]. Available: https://www.sciencedirect.com/science/article/pii/S0169743917300473.

[49] A. D. Polianin, *Handbook of linear partial differential equations for engineers and scientists*. Chapman & Hall/CRC, 2002, ISBN: 1-58488-299-9.

[50] N. Yang, Y. Liu, and Z. Cui, "Pricing Continuously Monitored Barrier Options under the SABR Model: A Closed-Form Approximation," *Journal of Management Science and Engineering*, vol. 2, no. 2, pp. 116–131, Jun. 2017, ISSN: 25895532. DOI: 10.3724/SP.J.1383.202006.

[51] M. Kozdron, *Lecture #33, 34: The Characteristic Function for a Diffusion*, Nov. 2014.

[52] P. Salminen, "On the First Hitting Time and the Last Exit Time for a Brownian Motion to/from a Moving Boundary," *Advances in Applied Probability*, vol. 20, no. 2, pp. 411–426, 1988. [Online]. Available: https://www.jstor.org/stable/1427397?seq=1&cid=pdf-.

[53] R. Cont and E. Voltchkova, "Integro-differential equations for option prices in exponential Lévy models," *Finance and Stochastics*, vol. 9, pp. 299–325, 2005. DOI: 10.1007/s00780-005-0153-z.

[54] P. Carr, A. Itkin, and D. Muravey, "Semi-analytical pricing of barrier options in the time-dependent Heston model," Feb. 2022. [Online]. Available: http://arxiv.org/abs/2202.06177.

[55] C. C. Kwan, "Solving the Black-Scholes Partial Differential Equation via the Solution Method for a One-Dimensional Heat Equation: A Pedagogic Approach with a Spreadsheet-Based Illustration," *Spreadsheets in Education*, vol. 12, no. 1, Sep. 2019. [Online]. Available: https://sie.scholasticahq.com.

[56] A. Pelsser, "Pricing Double Barrier Options: An Analytical Approach," Tinbergen Institute, Tech. Rep., 1997.

9

[57] T. Hillen, I. E. Leonard, and H. van Roessel, *Partial Differential Equations: Theory and Completely Solved Problems*. John Wiley & Sons, Inc., 2012, ISBN: 978-1-118-06330-9.

[58] Z. Cheng, "Dimension Reduction Techniques for Multi-dimensional Numerical Integrations Based on Fourier-cosine Series Expansion," 2022. [Online]. Available: https://repository.tudelft.nl/islandora/object/uuid:f6ffbcd6-df14-425b-84bb-63e4e105205c?collection=education.

[59] M. Dell'Era, "Closed Form Solution For Heston PDE by Geometrical Transformations," *Asian Economic and Financial Review*, vol. 4, no. 6, pp. 793–807, 2014. [Online]. Available: http://www.aessweb.com/journals/5002.

[60] C. Vuik and D. J. P. Lahaye, *Scientific Computing (WI4201)*, 2019.

[61] D. J. Duffy, *Finite Difference methods in financial engineering: a Partial Differential Equation approach*. John Wiley & Sons, 2013.

A

ADDITIONAL RESULTS

This appendix contains additional results showcasing the accuracy of the approach in Chapter 5 for other types of knock-out barrier options. In fact, as discussed before, our approach can be applied to the valuation of double barrier options, up-and-out and down-and-out barrier options. It is only necessary to change the range $[a,b]$ of the possible values assumed by the asset price process S_t accordingly. Moreover, since information about the type of option is only contained in the payoff coefficients V_p, these can easily be changed to provide the payoff coefficients of a put option, instead of a call option, as done in previous chapters.

Figure A.1 displays the price and error of an down-and-out put option for parameters $(r,\gamma,\bar{v},\kappa,\rho,v,K,B) = (0.1,0.1,0.02,2.0,-0.5,0.01,100,70)$, using $N = M = 32$. This means that $a = B$ and b should be chosen big enough. For put options, the payoff coefficients are given by

$$V_p = \int_a^b (K-y)^+ \sin\left(p\pi\frac{y-a}{b-a}\right) dy,$$

for which there is a closed-form expression.

Figure A.2 shows the price and error of an double barrier call option with lower barrier level B_l and upper barrier level B_u. The option is computed for parameters $(r,\gamma,\bar{v},\kappa,\rho,v,K,B_l,B_u) = (0.1,0.1,0.02,2.0,-0.5,0.01,90,80,120)$, using $N = M = 32$. This means that $a = B_l$ and $b = B_u$.

In both cases, the respective result is benchmarked against a Monte Carlo simulation with 100,000 paths and 1,000 time steps.

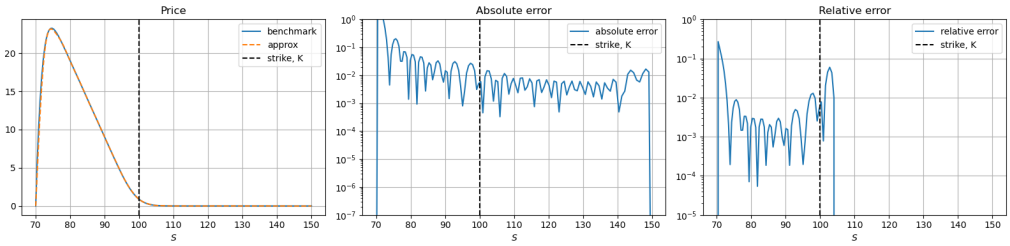

(a) Price, absolute and relative errors for $\tau = 0.1$.

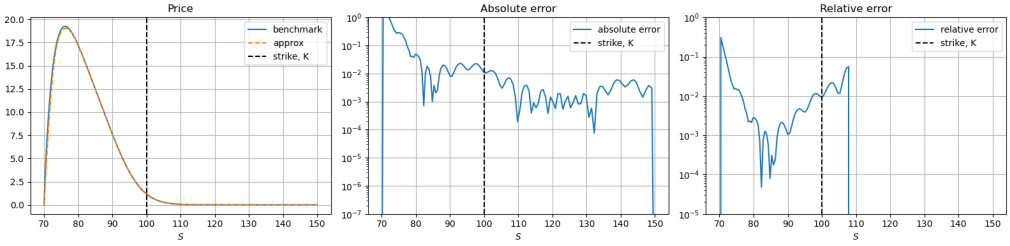

(b) Price, absolute and relative errors for $\tau = 0.25$.

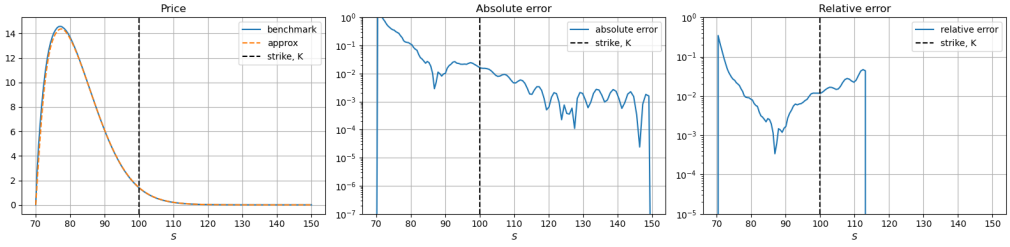

(c) Price, absolute and relative errors for $\tau = 0.5$.

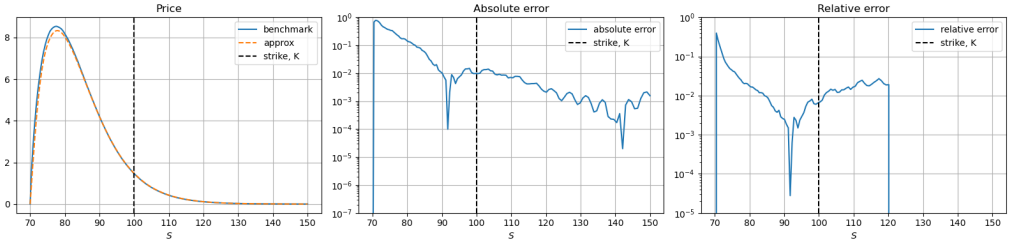

(d) Price, absolute and relative errors for $\tau = 1$.

Figure A.1: Price and respective errors of a down-and-out put option for τ, using our approach vs. MC formulation.

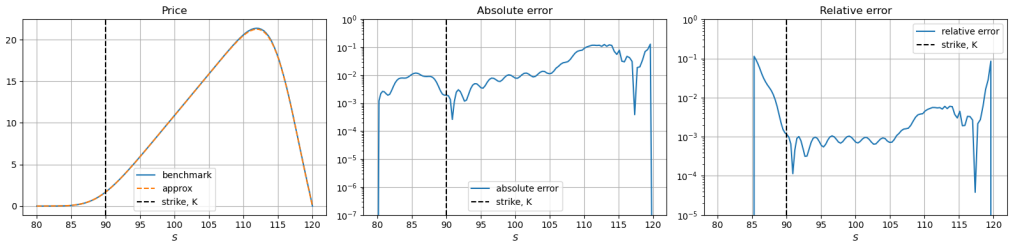

(a) Price, absolute and relative errors for $\tau = 0.1$.

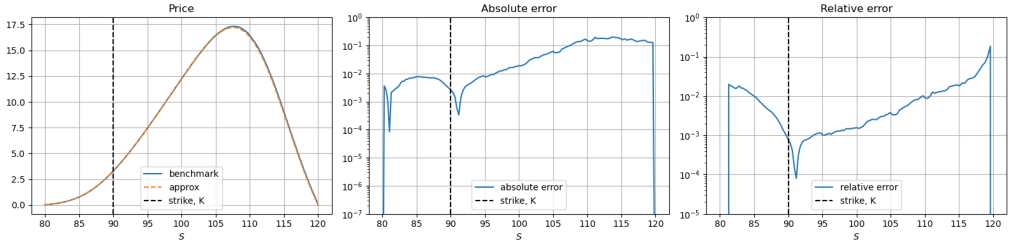

(b) Price, absolute and relative errors for $\tau = 0.25$.

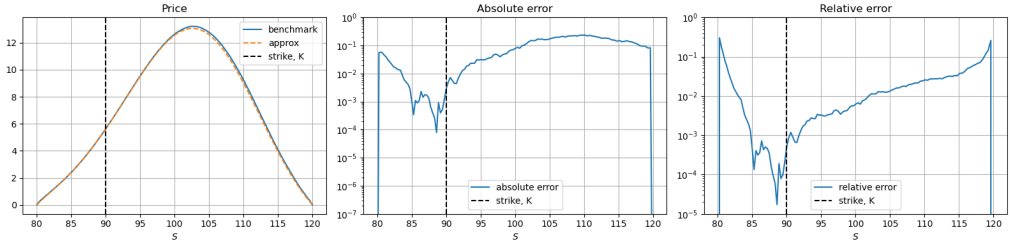

(c) Price, absolute and relative errors for $\tau = 0.5$.

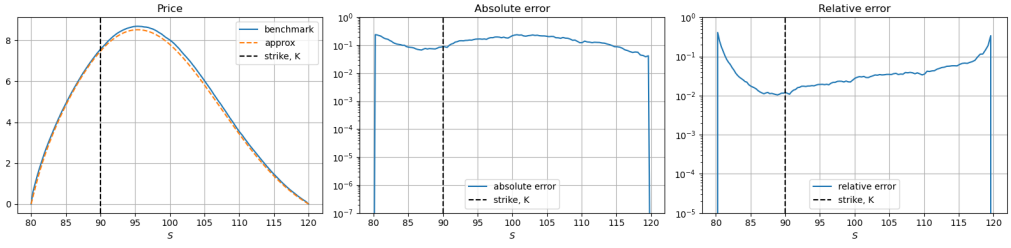

(d) Price, absolute and relative errors for $\tau = 1$.

Figure A.2: Price and respective errors of a a double barrier call option for different values of τ, using our approach vs. MC formulation.